

https://dspace.org/

Commissioning and evaluation of electron Monte Carlo dose calculation algorithm in the Monaco treatment planning system

Motseki, Masupha

2025-06
University of the Witwatersrand, Johannesburg
https://hdl.handle.net/10539/48753

Motseki, Masupha. (2025). Commissioning and evaluation of electron Monte Carlo dose calculation algorithm in the Monaco treatment planning system. [Master's dissertation, University of the Witwatersrand, Johannesburg]. WIReDSpace. https://hdl.handle.net/10539/48753

Downloaded from a DSpace repository. https://dspace.org/

Commissioning and evaluation of electron Monte Carlo dose calculation algorithm in the Monaco treatment planning system.

Masupha Motseki (913627)

A research report submitted to the Faculty of Science, University of the Witwatersrand, Johannesburg, in partial fulfillment of the requirements for the degree of Master of Science.

School of Physics

Faculty of Science

University of the Witwatersrand

Supervisor: Dr Sonwabile Ngcezu

Co-supervisor: Prof. Debbie van der Merwe

Administrative supervisor: Ms. Lehlabile Sekone

09 June 2025

Declaration

I, Masupha David Motseki (Student number: 913627), hereby declare that this research report is my original work, except where acknowledged in the references and acknowledgements. It is submitted in partial fulfilment of the requirements for the Master of Science degree in Medical Physics at the University of the Witwatersrand, Johannesburg. This work has not been submitted previously for any degree or examination at this or any other university.



Masupha Motseki

Signed at Johannesburg, on 09 June 2025

Abstract

This study aimed to validate and commission the electron Monte Carlo (eMC) algorithm integrated into the Monaco Treatment Planning System (TPS) (version 6.1.2) in accordance with the American Association of Physicists in Medicine (AAPM) Medical Physics Practice Guideline (MPPG) 5a of 2015. The initial task involved validating the beam data used for beam modelling, followed by three verification tests using a homogeneous water-equivalent and a locally designed inhomogeneous phantom. The computed dose distributions from the eMC algorithm were evaluated against the measured data. In the homogeneous water-equivalent phantom, profiles, output factors and percentage depth dose (PDD) curves were evaluated for multiple electron energies at standard and extended source-to-surface distances (SSDs) using different applicators, including an irregularly shaped trapezoid cutout. PDDs and profiles were also computed at an oblique gantry angle of 20°. For the heterogeneity tests, low-density polystyrene was used to simulate lung tissue and solid Plaster of Paris (POP) was utilized to simulate bone. Cross-plane profiles distal to the inhomogeneities were computed by the eMC algorithm and compared to those measured with a planar detector. The study also investigated the performance of the algorithm by varying grid spacing and the number of histories. A one-dimensional gamma analysis with 3 %/3 mm criterion was utilized to compare measured and computed PDDs. The eMC algorithm demonstrated agreement within 3 %/3 mm for PDDs and profiles across all applicators and beam energies. However, discrepancies were observed for the irregular trapezoid cutout, where the agreement fell below 90 percent, indicating that limitations exist in the dosimetry of field sizes below 3 cm radius at beam energies greater than 12 MeV. Additionally, deviations in output factors were noted, with a maximum error of 6.5 percent. Overall, the eMC algorithm computed the dose distributions with sufficient accuracy in both homogeneous and inhomogeneous phantoms, and the optimal input parameters were identified as a 0.2 cm grid spacing and 500,000 histories for all energies.

Dedication

This research report is devoted to the memory of my late father, John Hopolang Motseki, who passed away in 2013. It was his dream for me to become a graduate, but he did not live to see it come true. May his soul rest in peace.

Acknowledgements

I sincerely appreciate and thank my supervisor, Dr Sonwabile Ngcezu, for providing guidance, assistance and introducing me to my research topic. I am also grateful to my co-supervisor, Prof. Debbie van der Merwe, for her guidance, dedication and support. Her patience with my shortcomings was truly appreciated. I sincerely thank my partner, Dr. Ntaote Matseliso and my mother, Maseeiso Veronica Motseki, for their unwavering financial and emotional support throughout this research. Finally, I express my gratitude to the medical physics staff at Charlotte Maxeke Johannesburg Academic Hospital, particularly Mr. Khotle Thekiso, for providing relevant articles and sharing his previous work on commissioning, as well as to the medical physics interns for their assistance with the equipment.

List of figures

Figure 2.1: A typical PDD curve for a clinical electron beam illustrating key parameters such as d_{max}, R_{80}, R_{90}, R_{50} and R_p, which are critical for dose prescription, calibration and treatment planning. The blue curve represents the measured dose distribution, while the red curve highlights the bremsstrahlung tail and a gradient line passing through R_{50} (Oncology Medical Physics, 2020). 6

Figure 2.2: A general electron beam profile illustrating the penumbra, umbra and central region. The ideal dose profile demonstrates a theoretical uniform dose, while the actual dose profile reflects real-world deviations caused by internal scattering and beam collimation (Quizlet, 2023). 7

Figure 3.1: In-air measurement setup without an applicator, showing the PTW Semiflex 31021 placed at 80 cm SDD, and the reference chamber used to correct fluctuations in measurements taken by the field chamber…… 18

Figure 3.2: PDD generation using Monaco TPS. 19

Figure 3.3: (a) Lung-equivalent setup at 100 cm SSD, with lung-equivalent material positioned within the 10 cm × 10 cm applicator-defined field. (b) Bone-equivalent setup at 100 cm SSD, with Plaster of Paris (POP) slab positioned within the 10 cm x 10 cm field. 21

Figure 3.4:(a) Lateral lung-equivalent setup: The lung-equivalent material and Perspex are offset to half of the field, creating an interface along the in-plane axis with the SSD set to 100 cm.(b) Lateral bone-equivalent setup: The POP and Perspex are offset to half of the field (10 cm × 10 cm) , similarly creating an interface along the in-plane axis with the SSD set to 100 cm. 23

Figure 4.1: Comparison of CMJAH and measured PDDs in water, employing an applicator sized 10 cm x 10 cm to confine the field, indicating the percentage difference obtained from 1D gamma analysis. (a) 6 MeV PDD. (b) 9 MeV PDD. (c) 12 MeV PDD. (d) 15 MeV PDD…….. 27

Figure 4.2: Cross-plane profiles in water for an applicator sized 10 cm x 10 cm, indicating the percentage difference obtained from 1D gamma analysis comparing measured and CMJAH profiles. The data are normalized to the central axis dose. (a) 6 MeV profile measured at 1 cm depth. (b) 9 MeV profile measured at 2 cm depth. (c) 12 MeV profile measured at 2 cm depth. (d) 15 MeV profile measured at 2 cm depth. 29

Figure 4.3: Cross-plane bremsstrahlung profiles in water for an applicator sized 10 cm x 10 cm, indicating the percentage difference obtained from 1D gamma analysis by comparing measured and CMJAH profiles. The data are normalized to the central axis dose. (a) 6 MeV bremsstrahlung profile measured at 5 cm depth. (b) 9 MeV bremsstrahlung profile measured at 15 cm depth. (c) 12 MeV profile measured at 15 cm depth. (d) 15 MeV bremsstrahlung profile measured at 15 cm depth.....31
Figure 4.4: A comparison of CMJAH and measured PDDs in water, for the 40 cm × 40 cm set field size, indicating the percentage difference from 1D gamma analysis. (a) 6 MeV PDD. (b) 9 MeV PDD. (c) 12 MeV PDD. (d) 15 MeV PDD.....33
Figure 4.5: Comparison of CMJAH and measured cross-plane profiles in air for a set field size of 8 cm × 8 cm, showing the percentage difference obtained from 1D gamma analysis. The data are normalized to the central axis dose. (a) 6 MeV profile. (b) 9 MeV profile. (c) 12 MeV profile. (d) 15 MeV profile. 36
Figure 4.6: Cross-plane profiles in air with the field size set to 40 cm × 40 cm, Indicating the percentage difference obtained from 1D gamma analysis comparing measured and CMJAH profiles. The data are normalized to the central axis dose. (a) 6 MeV profile. (b) 9 MeV profile. (c) 12 MeV profile. (d) 15 MeV profile.....38
Figure 4.7: Comparison of computed and measured PDDs in water at 100 cm SSD, employing the trapezoid cutout to confine the field, indicating the percentage difference obtained from 1D gamma analysis. (a) 6 MeV. (b) 9 MeV. (c) 12 MeV. (d) 15 MeV.....41
Figure 4.8: Comparison of measured and calculated PDDs in water, for an applicator sized 6 cm x 6 cm, indicating the percentage difference obtained from 1D gamma analysis at 100 cm SSD. (a) 6 MeV. (b) 9 MeV. (c) 12 MeV. (d) 15 MeV. 43
Figure 4.9: Comparison of measured and calculated PDDs in water at 110 cm SSD with a trapezoid cutout, indicating the percentage difference obtained from 1D gamma analysis. (a) 6 MeV. (b) 9 MeV. (c) 12 MeV. (d) 15 MeV.....45
Figure 4.10: Comparison of calculated and measured PDDs in water, employing an applicator sized 6 cm x 6 cm to confine the field at 110 cm SSD, showing the percentage difference obtained from 1D gamma analysis. (a) 6 MeV. (b) 9 MeV. (c) 12 MeV. (d) 15 MeV. 47
Figure 4.11: Cross-plane profiles in water at 110 cm SSD, employing an applicator sized 14 cm x 14 cm to confine the field, indicating the percentage difference obtained from 1D gamma analysis comparing measured and calculated profiles at R_{90}. (a) 6 MeV. (b) 9 MeV. (c) 12 MeV. (d) 15 MeV.....50

Figure 4.12: Cross-plane profiles at 110 cm SSD in water, for an applicator sized 14 cm × 14 cm, indicating the percentage difference obtained from 1D gamma analysis comparing measured and calculated profiles at R_{50}. (a) 6 MeV. (b) 9 MeV. (c) 12 MeV. (d) 15 MeV....52
Figure 4.13: Cross-plane profiles at 100 cm SSD with the lung and Perspex offset to half of the field, indicating the 1D gamma analysis comparing computed and measured profiles. The data are normalized to the central axis dose. (a) 6 MeV profile measured at 1.9 cm depth. (b) 9 MeV profile measured at 2.7 cm. (c) 12 MeV profile measured at 2.7 cm. (d) 15 MeV profile measured at 2.7 cm depth.....58
Figure 4.14: Cross-plane profiles at 100 cm SSD with lung-equivalent material positioned within the 10 cm × 10 cm field, indicating the 1D gamma analysis comparing calculated and measured profiles. (a) 6 MeV profile measured at 1.9 cm depth. (b) 9 MeV profile measured at 2.7 cm depth. (c) 12 MeV profile measured at 2.7 cm. (d) 15 MeV profile measured at 2.7 cm. 61
Figure 4.15: Cross-plane profiles at 100 cm SSD with the POP and Perspex offset to half the field, indicating the 1D gamma analysis comparing computed and measured profiles. The data are normalized to the central axis dose. (a) 6 MeV profile measured at 1.6 cm depth. (b) 9 MeV profile measured at 2.4 cm depth. (c) 12 MeV profile measured at 2.4 cm. (d) 15 MeV profile measured at 2.4 cm depth.....64
Figure 4.16: Cross-plane profiles at 100 cm SSD with the POP material positioned within the field, indicating the 1D gamma analysis comparing measured and calculated profiles. (a) 6 MeV profile measured at 1.6 cm depth. (b) 9 MeV profile measured at 2.4 cm depth. (c) 12 MeV profile measured at 2.4 cm. (d) 15 MeV profile measured at 2.4 cm depth. 67
Figure 4.17: A comparison of computed and measured PDDs in water at a gantry angle of 20 degrees, indicating the percentage difference obtained from 1D gamma analysis. (a) 6 MeV. (b) 9 MeV. (c) 12 MeV. (d) 15 MeV. 70
Figure 4.18: Cross-plane profiles in water at a depth of R_{90}, with the gantry angle set to 20 degrees, indicating the percentage difference obtained from 1D gamma analysis comparing calculated and measured profiles. (a) 6 MeV. (b) 9 MeV. (c) 12 MeV. (d) 15 MeV. 72
Figure 4.19: 9 MeV PDDs in water at 100 cm SSD, indicating the percentage difference obtained from 1D gamma analysis comparing computed and measured PDDs for different grid spacings. (a) 0.1 cm grid spacing (b) 0.3 cm grid spacing. (c) 0.5 cm grid spacing. (d) 0.8 cm grid spacing. 75
Figure 4.20: Comparison of measured and computed PDDs in water for the 9 MeV beam, indicating the percentage difference obtained from 1D gamma analysis for different number of

histories. (a) 50 000 histories. (b) 100 000 histories. (c) 200 000 histories. (d) 300 000 histories 78

List of Tables

Table 3.1: Initial depth for scanning depth ionization curves.....16
Table 3.2: Scanning depth for beam profiles and bremsstrahlung profiles. 17
Table 4.1: Summary of the 1D gamma analysis comparing calculated and measured PDDs in water, with the SSD of 100 cm, for different beam energies and applicators……48
Table 4.2: Summary of the 1D gamma analysis comparing computed and measured PDDs in water, with the SSD of 110 cm, for different electron beam energies and applicators. 48
Table 4.3: Summary of the 1D gamma analysis comparing computed and measured cross-plane profiles, scanned at R_{90} in water at 100 cm SSD for the different applicators and the trapezoid cutout, for all energies.....53
Table 4.4: Summary of the 1D gamma analysis comparing measured and computed cross-plane profiles, scanned at R_{50} in water with the SSD set to 100 cm, for the different applicators and the trapezoid cutout, for all energies.....53
Table 4.5: Summary of the 1D gamma analysis comparing computed and measured profiles, scanned at R_{90} in water at 110 cm SSD, for the different applicators and the trapezoid cutout,for all energies. 53
Table 4.6: Summary of the 1D gamma analysis comparing measured and computed cross-plane profiles, scanned at R_{50} in water with the SSD set to 110 cm , for the different applicators and the trapezoid cutout, for all energies.....54
Table 4.7: Percentage differences obtained from comparing measured and computed output factors in water with the SSD set to 100 cm for the different applicators and the trapezoid cutout, for all energies.....55
Table 4.8: Percentage differences obtained from comparing measured and computed output factors in water with the SSD set to 110 cm for the different applicators and the trapezoid cutout, for all energies.....55
Table 4.9: Summary of the 1D gamma analysis comparing computed and measured cross-plane profiles for different electron beam energies and 1D gamma analysis criteria, with the lung and Perspex offset to half of the field.....59
Table 4.10: Summary of the 1D gamma analysis comparing calculated and measured cross-plane profiles for different electron beam energies and 1D gamma analysis criteria at 100 cm SSD, with the lung-equivalent material positioned within field.....62

Table 4.11: Summary of the 1D gamma analysis comparing calculated and measured cross-plane profiles for different 1D gamma analysis criteria and beam energies, with POP and Perspex offset to half of the field. 65
Table 4.12: Summary of the 1D gamma analysis comparing calculated and measured cross-plane profiles for different beam energies and 1D gamma analysis criteria, with the POP material positioned within the field. 68
Table 4.13: Summary of the 1D gamma analysis comparing measured and computed PDDs for different grid spacings and beam energies. 76
Table 4.14: Summary of the 1D gamma analysis comparing calculated and measured PDDs for different electron beam energies and number of histories. 79

Acronyms

AAMP	American Association of Physicist in Medicine
CMJAH	Charlotte Maxeke Johannesburg Academic Hospital
CT	Computed tomography
DTA	Distance to agreement
eMC	electron Monte Carlo
LINAC	Linear accelerator
IAEA	International Atomic Energy Agency
MMC	Macro Monte Carlo
MPPG	Medical Physics Practice Guideline
MC	Monte Carlo
MLC	Multileaf collimator
PDD	Percentage depth dose
SDD	Source-to-detector distance
SSD	Source-to-surface distance
STOPS	Simultaneous-Transport-Of-Particle
TPS	Treatment Planning System
VMC	Voxel Monte Carlo

Table of contents

Declaration.....ii
Abstract..... iii
Dedication.....iv
Acknowledgements.....v
List of figures.....vi
Acronyms.....xii
1. Introduction.....1
1.1. Background.....1
1.2. Problem Statement.....1
1.3. Motivation of the study.....1
1.4. Aims and Objectives.....3
1.5. Report Structure.....3
2. Theoretical Background and Literature Review.....5
2.1. Electron interaction with matter.....5
2.2. Properties of electron Beams.....5
2.2.1. Percentage Depth dose curves.....5
2.2.2. Dose profile.....6
2.3. Applicators.....7
2.3.1. Irregular field.....7
2.4. Treatment planning.....8
2.4.1. Monaco Treatment planning system.....8
2.4.1.1. Coupled multi-source phase space.....8
2.4.1.2. Monte Carlo Method.....9
2.4.1.3. VMC++.....10
2.4.1.4. Input parameters of VMC++.....10
2.4.1.5. Advantages of VMC++.....11
2.5. Commissioning a dose calculation algorithm.....11
2.5.1. Commissioning beam data.....11
2.5.2. Validation test.....12
2.5.2.1. Model verification Test.....12
2.5.2.1.1. Output factor.....12
2.5.2.2. Heterogeneity test.....13
2.5.2.3. Oblique incidence test.....13
2.5.3. One Dimensional gamma.....13

3. Methodology and Materials 15
3.2. Commissioning Beam Data 15
3.2.1. Beam data collection 16
3.2.1.1. In-water measurements 16
3.2.1.2. In air measurements 17
3.3. Validation Test 18
3.3.1. Model verification 18
3.3.2. Heterogeneity test 20
3.3.3. Oblique incidence test 24
3.4. Input parameters 24
4. Results 25
4.1. Comparison of beam data 25
4.2. Validation Tests 39
4.2.1. Model verification 39
4.2.2. Heterogeneity test 56
4.2.3. Oblique incidence test 68
4.3. Input parameters 73
5. Discussion 80
6. Conclusion 85
References 86
APPENDIX 90

1. Introduction

1.1. Background

Accurate dose calculations in radiotherapy contribute to optimal treatment planning. An effective dose calculation algorithm strikes a balance between efficiency and accuracy (Gardner, 2005). Monte Carlo (MC) techniques, which model radiation transport from first principles, have been widely adopted for treatment planning of clinical electron beams. These techniques are generally regarded as more accurate and efficient (Ali, et al., 2022; Huang, et al., 2019; Reynaert, et al., 2006; Snyder, et al., 2019). Before clinical deployment, it is essential to commission and validate the dose calculation algorithms of treatment planning systems (TPS) to guarantee the accurate administration of therapeutic doses. This study aims to validate the electron Monte Carlo (eMC) algorithm integrated into the Monaco TPS (version 6.1.2) at Charlotte Maxeke Johannesburg Academic Hospital (CMJAH).

1.2. Problem Statement

The electron beam therapy planning process at CMJAH traditionally and currently relies on manual techniques, utilizing lookup tables to select beam energy and clinical output factors for dose rate calculations. In the manual technique, aids (devices) are manufactured to homogenize dose to the treatment volume (Khan, 2014). However, an individualized graphical representation of the treatment is not recorded. The lack of individualized graphical treatment plans and reliance on manual corrections limit versatility in treatment and may lead to greater dosimetric uncertainty.

1.3. Motivation of the study

Guidance on dose accuracy in radiotherapy is outlined by the American Association of Physicists in Medicine (AAPM) and the International Atomic Energy Agency (Human Health series No.31) (AAPM, 1994; AAPM, 2004; Huq, et al., 2015). The AAPM Report No. 85 from Task Group 65 (Huq, et al., 2015) emphasizes the uncertainties in treatment planning, indicating that a 5% dose deviation may result in tumor control probability changes ranging from 10% to 20%. Utilizing a dose computation engine like eMC can help reduce uncertainties in the delivered dose to within 3% (Pascal, et al., 2022; Reynaert, et al., 2006). Before the introduction of eMC algorithm in radiation oncology, the pencil beam algorithm, based on

small-angle multiple scattering and the Gaussian distribution, was the most advanced dose calculation algorithm (Khan, 2014; Podgorsak, 2005).

The pencil beam algorithm functions by modelling the fluence incident on the patient or medium as numerous small, narrow "pencil beams" (Carolan, 2010). To calculate the dose, the superposition technique is used. This technique involves segmenting the computation volume into uniformly sized voxels, where the precomputed dose values for each pencil beam kernel are mapped onto the corresponding voxel grid. To correct for inhomogeneities, scale factors are derived by adjusting the shape of the pre-calculated, teardrop-shaped dose kernels. For high-density materials, the dose kernel shrinks, whereas for low-density materials, the dose kernel elongates and widens to account for lower attenuation coefficient. These corrections are applied before the superposition technique is used for dose calculation. However, even with these corrections, the computed dose may still contain errors, particularly near complex tissue interfaces, because the algorithm neglects large-angle scattering (Carolan, 2010; Khan, 2014).

Unlike the pencil beam algorithm, the eMC algorithm employs stochastic sampling for radiation transport within a patient or medium. The eMC algorithm does not rely on pre-calculated dose kernels for dose calculation or dose kernel modifications to handle inhomogeneities. Instead, electrons are initially propagated through water, and the distance travelled by each electron is rescaled by the ratio of energy loss per unit path length in the voxel to that of water, enabling electron transport through a heterogeneous medium. To compute the dose, the distance travelled within the voxel is multiplied by the voxel's stopping power.

The AAPM Report No. 85 suggests that employing an accurate dose calculation algorithm reduces the uncertainty by 2.5% (AAPM, 2004). The eMC algorithm can reduce dose computation uncertainty to approximately 2% to 3%, regardless of beam obliquity or variations in tissue density (Reynaert, et al., 2006). Beyond accuracy, the eMC algorithm offers advantages similar to those of the pencil beam algorithm, including the direct prediction of monitor units, the display and identification of hot and cold spots during treatment planning and the assessment of ICRU volume coverage through Dose Volume Histograms (Fraass & James, 2003). Although the pencil beam algorithm provides some of these advantages, it falls short in accurately calculating dose distributions in heterogeneous media (Carolan, 2010; Chamberland, et al., 2015).

1.4. Aims and Objectives

This study aims to commission the Elekta Monaco eMC dose calculation algorithm (version 6.1.2). This will involve a systematic approach, starting with the collection of beam data under standard conditions, comprising output factors, profiles and percentage depth dose (PDD) curves, following the specifications outlined in the Elekta beam data document. Subsequently, the collected beam data will be compared to the existing CMJAH beam data utilizing a tolerance of two percent and overall comparability of one percent, as outlined in the AAPM Task Group-106 report (AAPM, 2008) and the AAPM Task Group-198 report (Li, et al., 2021). If the compared beam data demonstrate acceptable agreement, the beam model currently employed at CMJAH will be validated for further use, eliminating the need to send the collected beam data to Elekta for beam modeling. Three validation tests will be conducted to evaluate the ability of the algorithm to compute accurate output factors, profiles and PDDs under non-standard conditions.

These validation tests are the model verification for all applicators and an irregular cutout (a trapezoid was used in this study), evaluating oblique beam incidence and assessing dosimetric perturbations created by typical tissue heterogeneities. The eMC algorithm calculated dose distributions (PDDs and profiles) will be compared to measured dose distributions using one-dimensional gamma analysis. The tolerances used for these comparisons are obtained from the AAPM Medical Physics Practice Guideline (MPPG) 5a (Huq, et al., 2015) and the International Atomic Energy Agency Technical Reports Series No.430 (IAEA, 2004). Conducting these tests is essential to ensure the system can accurately compute dose distributions across various clinical scenarios. (Huq, et al., 2015) (IAEA, 2004).

To this end, the study includes:

- Measurement of beam data to be used for beam modelling.
- Verification and validation tests under standard and non-standard conditions.
- Investigation of the influence of eMC algorithm input parameters on the accuracy and efficiency of the algorithm in a homogeneous medium.

1.5. Report Structure

The report is structured to systematically address the objectives, methods and findings of the study.

Chapter one introduces the commissioning of dose computation algorithms, challenges encountered in manual planning, the motivation for commissioning the eMC algorithm and the aim of this study.

Chapter two reviews the background theory and literature, focusing on electron interactions, characteristics, the Monte Carlo technique, the eMC algorithm, input parameters and advantages, all discussed in detail.

Chapter three describes the methods and apparatus used to commission the eMC algorithm and investigate the associated limitations.

Chapter four presents the results obtained in this study.

Chapter five discusses the findings and compares them to results from previous studies, provides recommendations for future work and highlights the limitations of the study.

Chapter six concludes the study.

This structure ensures a systematic approach to commissioning the eMC algorithm and addressing the limitations associated with the algorithm.

2. Theoretical Background and Literature Review

This section covers electron interactions and properties, a description of the eMC algorithm, the process of commissioning the algorithm and the input parameters required.

2.1. Electron interaction with matter

When an electron beam passes through matter, it experiences a range of processes resulting from Coulomb interactions (Khan, 2014). These processes include inelastic and elastic interactions with atomic electrons and the atomic nucleus. In inelastic interactions, electrons lose energy through excitations, ionizations and bremsstrahlung production. Conversely, in elastic interactions, there is no loss of energy, but the energy is redistributed to particles emerging from the collision. Electron interaction with matter is influenced by the atomic number (Z) of the material being traversed and the energy of the electron beam. In low-Z materials like human tissue and water, inelastic collisions with atomic electrons are predominant, while in high-Z materials, bremsstrahlung production is dominant (Khan, 2014; Podgorsak, 2005). At low energies, the collisional losses (ionizations) are predominant. Conversely, at high energies, radiative losses through bremsstrahlung dominate.

2.2. Properties of electron Beams

2.2.1. Percentage Depth dose curves

The PDD curves illustrate the relationship between the relative dose and depth in water for a specified SSD, normalized at the depth of maximum dose along the central axis of an electron beam. These curves are obtained by measuring toward the surface using a detector with a small collection volume. Figure 2.1 displays a typical clinical electron beam PDD. There is a buildup region due to knock-on electrons, followed by the region of dose maximum (D_{max}). Beyond this D_{max}, a steep dose falloff occurs, followed by a bremsstrahlung tail.

Key regions of interest on a PDD curve include:

- Practical range (R_p): represents an intersection of a tangent drawn on the dose falloff region and the extrapolation of the bremsstrahlung tail.
- R_{90}**:** Represents the depth where the dose decreases to 90% of the peak dose in the falloff region.
- R_{80}: Represents the depth where the dose is 80% of the peak dose in the falloff region.

- R_{50}: Represents the depth where the dose reaches 50% of the peak dose.
- d_{max}: Represents the depth of maximum dose.

R_{90}, R_{85} and R_{80} are typically utilized for dose prescription, while R_{50} is utilized for estimating the beam quality (Amjad & Muhammad, 2017; Khan, 2014; Podgorsak, 2005).

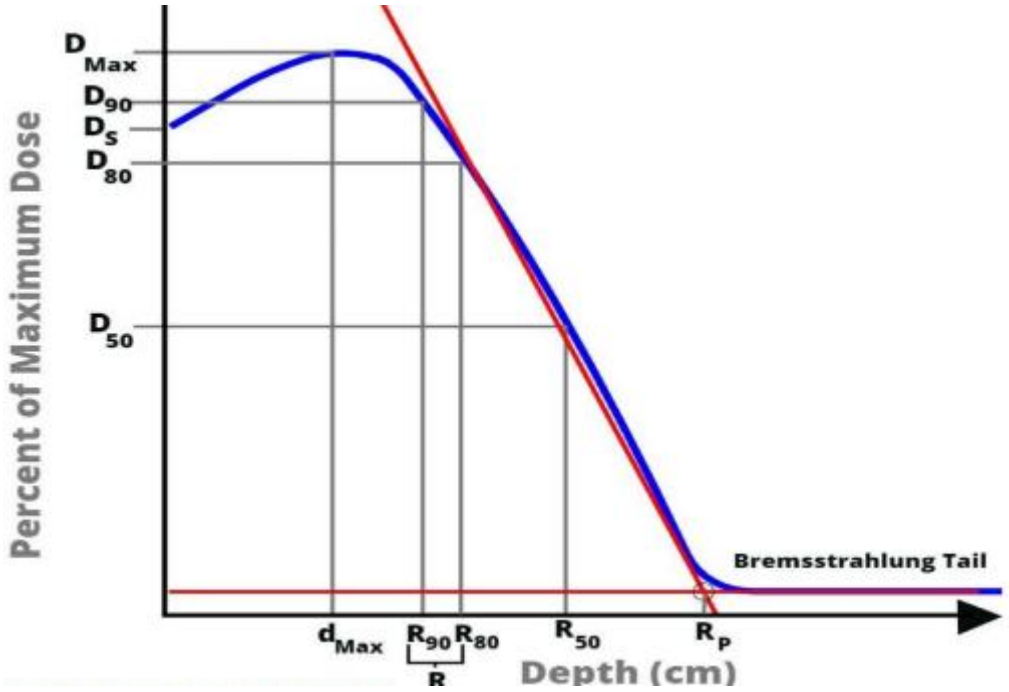

Figure 2.1: A typical PDD curve for a clinical electron beam illustrating key parameters such as d_{max}, R_{80}, R_{90}, R_{50} and R_p, which are critical for dose prescription, calibration and treatment planning. The blue curve represents the measured dose distribution, while the red curve highlights the bremsstrahlung tail and a gradient line passing through R_{50} (Oncology Medical Physics, 2020).

2.2.2. **Dose profile**

A dose profile indicates the relationship between the relative dose and the off-axis distance (Podgorsak, 2005). The dose profile features are the central region, penumbra and umbra region (see Figure 2.2). The penumbra defines a region located towards the periphery of an electron beam and the dose rate varies with the off-axis distance (Amestoy, 2015; Podgorsak, 2005). The umbra is located beyond the radiation field. In this region, the dose level is relatively low, as the dose results from indirect electrons that interacted with the linear accelerator (LINAC) head components and the applicator (Khan, 2014; Podgorsak, 2005).

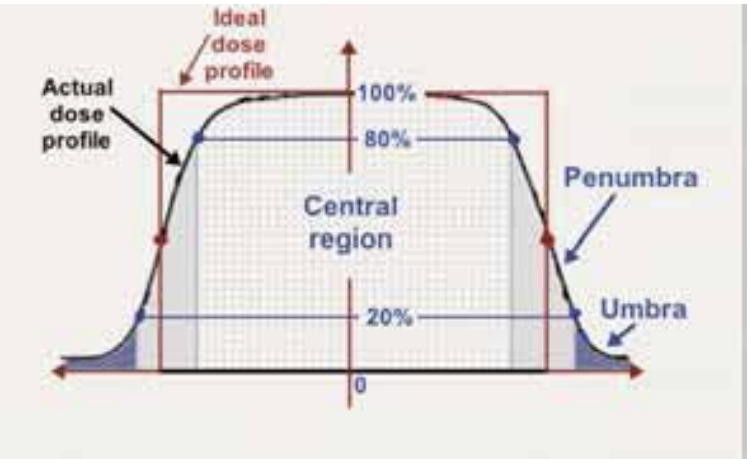

Figure 2.2: A general electron beam profile illustrating the penumbra, umbra and central region. The ideal dose profile demonstrates a theoretical uniform dose, while the actual dose profile reflects real-world deviations caused by internal scattering and beam collimation (Quizlet, 2023).

2.3. **Applicators**

Electron beams have a large geometrical spread due to Coulomb scattering and applicators are used to confine the beams to the therapeutic volume. These devices define the treatment field at the standard treatment SSD and are typically equipped with 2 to 4 scraper layers to enhance beam control and precision. Most applicators are designed to maintain a gap of 5 cm between the applicator endface and the patient at 100 cm SSD (Khan, 2014; Xing, 2007).

2.3.1. **Irregular field**

An irregular field is a radiation field that is not circular, square or rectangular (Podgorsak, 2005). In certain clinical scenarios, the square field shaped by the applicator insert does not provide sufficient shielding for organs at risk or normal tissues during treatment. In such cases, an irregularly shaped cutout is designed to conform the field to the treatment area while reducing dose to healthy tissues. These irregular cutouts are typically made from thin lead, and in some instances, a low-melting-point alloy is used, particularly for electron shielding. Irregular fields affect electron beam dosimetry, including PDDs and output factors (Khan, 2014; Podgorsak, 2005).

2.4. Treatment planning

The process of modelling and creating a graphical radiation delivery strategy to treat a patient's tumor while minimizing dose to healthy tissues is called treatment planning. During this procedure, beam angles and shapes are chosen to ensure the target region receives the required dose while minimizing exposure to surrounding healthy tissues. (Gardner, 2005). The TPS generates computed dose distributions based on beam information and patient information. Patient information is represented as a 3D electron density matrix obtained from computed tomography (CT) images.

2.4.1. Monaco Treatment planning system

As detailed in the Monaco training guide, the Monaco TPS is a template-based TPS that utilizes a coupled multi-source phase space along with voxel Monte Carlo (VMC++). VMC++ is employed to transport particles into the patient matrix obtained from the CT scan and calculate the dose.

2.4.1.1. Coupled multi-source phase space

A coupled multi-source phase space is the combination of the exit phase space and the source phase space (Huang, et al., 2019). This configuration has the advantage of giving the user full control of beam characterization. The source phase space is situated in an x-y plane distal to the secondary scattering foil within the LINAC treatment head, serving as a representation of a stream of particles with specific properties (Ding, et al., 2005; Huang, et al., 2019). Building blocks of the source phase space are the energy spectrum and 5 spatial parameters. Fluence components of the source phase space are direct electrons and bremsstrahlung photons. The source phase space is not influenced by the applicator (Ferretti, et al., 2014; Ding, et al., 2005).

The exit phase space between the ion chamber and the patient specific insert encompasses fluence components such as direct and indirect electrons, including bremsstrahlung photons. A coupled multi-source phase space integrates information regarding particle properties, including energy, position, weight, direction and more. This information is sampled by VMC++ during electron transportation and dose calculation (Huang, et al., 2019).

In electron mode, the Elekta Versa HD LINAC head is designed with a specific configuration. It begins with the entrance window, followed by the collimator (Pascal, et al., 2022). Below the collimator is the scattering foil assembly, which utilizes a dual-scattering foil technique

(Metcalfe, et al., 2007). The primary scattering foil, located at the top, is made of high-Z material, with a thickness varying between 0.05 mm and 0.4 mm. The secondary scattering foil, positioned below the primary foil, is made of low-Z material and has a thickness of less than 0.3 mm. The material and thickness of these scattering foils vary depending on the beam energy and is proprietary information. Below the scattering foils is the ionization chamber, followed by a multi-leaf collimator (MLC). The MLCs retracts in electron mode. In terms of how the Elekta Versa head is designed, the source phase space is independent of the secondary collimation and the applicator but depends on the primary collimation (Bedford, et al., 2022).

2.4.1.2. **Monte Carlo Method**

The MC method simulates particle transport within a specified geometry, with each initial particle transported through the defined geometry referred to as a "history". In this process, the computer makes several decisions regarding factors such as the distance to the particle's next interaction, the energy of the particle, the type of collision the particle will undergo and at what energy and angle the particle will exit the collision, based on a random number generator and the probability density function. Every random decision made by the computer is termed a sample (Gardner, 2005; Herwiningsih, 2017).

The computer first samples the initial position of each particle, as well as the direction and energy in the source phase space. In the second step, depending on the material the particle is propagated through, the path length to the next collision is sampled, and the voxel through which the collision will occur is noted. The particle history is terminated when particles leave the computational domain (Gardner, 2005).

Moving to the third step, the computer samples the type of collision experienced by the particle depending on the energy and type of material traversed by the particle. If the particle gets absorbed, the history is terminated; if the particle does not, the outgoing energy and direction are sampled. The energy of the outgoing particle should not be below the cut-off energy; if that is the case, the history of the particle is terminated (Herwiningsih, 2017). Any new particles generated from the collision are stored in a stack for future sampling.

In the fourth step, the computer scores the energy deposition in the voxel where the collision occurred. Steps two through three are repeated up to the point where the particle escapes the geometry or is absorbed by the material. The energy depositions of the existing history are added, and the total dose is computed by summing all history scores (Gardner, 2005).

2.4.1.3. **VMC++**

The VMC++ dose calculation algorithm used in the Monaco TPS for particle transport and dose calculation was developed by Iwan Kawrakow in 2000. The code was developed in C++ as an improved version of the previous VMC release. The code first transports electrons in a homogeneous medium (water) and then rescales the distance traversed in each voxel based on the voxel-dependent stopping power ratio to water, enabling transport through a heterogeneous medium. (Gardner, 2005; Kawrakow, et al., 1996). The rescaling of the path length ensures that the energy lost in the homogeneous medium is the same as in the heterogeneous medium. To determine the energy deposition in each voxel, the code multiplies the path length travelled by the electrons within the voxel by the voxel's stopping power. (Ferretti, et al., 2014; Gardner, 2005; Kawrakow & Fippel, 2000; Kawrakow, et al., 1996; Kawrakow, 2001).

2.4.1.4. **Input parameters of VMC++**

The accuracy of the eMC algorithm depends on three parameters: grid spacing (dose voxel size), statistical uncertainty and the number of histories (Chetty, et al., 2007; Reynaert, et al., 2006). In MC computations, the dose computational grid is divided into voxels of equal volumes. These voxels are referred to as grid spacing in the Monaco TPS. The grid spacing defines the volume in which dose computation occurs and directly impacts the accuracy of the computed dose (Ebert & Goodall, 2020).

Increasing the voxel size reduces statistical uncertainty and enhances the efficiency of the eMC algorithm. However, it may also introduce errors in the final computed dose. This is because electron beams have steep dose gradients, and larger voxels can prevent the algorithm from capturing the spatial details of the beam accurately. Additionally, larger voxel sizes result in the algorithm averaging over a larger volume, which can further contribute to errors in dose calculation. Conversely, decreasing voxel size improves spatial resolution but increases statistical uncertainty and the computation time. This is due to fewer particles entering each voxel, which reduces the sampling of particle interactions, energy, position and other relevant characteristics. Although increased statistical uncertainty can be a drawback, smaller voxel size enhances dose accuracy by providing better spatial resolution (Chetty, et al., 2007).

The level of noise in the final computed dose is influenced by statistical uncertainty, which depends on the effectiveness of particle sampling. The number of histories also affects dose accuracy; increasing the number of histories improves spatial resolution and decreases

statistical uncertainty. In the Monaco TPS, users can adjust the number of histories and the grid spacing but not the statistical uncertainty directly.

2.4.1.5. **Advantages of VMC++**

The VMC++ is accurate and efficient. In 2001, Iwan Kawrakow introduced a variance reduction technique aimed at reducing dose computation time. This technique, termed "STOPS" (Simultaneous Transport of Particle Sets), involves transporting a set of particles with identical energy but varying weights, positions and directions simultaneously (Jabbari, 2012). Unlike the traditional repetition variance reduction techniques used in VMC, where a single particle history is repeated, in STOPS, a set of particles is repeated (Gardner, 2005). This approach allows for the computation and sampling of material-dependent quantities, such as azimuthal scattering angles, maximum acceptable step length and interpolation indices, to be performed just once. Therefore, STOPS enhances the efficiency of VMC++ without compromising the accuracy of the algorithm.

2.5. **Commissioning a dose calculation algorithm**

Commissioning a TPS dose computation algorithm, as outlined in the AAPM MPPG 5a (Huq, et al., 2015), first requires collecting commissioning beam data and then performing verification followed by validation tests in non-standard geometries (Huq, et al., 2015; IAEA, 2006).

2.5.1. **Commissioning beam data**

Commissioning beam data is essential for institutional beam modelling (AAPM, 2008). Input data is comprised of both scanned (obtained utilizing a scanning system with a detector of small collection volume) and non-scanned data, depending on the vendor's recommendations. Characteristics of the machine, such as information about the position and thickness of jaws and MLCs, electron scraper layers, the location of primary and secondary scattering foil, applicator-specific jaw settings and energy, are obtained to simulate the LINAC beamline in order to generate the exit phase (Huang, et al., 2019).

Commissioning Monaco beam data for electrons, following vendor recommendations, involves collecting measurements in air and water. In-water data is categorized into two groups: with and without an applicator. Unlike photons, electron beams originate from a virtual source point rather than a physical source in the treatment head (Khan, 2014). As a result, the incident

electron beam energy spectrum is not directly modelled but is instead derived by incorporating the measured open-field depth dose curve (obtained in water without an applicator) into the eMC-simulated depth dose curves. Meanwhile, fluence profiles measured in air are optimized with simulated fluence profiles to determine the spatial and angular parameters of the source phase space (Huang, et al., 2019).

2.5.2. **Validation test**

Upon collecting, processing, validating and entering commissioning beam data into the Monaco TPS, the AAPM MPPG 5a recommends performing three validation tests: model verification, heterogeneity tests and oblique incidence tests. These tests are conducted to ensure that eMC calculates correct output factors and dose distributions in these relevant clinical scenarios (Huq, et al., 2015; IAEA, 2006; Huang, et al., 2019).

2.5.2.1. **Model verification Test**

The model verification test is a procedure used to determine output factors, PDDs and profiles for each applicator in water, employing standard and non-standard SSDs in clinical use (Huq, et al., 2015; Huang, et al., 2019)

2.5.2.1.1. Output factor

An output factor is a ratio of the absorbed dose per monitor unit ($\frac{D(d_{max},r_a,SSD_{ra})}{MU}$), measured at d_{max} on the central axis for a specified field size and treatment SSD, to the absorbed dose per monitor unit ($\frac{D(d_{max},r_0,SSD_{r0})}{MU}$) measured under reference calibration conditions (AAPM, 2009). In equation form, it is represented as:

$$S_e = \frac{\frac{D(d_{max},r_a,SSD_{r_a})}{MU}}{\frac{D(d_{max},r_0,SSD_{r_o})}{MU}} \qquad (2.1)$$

Where:

- **S_e**: Output factor for a specified field size and treatment SSD.
- $\boldsymbol{SSD_{r_a}}$ (cm): represents both standard and non-standard treatment SSD.
- **d_{max}** (cm): depth of maximum dose.
- $\boldsymbol{r_a}$ (cm^2): treatment field created by an applicator insert or cutout.
- $\boldsymbol{SSD_{r_o}}$(cm): standard treatment SSD (100 cm).

The change in the output factor of an electron beam is attributed to electron scattering between the electron source, inner wall of a collimator, applicator and patient tissue. (AAPM, 2009; Amjad & Muhammad, 2017). Extended SSD can be utilized in the clinical application of electron beams to ensure that the applicator does not collide with the patient during treatment (AAPM, 2009). Therefore, determining output factors at extended SSDs, using measurements and comparing to calculations by eMC algorithm, establishes whether the eMC algorithm can account for the effects of extended SSDs on the output factor value and the dose distribution.

2.5.2.2. **Heterogeneity test**

Tissue heterogeneity is defined as the difference in material density and atomic composition, such as lung, air cavity and bone (AAPM, 2009; Khan, 2014). Tissue heterogeneity affects the electron beam penetration and angular scattering power. In most clinical scenarios, scattering power has the most impact on the dose distribution (Khan, et al., 1991). The localized cold and hot spots are a result of the altered lateral scattering in the presence of localized small inhomogeneities (AAPM, 2009).

2.5.2.3. **Oblique incidence test**

Oblique beam incidence occurs when an electron beam irradiates tangentially to the patient's surface rather than perpendicularly. The tilt is often caused by surface irregularities, which can affect the electron dose distribution. When treating curved volumes, the dose distribution undergoes changes due to oblique incidence. An increase in the angle of beam incidence leads to several effects: a change in the penumbra, a decrease in d_{max} and R_{90} (IAEA, 2006; Khan, 2014). Consequently, an oblique incidence test is performed to determine whether the eMC algorithm can account for the effect of the tangential beam on the penumbra and PDD (Huq, et al., 2015).

2.5.3. **One Dimensional gamma**

A one-dimensional gamma analysis is a technique that compares measured and calculated dose distributions, point by point. This technique calculates the gamma index value at each point using the following formula:

$$\boldsymbol{\Gamma = min}\sqrt{\left(\frac{\boldsymbol{\Delta D}}{\boldsymbol{\delta D}}\right)^{\boldsymbol{2}} + \left(\frac{\boldsymbol{\Delta d}}{\boldsymbol{\delta d}}\right)^{\boldsymbol{2}}} \quad \textbf{(}2.3\textbf{)}$$

Where:

- $\Delta \boldsymbol{D}$ (%): The deviation between the corresponding measured and computed doses.
- $\Delta \boldsymbol{d}$ (mm): The difference between the positions of the measured and computed doses within the dose distribution.
- $\boldsymbol{\delta d}$ (mm): Distance-to-agreement tolerance.
- $\boldsymbol{\delta D}$ (%): Dose difference tolerance.

When the values for δD and δd, which define the gamma criteria are known, the gamma index can be calculated. If the gamma index is one or greater, the comparison does not meet the specified criteria (Duong, et al., 2023; Low, et al., 1998).

3. Methodology and Materials

3.1. Introduction

This section describes the apparatus and procedures used for acquiring beam data, conducting validation tests and evaluating input parameters that influence the performance of the eMC algorithm. The setups for data acquisition, including measurements of PDD curves, dose profiles and output factors, are outlined. These methods are designed to ensure the successful commissioning of the eMC algorithm for clinical use.

3.2. Commissioning Beam Data

The following is the description of the apparatus used for beam data collection as recommended by ELEKTA.

- Detector

  The ionization chamber selected for collecting beam data was the PTW Semiflex 31021 3D chamber. The PTW Semiflex 31021 has a nominal collection volume of 0.07 cc and is primarily utilized for reference and relative dose measurements. The PTW Semiflex 31021 was selected due to the small nominal collection volume, offering high spatial resolution, which is ideal for handling the steep gradients in electron beams.
- Water Phantom

  A PTW Beamscan automatic beam acquisition system with a water tank of 2500 cm^3 was utilized. The size of the tank allows scanning profiles across the maximum field size and provide a 5 cm extension on all four sides of the employed applicator.
- Beamscan software

  The PTW Beamscan software (version 4.4.78) was utilized to control the acquisition parameters of point dose measurements, depth ionization curves and profiles, as well as to display, process and analyze the measurements.
- Elekta HD versa LINAC.

  The Elekta HD Versa LINAC was employed to deliver 6 MeV, 9 MeV, 12 MeV and 15 MeV beams.
- Applicators

  Applicators of 6 cm x 6 cm, 10 cm x 10 cm, 14 cm x 14 cm, 20 cm x 20 cm and 25 cm x 25 cm, defined at the standard SSD of 100 cm, were employed. These applicators are

designed so that when attached to the LINAC, the gap between the applicator endface and the phantom or patient is 5 cm in order to achieve a setup of 100 cm SSD.

3.2.1. Beam data collection

Beam data were collected both in air and in water, with and without the applicator, in accordance with the Elekta document for electron beam data (refer to Appendix I).

3.2.1.1. In-water measurements

In-water measurements consisted of measurements in water with and without an applicator.

- With Applicator measurements

  Depth ionization curves for all five applicators attached to the treatment head were scanned at 100 cm SSD (see Table 3.1 for the initial depths). The depth ionization curves were measured up to 0.5 cm above the water surface, with a depth increment of 0.1 cm and a sample time of 0.5 seconds. The PTW Beamscan software was then utilized to convert the depth ionization curves into PDDs.

  Table 3.1: Initial depth for scanning depth ionization curves.

Energy (MeV)	Initial scan depth (cm)
6	5.5
9	7
12	12
15	15

  Beam and bremsstrahlung profiles were scanned for all five applicators at 100 cm SDD and at different scanning depths (see table 3.2). The scans extended 6 cm beyond the geometric field edge for both the beam and bremsstrahlung profiles, with the scan increment set to 0.1 cm.

Table 3.2: Scanning depth for beam profiles and bremsstrahlung profiles.

Energy (MeV)	Beam profiles scanning depth (cm)	Bremsstrahlung profiles scanning depth (cm)
6	1	5
9	2	15
12	2	15
15	2	15

- Without Applicator

  Only depth ionization curves were scanned without an applicator, as recommended by the vendor. These curves were scanned in water, with a maximum set field size of 40 cm × 40 cm at 100 cm SSD. The sample time, depth increment and initial scanning depth were the same as those used for the applicator measurements.

3.2.1.2. In air measurements

In-air measurements included scanning fluence profiles and acquiring the chamber "output factors". Elekta recommends scanning profiles at 70 cm and 90 cm source-to-detector distance (SDD). However, due to mechanical issues, specifically, the inability to achieve the 70 cm SDD since the tank control mechanism was colliding with the accelerator touch guard, the fluence profiles were acquired at 80 cm and 100 cm SDD. Refer to Figure 3.1 for setup.

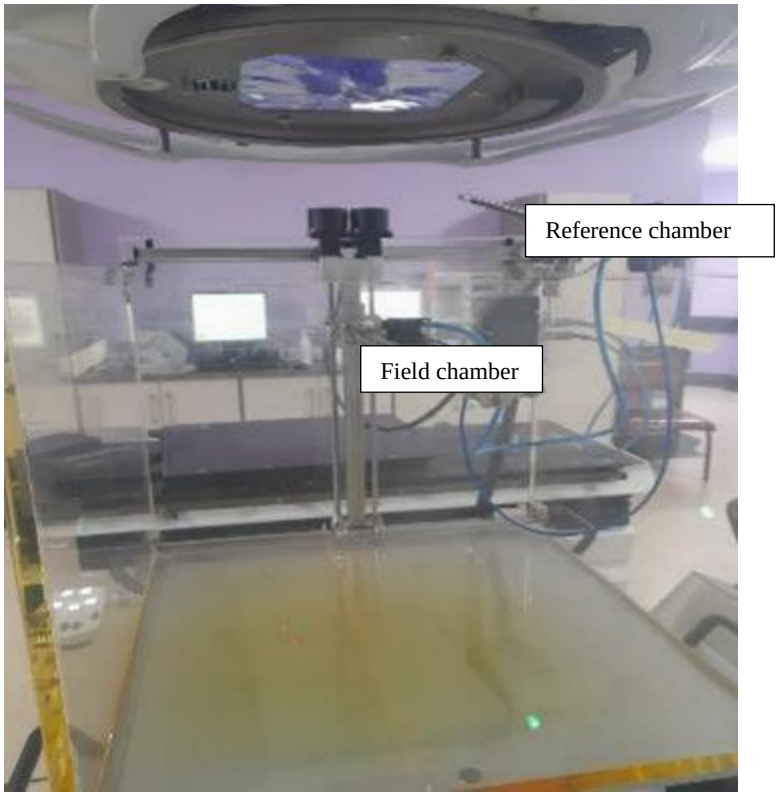

Figure 3.1: In-air measurement setup without an applicator, showing the PTW Semiflex 31021 placed at 80 cm SDD, and the reference chamber used to correct fluctuations in measurements taken by the field chamber.

The PTW Semiflex 31021 was placed at 80 cm and 100 cm SDD in an empty tank without a build cap. Fluence profile scans were acquired for 8 cm x 8 cm, 8 cm x 20 cm, 8 cm x 40 cm and 40 cm x 40 cm set field sizes. Scans were taken with a scan increment of 0.1 cm and a sample time of 0.5 seconds.

3.3. Validation Test

3.3.1. Model verification

A homogeneous phantom measuring 40 cm x 40 cm x 30 cm was created in the TPS, and the electron density was set to 1.00 to make the phantom water equivalent. Treatment plans were generated for 6 MeV, 9 MeV, 12 MeV and 15 MeV beams, utilizing all applicators used for beam data collection, along with the trapezoid cutout with non-parallel sides measuring 4 cm, a long base of 8 cm parallel to a shorter side of 6 cm. One hundred monitor units were delivered, and treatment plans were generated for defined SSDs of 110 cm and 100 cm.

The eMC algorithm was run with a 0.2 cm grid spacing and 500,000 histories for the 6 MeV beam, and with a 0.25 cm grid spacing and 500,000 histories for the 9 MeV beam. For calculations involving beam energies of 15 MeV and 12 MeV, a 0.3 cm grid spacing and 500,000 histories were used. After generating the treatment plans, points of interest were added within the computed dose distribution to construct PDD curves and profiles within the TPS (see Figure 3.3).

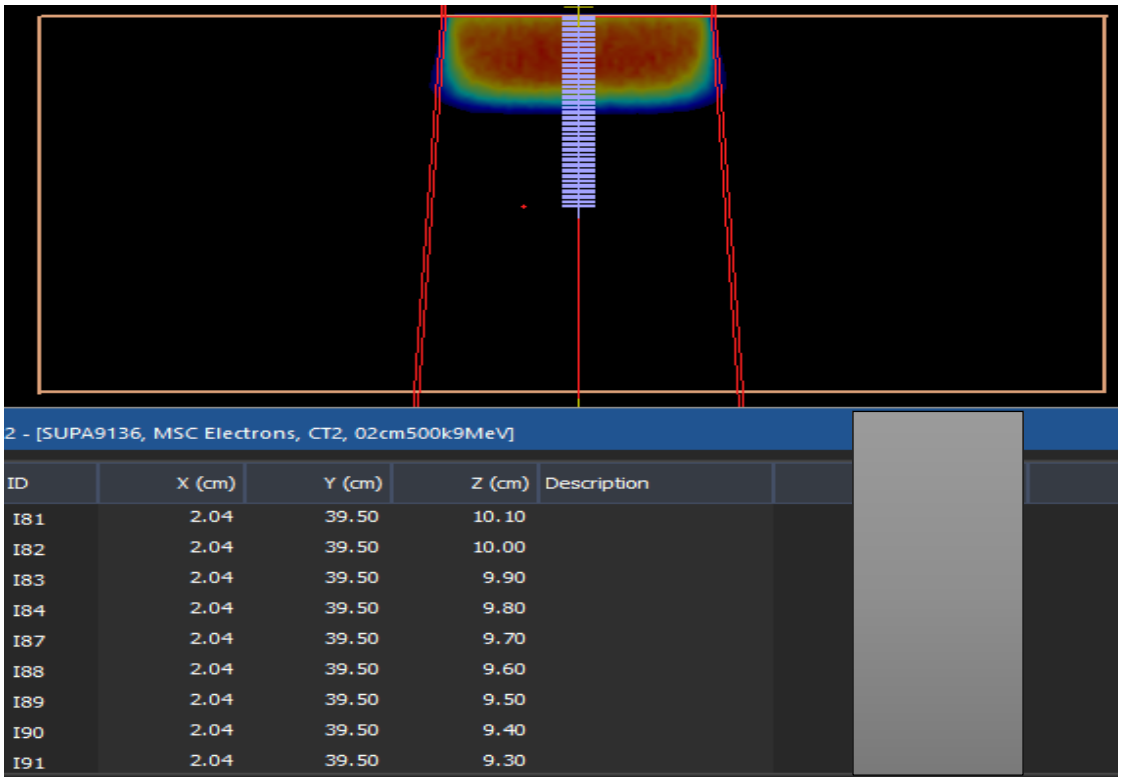

Figure 3.2: PDD generation using Monaco TPS.

A PTW Semiflex 31021 connected to the Beamscan software was utilized to scan the depth ionization curves and profiles. The tank was irradiated using an Elekta Versa HD LINAC. The depth increment for scanning PDDs was 1 mm, while the profile scan increment was also 1 mm. Profiles were scanned at R_{90} and R_{50} for both 100 cm and 110 cm SSDs. The trapezoid cutout, along with 14 cm × 14 cm and 6 cm × 6 cm applicators were used to confine the field for profile measurements. PDDs were scanned for all applicators used in this study.

Output factors

Output factors were measured using a PTW Semiflex 31021 at d_{max} for all electron beams. Measurements were taken for the trapezoid cutout and all applicators. These measurements were performed at 100 cm and 110 cm SDDs in water, with 100 monitor units delivered for

each setup. Output factors were then computed using the eMC algorithm in a homogeneous water-equivalent phantom under the same conditions as the measurements.

3.3.2. Heterogeneity test

Four phantoms were created to perform the heterogeneity test. The first phantom was designed to mimic lung tissue using low-density polystyrene with a relative electron density of 0.16. The polystyrene slab measured 15 cm in both width and length, with a thickness of 1.2 cm. The setup included a 1 cm thick Perspex buildup layer (water equivalent) and a 5 cm thick Perspex backscatter layer. The width and length of the Perspex were 30 cm (see Figure 3.3 for setup). For the 6 MeV setup with the lung-equivalent material, a 2 mm thick buildup layer was used instead of the 1 cm layer. The phantom was scanned with CT, with the PTW Octavius detector 1500 placed 2.2 cm below the low-density polystyrene, and the data was imported into the TPS.

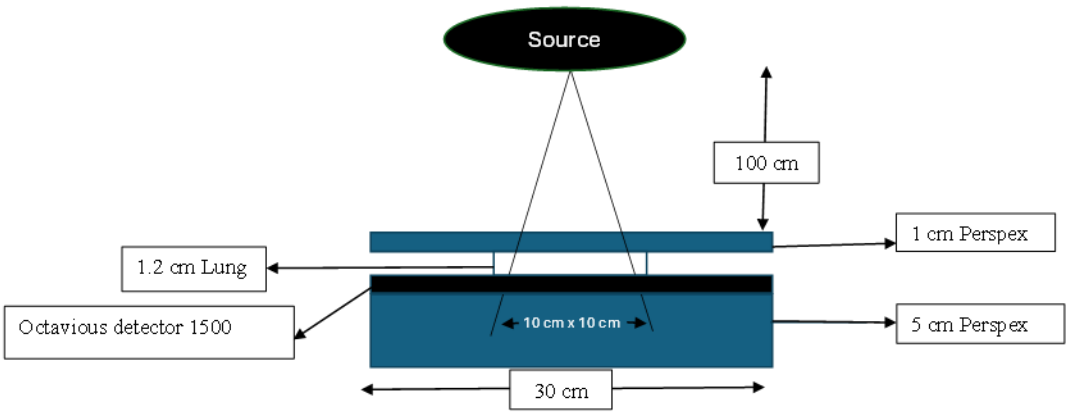

(a)

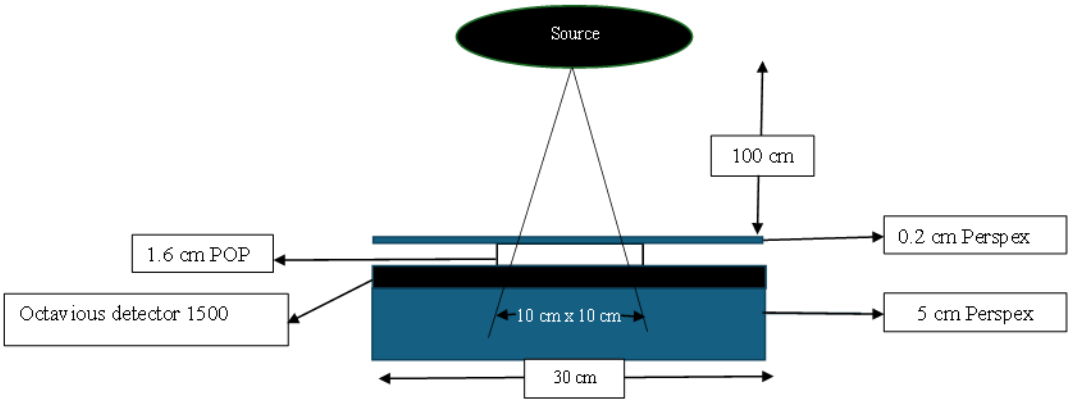

(b)

Figure 3.3: (a) Lung-equivalent setup at 100 cm SSD, with lung-equivalent material positioned within the 10 cm × 10 cm applicator-defined field. (b) Bone-equivalent setup at 100 cm SSD, with Plaster of Paris (POP) slab positioned within the 10 cm x 10 cm field.

A polystyrene slab was positioned within a 10 cm x 10 cm field. For both measurements and calculations, 250 monitor units were delivered. The eMC algorithm was run with a 0.2 cm grid spacing and 500,000 histories for all beam energies. The measured data were acquired using the PTW Octavius Detector 1500, which is a 2D array ionization chamber consisting of 1,405 plane-parallel chambers with a nominal collection volume of 0.06 cm^3. The dimensions of the

detector are 467 mm × 300 mm × 22 mm. The Octavius detector 1500 has an effective point of measurement situated 5 mm beneath the outer layer of the chamber housing, and acquisitions are transferred and processed using PTW VeriSoft software (version 7.2.0.68). The phantom was irradiated using an Elekta Versa HD LINAC, with the detector positioned at 2.2 cm.

The second phantom was designed to mimic a bone inhomogeneity. The phantom consisted of a solid Plaster of Paris (POP) slab with a relative electron density of 1.42, measuring 15 cm in both length and width, and 1.6 cm thick, sandwiched between a 0.2 cm thick buildup layer and a 5 cm thick backscatter layer made of Perspex. Both the width and length of the buildup and backscatter layers were 30 cm. The Octavious detector 1500 was positioned at 1.8 cm, as shown in Figure 3.4b. The setup and input parameters were identical to those used for the first phantom. Treatment plans were generated for 15 MeV,12 MeV and 9 MeV.

The third and fourth phantoms were similar to the first and second but with a different setup. In these phantoms, POP and low-density polystyrene slabs were offset to half of the field, respectively. Additionally, 1.2 cm and 1.6 cm thick Perspex layers were positioned lateral to the heterogeneity, respectively as shown in Figures 3.5a and 3.5b. All other set-up parameters were identical to those of the first and second phantoms. The four phantoms were CT scanned.

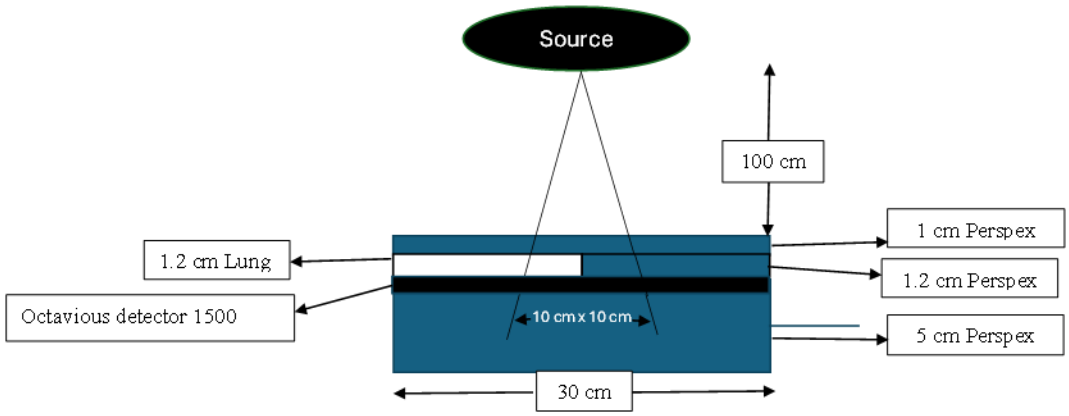

(a)

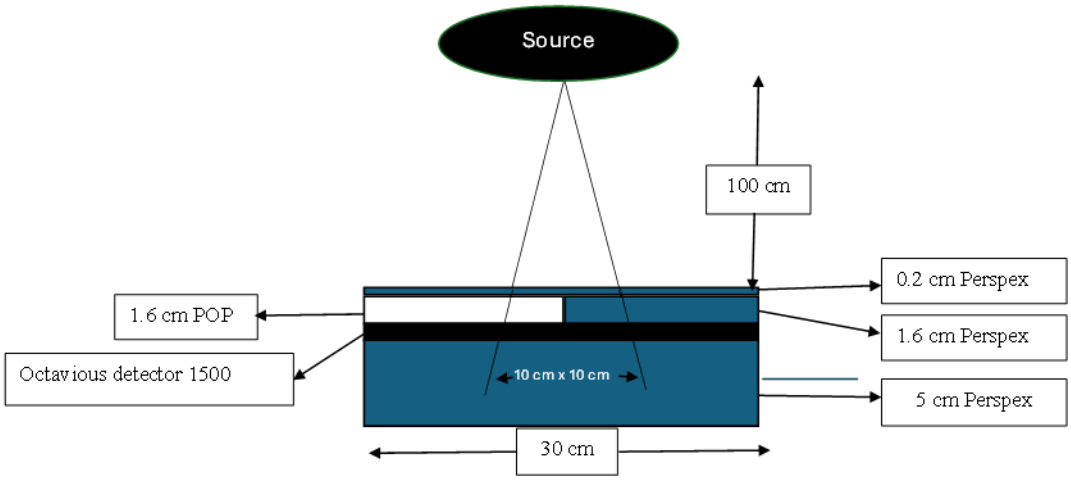

(b)

Figure 3.4:(a) Lateral lung-equivalent setup: The lung-equivalent material and Perspex are offset to half of the field, creating an interface along the in-plane axis with the SSD set to 100 cm.(b) Lateral bone-equivalent setup: The POP and Perspex are offset to half of the field (10 cm × 10 cm) , similarly creating an interface along the in-plane axis with the SSD set to 100 cm.

A different phantom was created to conduct the 6 MeV test using a bone-equivalent inhomogeneity. A POP slab with a thickness of 0.8 cm was used instead of the 1.6 cm slab

used for the other energies, as the latter resulted in complete attenuation. A 2 mm thick Perspex buildup layer and a 5 cm thick backscatter layer were employed. All heterogeneity tests were performed at 100 cm.

3.3.3. Oblique incidence test

A homogeneous water-equivalent phantom generated using the Monaco TPS was utilised to simulate cross-plane profiles and PDDs for the oblique incidence test. The gantry angle was set to 20°, and an applicator sized 10 cm × 10 cm was employed to confine the field. The eMC algorithm was run with a 0.2 cm grid spacing and 500,000 histories for the 6 MeV beam. The algorithm was then run with a 0.25 cm grid spacing and 500,000 histories for the 9 MeV beam. The grid spacing of 0.3 cm and 500,000 histories was utilized for 12 MeV and 15 MeV energies. Cross-plane profiles were generated by inserting interest points at R_{90}. Cross-plane profiles and PDDs were measured using the PTW Semiflex 31021. The scan increment for profiles and the depth increment for PDDs were both set to 1 mm. The SSD was set to 100 cm.

3.4. Input parameters

The grid spacing in the Monaco TPS ranges from 0.1 cm to 0.8 cm. To generate PDDs using the eMC algorithm, the grid spacing was varied in increments of 0.1 cm while maintaining a constant number of histories at 500,000. Depth ionization curves were scanned under the same conditions using a PTW Semiflex 31021 and converted to PDDs for comparison with the calculated PDDs. To assess how the number of histories affects the eMC algorithm in computing accurate dose distributions, the number of histories was varied from 50,000 to 1 million in increments of 100,000, with the grid spacing set to 0.2 cm. For both tests, PDDs were computed for all energies employing an applicator sized 10 cm × 10 cm to confine the field. The eMC-generated PDDs were then compared to the PDDs measured with the PTW Semiflex 31021. Measurements and calculations were conducted in water at 100 cm SSD.

4. Results

This section of the study outlines the results obtained from the verification of the CMJAH beam data, validation tests and the effect of varying input parameters on the calculations. All PDDs in this study were normalized at d_{max} and all profiles were normalized to the central axis before comparison using 1D gamma analysis.

4.1. Comparison of beam data

The measured electron beam data were compared to the CMJAH data, with a total of 96 profiles and PDDs analyzed. This comparison excluded absolute dose and output factors measured in air. A 1D gamma analysis technique with 2%/2 mm criterion was applied, yielding an overall agreement of 98.9%. The SSD was set to 100 cm for all measurements. Figure 4.1(a) to (d) presents a comparison between measured and CMJAH PDDs in water for 6 MeV, 9 MeV, 12 MeV and 15 MeV beams, employing an applicator sized 10 cm × 10 cm to confine the field. Figure 4.2(a) to (d) compare CMJAH and measured cross-plane profiles in water under the same applicator as Figure 4.1. Measurements were performed at depths of 1 cm and 2 cm, depending on the energy. Additionally, Figure 4.3(a) to (d) compare measured and CMJAH bremsstrahlung cross-plane profiles in water, using the same applicator. The bremsstrahlung profiles were measured at depths of 5 cm and 15 cm, depending on the beam energy. Beam data for applicators sized 6 cm × 6 cm, 14 cm × 14 cm, 20 cm × 20 cm and 25 cm × 25 cm were also analyzed and found to be consistent with the CMJAH data, though these results are not reproduced here.

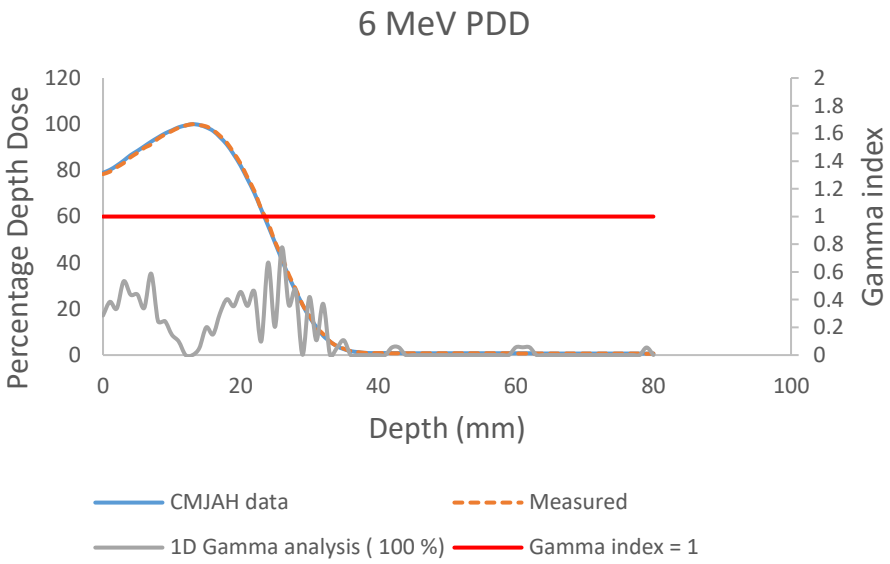
6 MeV PDD
Percentage Depth Dose
Gamma index
Depth (mm)
CMJAH data
Measured
1D Gamma analysis (100 %)
Gamma index = 1

(a)

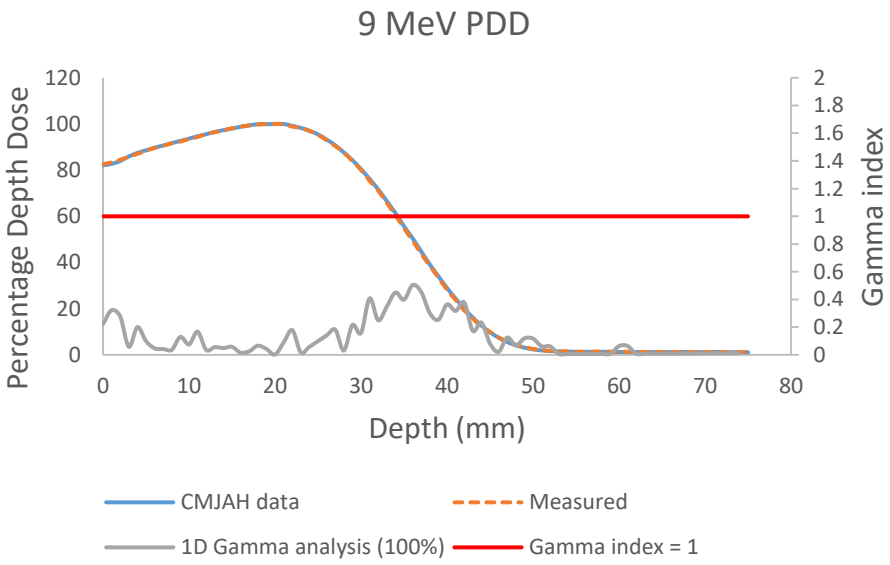
9 MeV PDD
Percentage Depth Dose
Gamma index
Depth (mm)
CMJAH data
Measured
1D Gamma analysis (100%)
Gamma index = 1

(b)

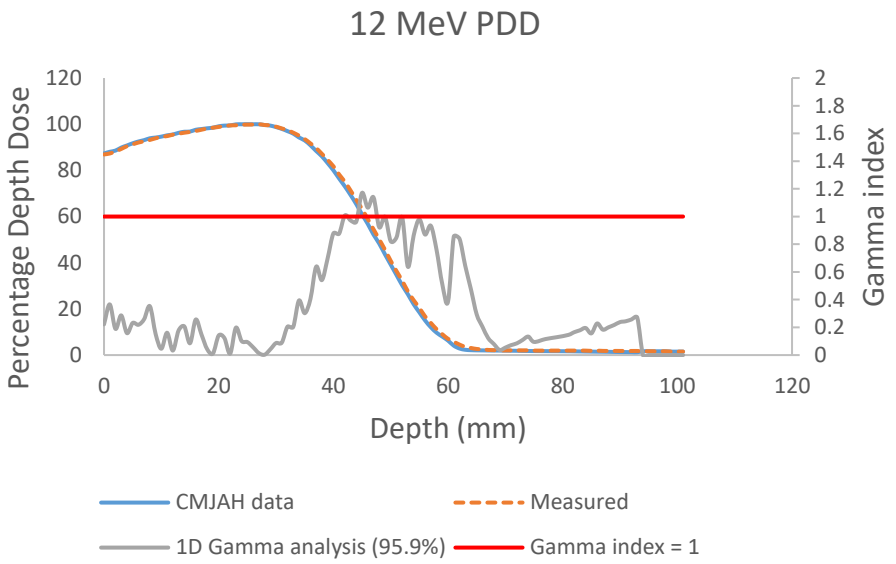

(c)

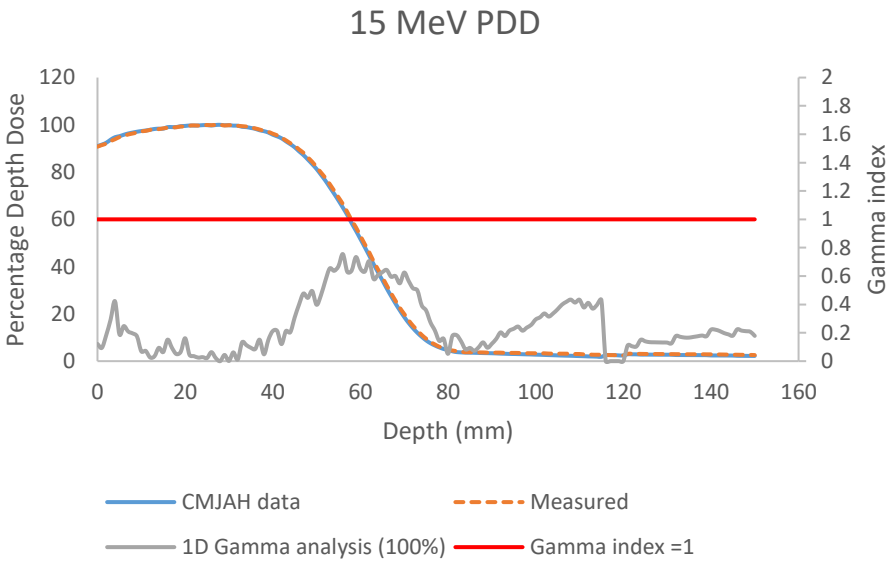

(d)

Figure 4.1: Comparison of CMJAH and measured PDDs in water, employing an applicator sized 10 cm x 10 cm to confine the field, indicating the percentage difference obtained from 1D gamma analysis. (a) 6 MeV PDD. (b) 9 MeV PDD. (c) 12 MeV PDD. (d) 15 MeV PDD.

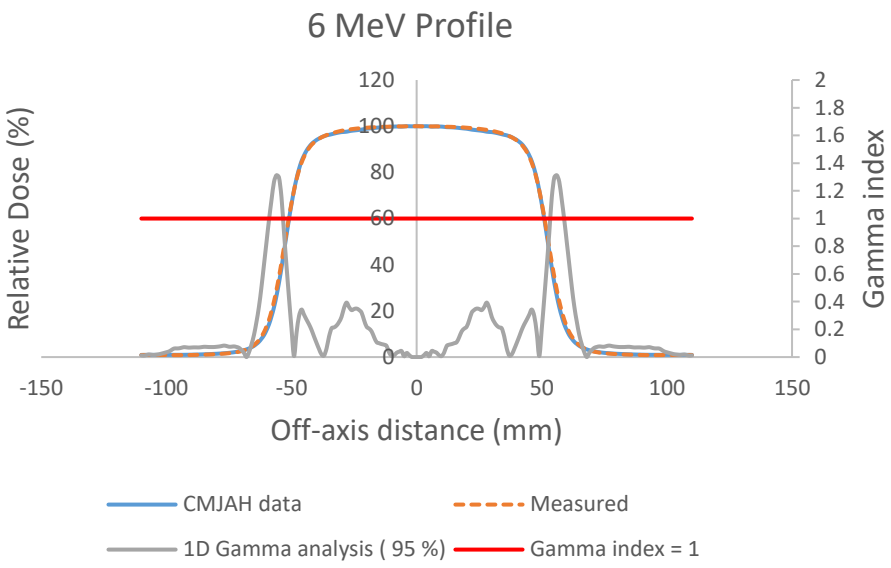
6 MeV Profile
Relative Dose (%)
Gamma index
Off-axis distance (mm)
120
100
80
60
40
20
0
2
1.8
1.6
1.4
1.2
1
0.8
0.6
0.4
0.2
0
-150
-100
-50
0
50
100
150
CMJAH data
Measured
1D Gamma analysis (95 %)
Gamma index = 1

(a)

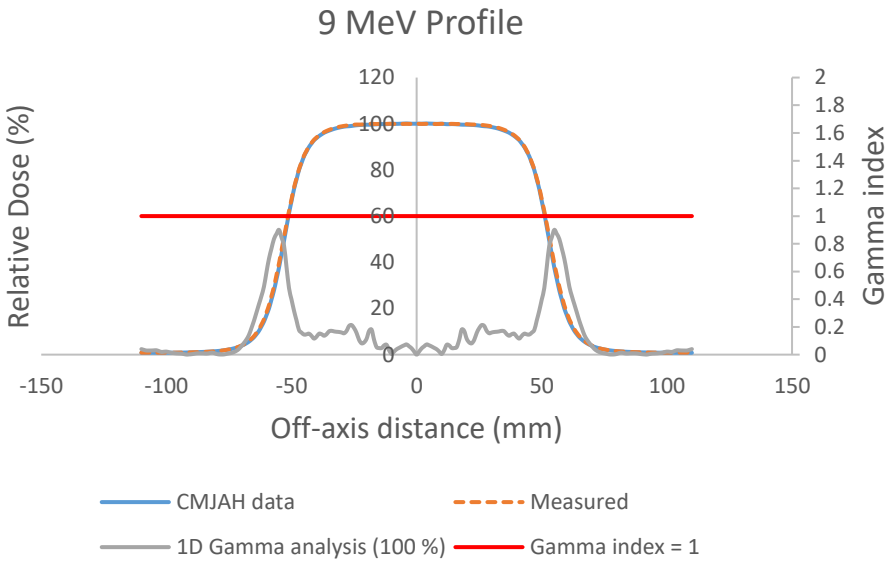
9 MeV Profile
Relative Dose (%)
Gamma index
Off-axis distance (mm)
120
100
80
60
40
20
0
2
1.8
1.6
1.4
1.2
1
0.8
0.6
0.4
0.2
0
-150
-100
-50
0
50
100
150
CMJAH data
Measured
1D Gamma analysis (100 %)
Gamma index = 1

(b)

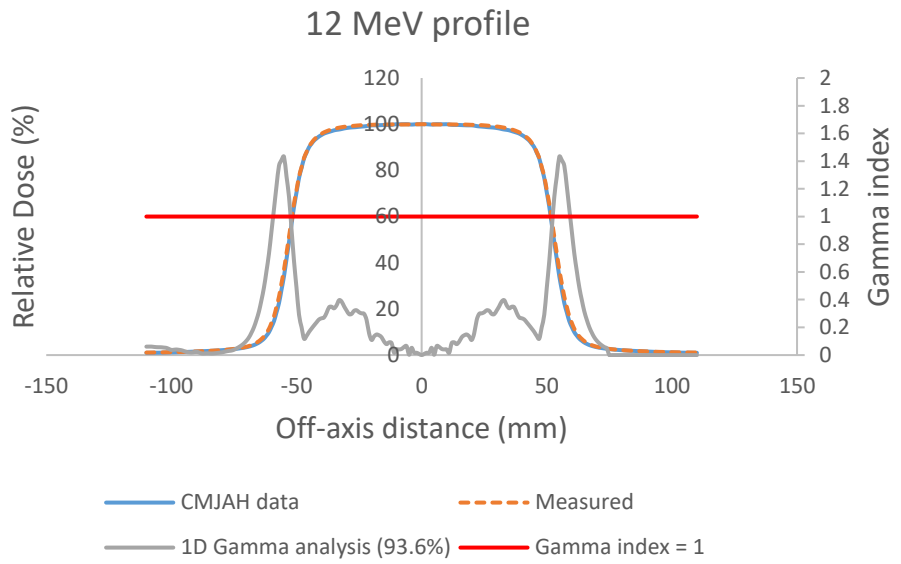

(c)

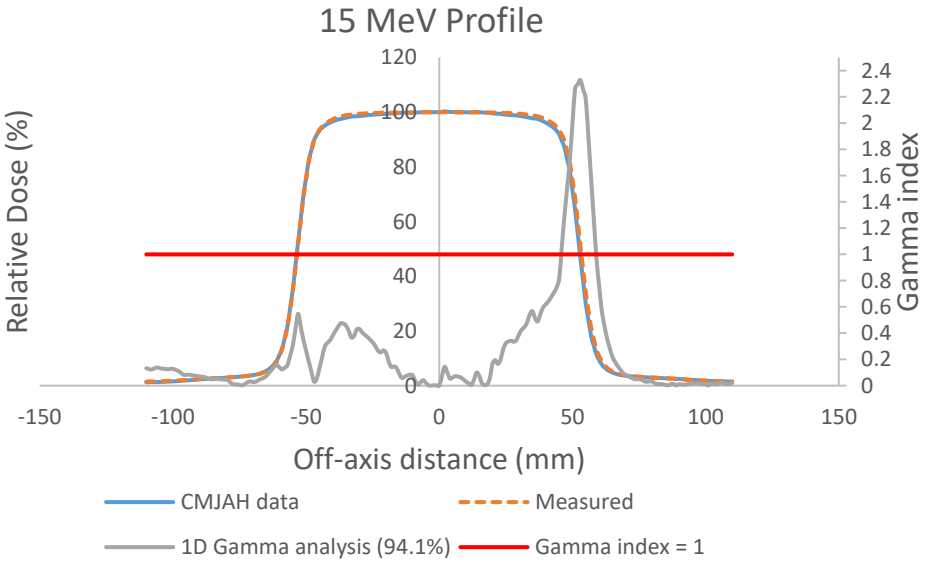

(d)

Figure 4.2: Cross-plane profiles in water for an applicator sized 10 cm x 10 cm, indicating the percentage difference obtained from 1D gamma analysis comparing measured and CMJAH profiles. The data are normalized to the central axis dose. (a) 6 MeV profile measured at 1 cm depth. (b) 9 MeV profile measured at 2 cm depth. (c) 12 MeV profile measured at 2 cm depth. (d) 15 MeV profile measured at 2 cm depth.

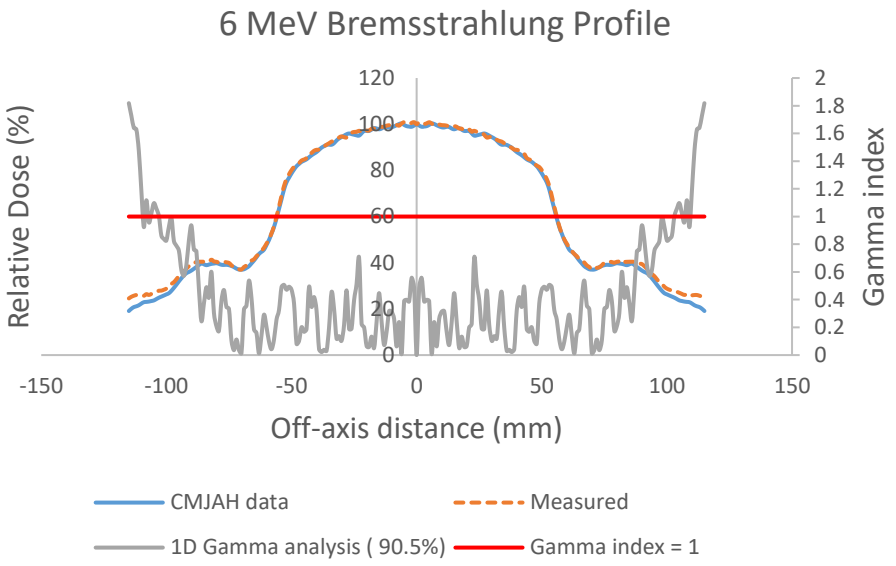
6 MeV Bremsstrahlung Profile
Relative Dose (%)
Gamma index
Off-axis distance (mm)
120
100
80
60
40
20
0
2
1.8
1.6
1.4
1.2
1
0.8
0.6
0.4
0.2
0
-150
-100
-50
0
50
100
150
CMJAH data
Measured
1D Gamma analysis (90.5%)
Gamma index = 1

(a)

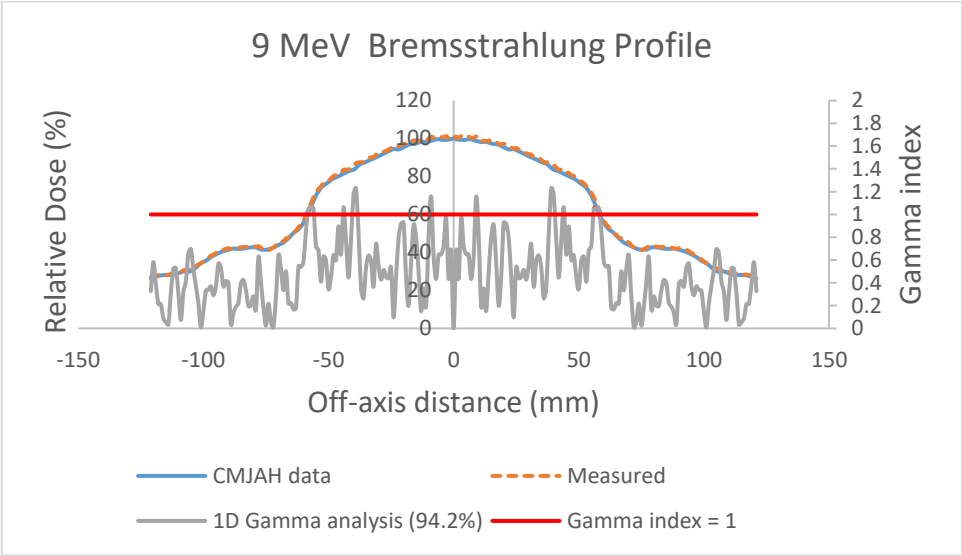
9 MeV Bremsstrahlung Profile
Relative Dose (%)
Gamma index
Off-axis distance (mm)
120
100
80
60
40
20
0
2
1.8
1.6
1.4
1.2
1
0.8
0.6
0.4
0.2
0
-150
-100
-50
0
50
100
150
CMJAH data
Measured
1D Gamma analysis (94.2%)
Gamma index = 1

(b)

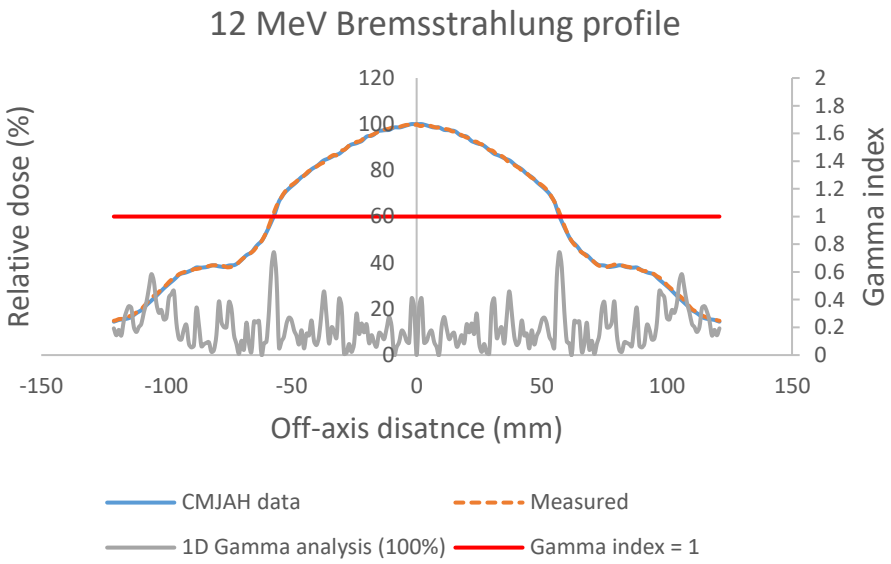

(c)

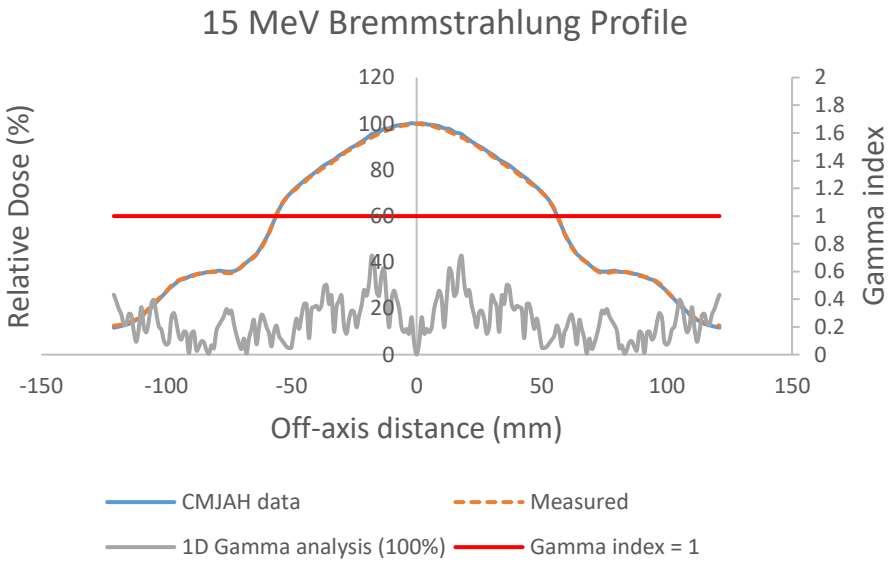

(d)

Figure 4.3: Cross-plane bremsstrahlung profiles in water for an applicator sized 10 cm x 10 cm, indicating the percentage difference obtained from 1D gamma analysis by comparing measured and CMJAH profiles. The data are normalized to the central axis dose. (a) 6 MeV bremsstrahlung profile measured at 5 cm depth. (b) 9 MeV bremsstrahlung profile measured at 15 cm depth. (c) 12 MeV profile measured at 15 cm depth. (d) 15 MeV bremsstrahlung profile measured at 15 cm depth.

Figure 4.4(a) to (d) compare CMJAH and measured PDDs obtained in water without an applicator for 6 MeV, 9 MeV, 12 MeV and 15 MeV beams, with a 40 cm × 40 cm set field size. The compared beam data met the 2%/2 mm criterion.

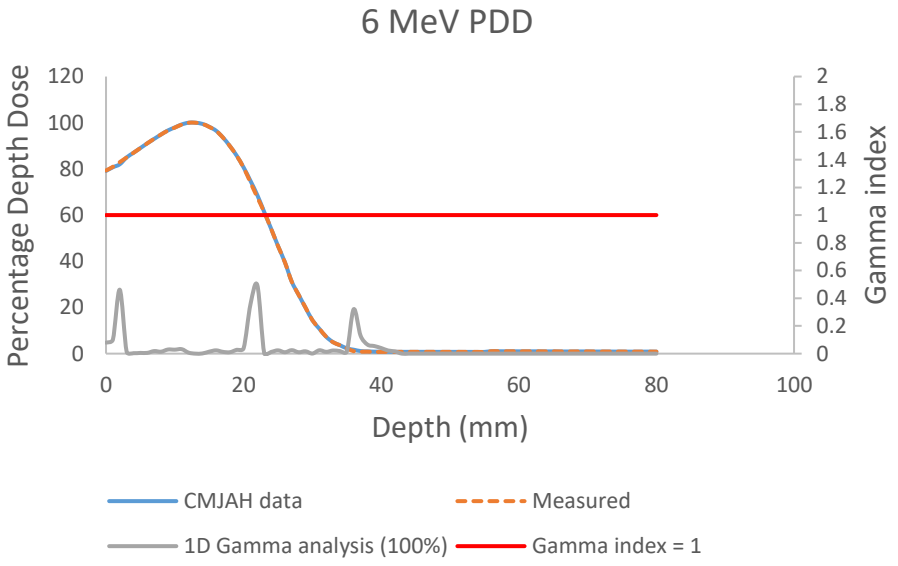

(a)

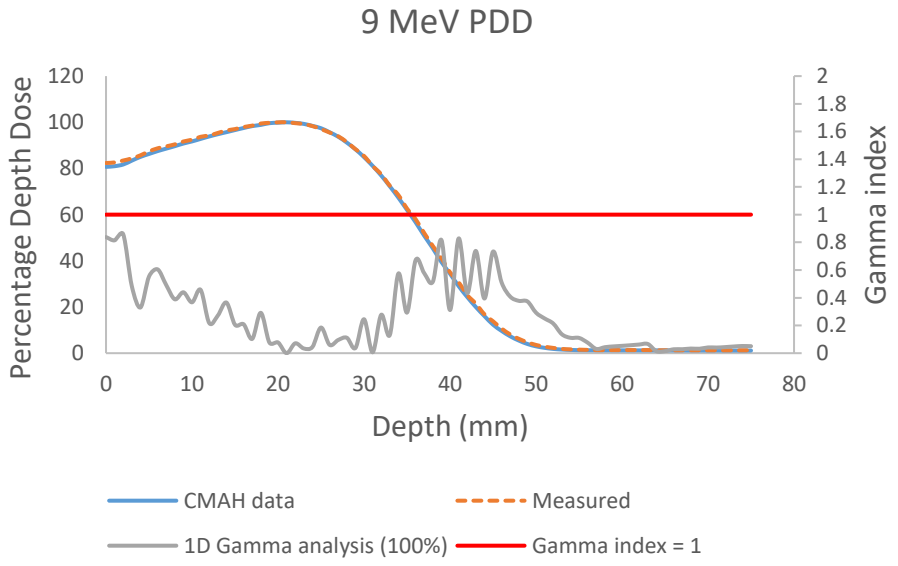

(b)

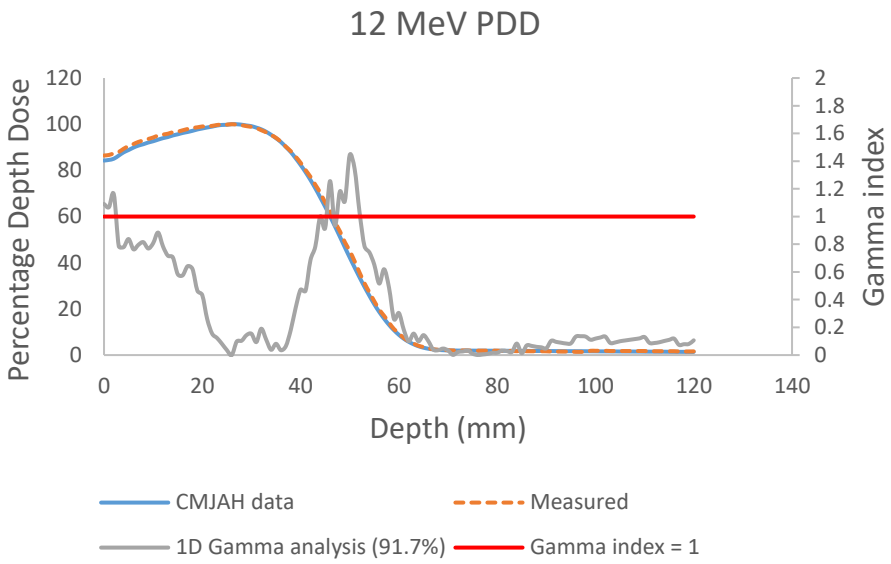

(c)

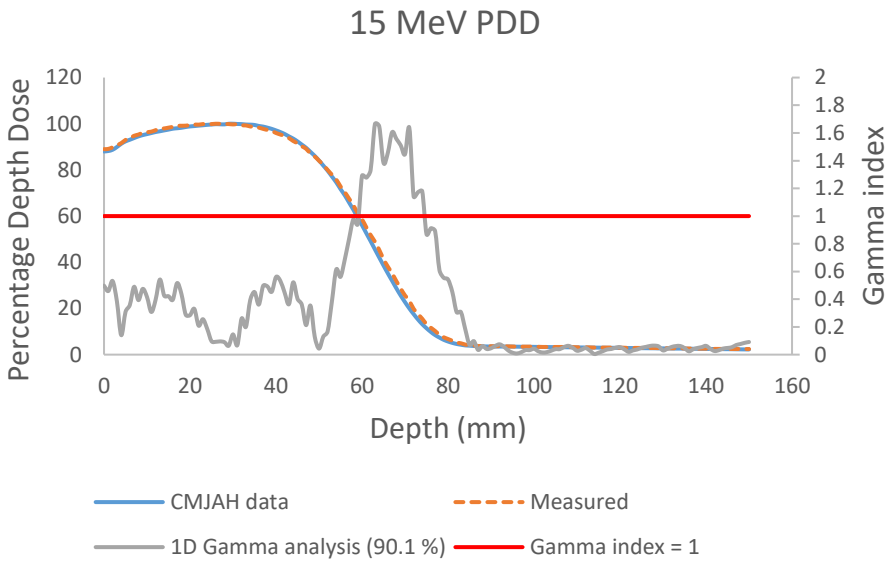

(d)

Figure 4.4: A comparison of CMJAH and measured PDDs in water, for the 40 cm × 40 cm set field size, indicating the percentage difference from 1D gamma analysis. (a) 6 MeV PDD. (b) 9 MeV PDD. (c) 12 MeV PDD. (d) 15 MeV PDD.

Figure 4.5(a) to (d) presents a comparison of cross-plane profiles in air between CMJAH and measured profiles without an applicator at 100 cm SDD, utilizing a set field size of 8 cm × 8 cm for all energies. The compared profiles were within the 2%/2 mm criterion. The comparison also included profiles obtained for 8 cm × 20 cm, 8 cm × 40 cm and 40 cm × 40 cm set field

sizes, all of which agreed within 2%/2 mm with the CMJAH in-air cross-plane profiles. Figure 4.6(a) to (d) show the comparison of cross-plane profiles between measured and CMJAH in-air fluence profiles without an applicator at 80 cm SDD for a 40 cm × 40 cm set field size. The 6 MeV, 9 MeV and 12 MeV measured profiles matched the CMJAH profiles, except for the 15 MeV profile, in which 88.7% of the compared relative dose points were within the 2%/2 mm criterion. The maximum deviation of 4% occurred at the arms or periphery of the 15 MeV profile and near the central axis. The 8 cm x 40 cm, 8 cm x 20 cm and 8 cm x 8 cm profile comparisons at 80 cm SDD were all consistent with the CMJAH profiles.

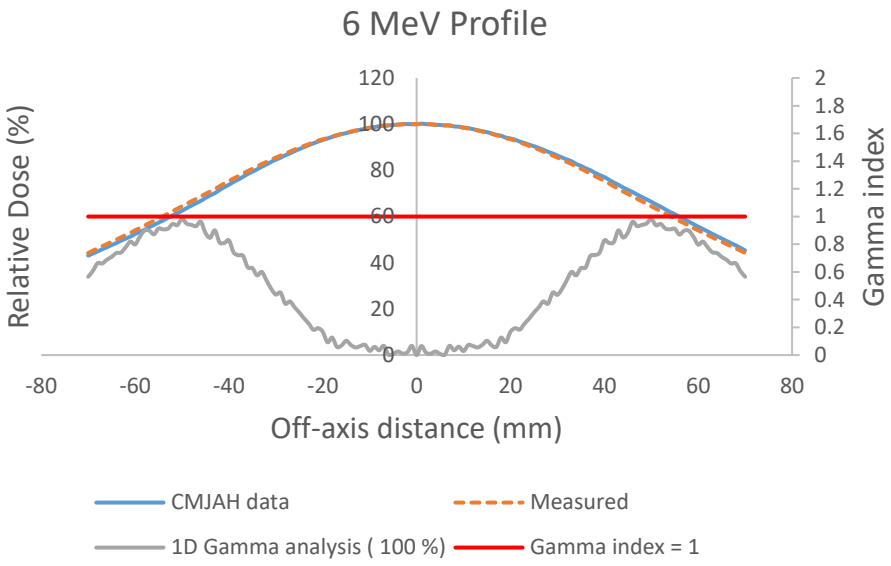
6 MeV Profile
Relative Dose (%)
Gamma index
Off-axis distance (mm)
120
100
80
60
40
20
0
2
1.8
1.6
1.4
1.2
1
0.8
0.6
0.4
0.2
0
-80
-60
-40
-20
0
20
40
60
80
CMJAH data
Measured
1D Gamma analysis (100 %)
Gamma index = 1

(a)

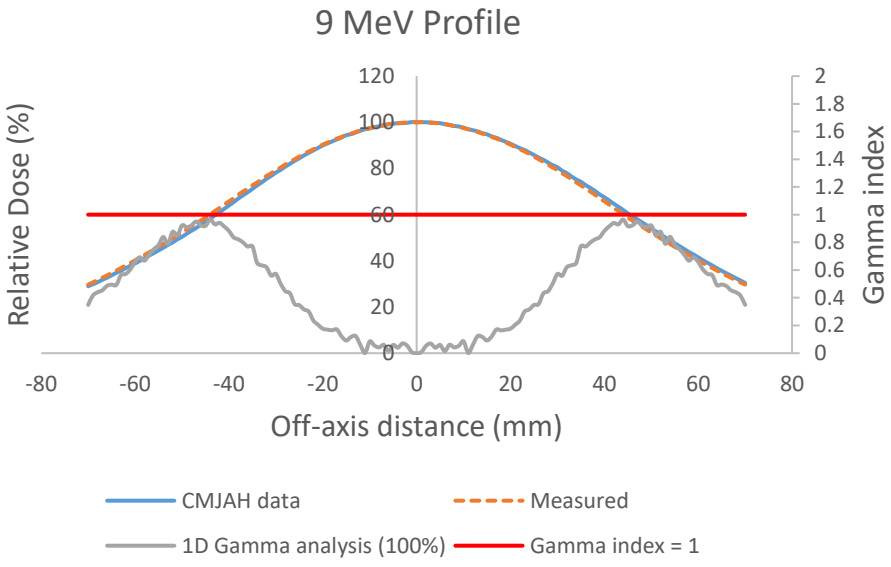
9 MeV Profile
Relative Dose (%)
Gamma index
Off-axis distance (mm)
120
100
80
60
40
20
0
2
1.8
1.6
1.4
1.2
1
0.8
0.6
0.4
0.2
0
-80
-60
-40
-20
0
20
40
60
80
CMJAH data
Measured
1D Gamma analysis (100%)
Gamma index = 1

(b)

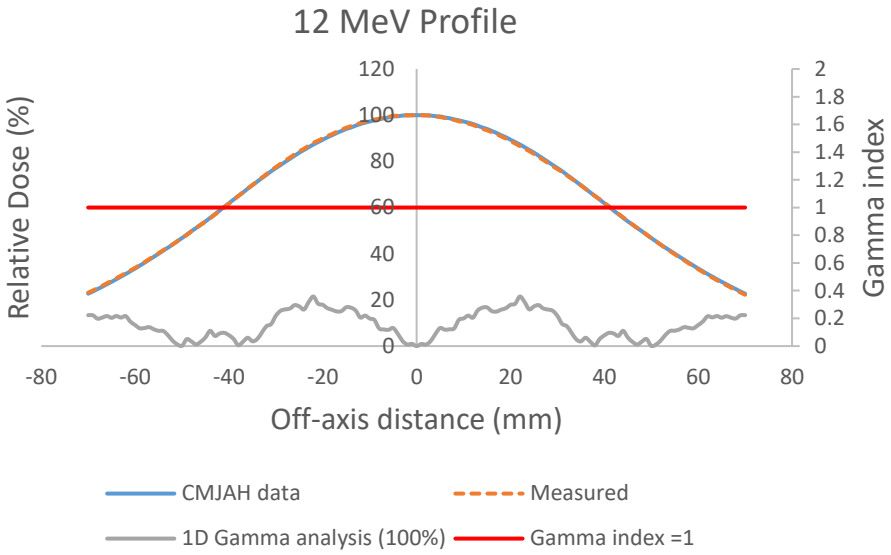

(c)

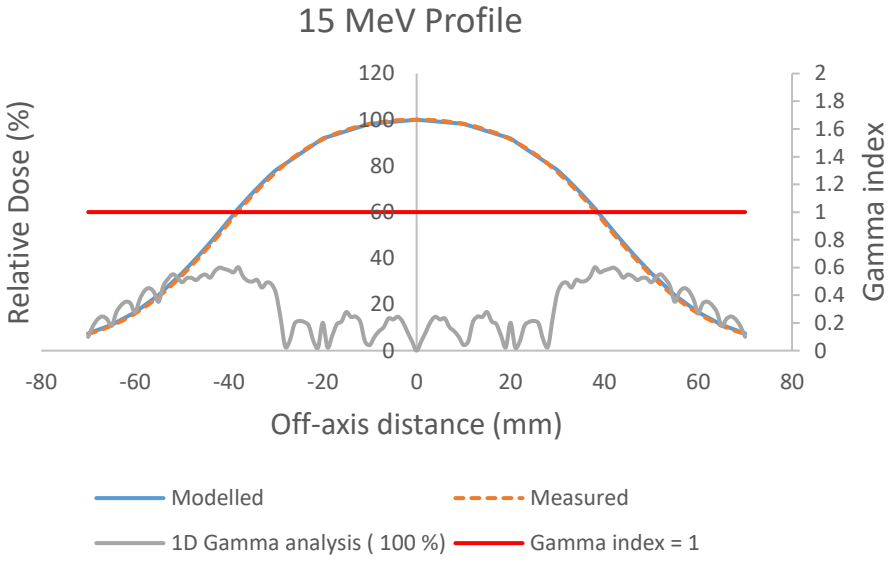

(d)

Figure 4.5: Comparison of CMJAH and measured cross-plane profiles in air for a set field size of 8 cm × 8 cm, showing the percentage difference obtained from 1D gamma analysis. The data are normalized to the central axis dose. (a) 6 MeV profile. (b) 9 MeV profile. (c) 12 MeV profile. (d) 15 MeV profile.

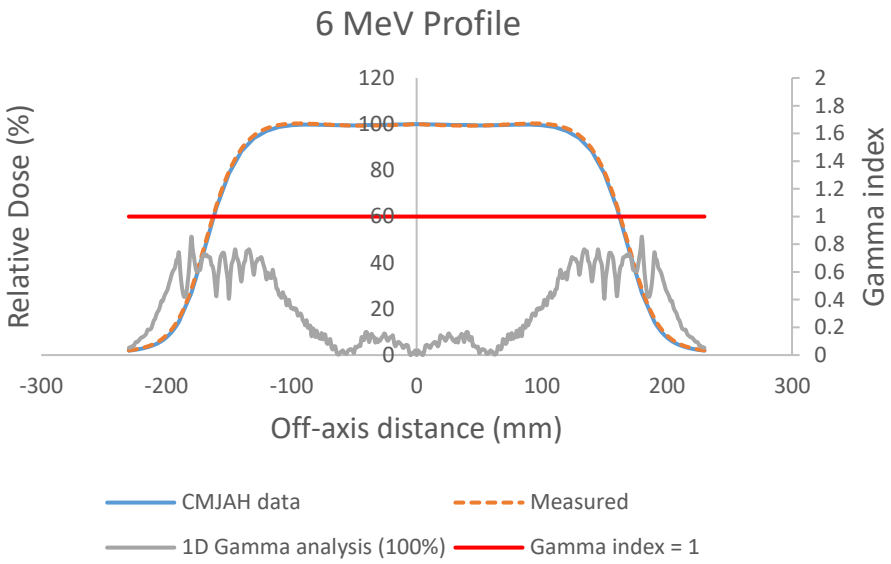
6 MeV Profile
Relative Dose (%)
Gamma index
Off-axis distance (mm)
120
100
80
60
40
20
0
2
1.8
1.6
1.4
1.2
1
0.8
0.6
0.4
0.2
0
-300
-200
-100
0
100
200
300
CMJAH data
Measured
1D Gamma analysis (100%)
Gamma index = 1

(a)

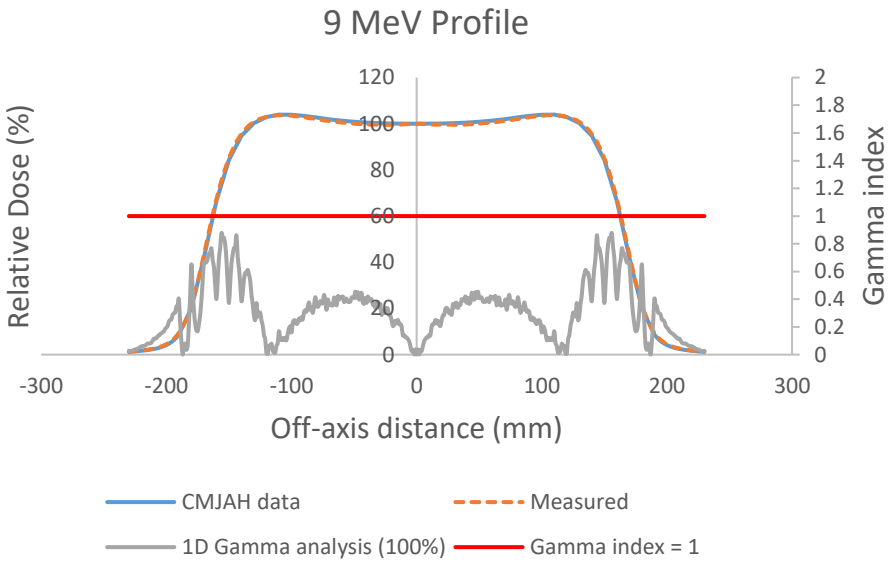
9 MeV Profile
Relative Dose (%)
Gamma index
Off-axis distance (mm)
120
100
80
60
40
20
0
2
1.8
1.6
1.4
1.2
1
0.8
0.6
0.4
0.2
0
-300
-200
-100
0
100
200
300
CMJAH data
Measured
1D Gamma analysis (100%)
Gamma index = 1

(b)

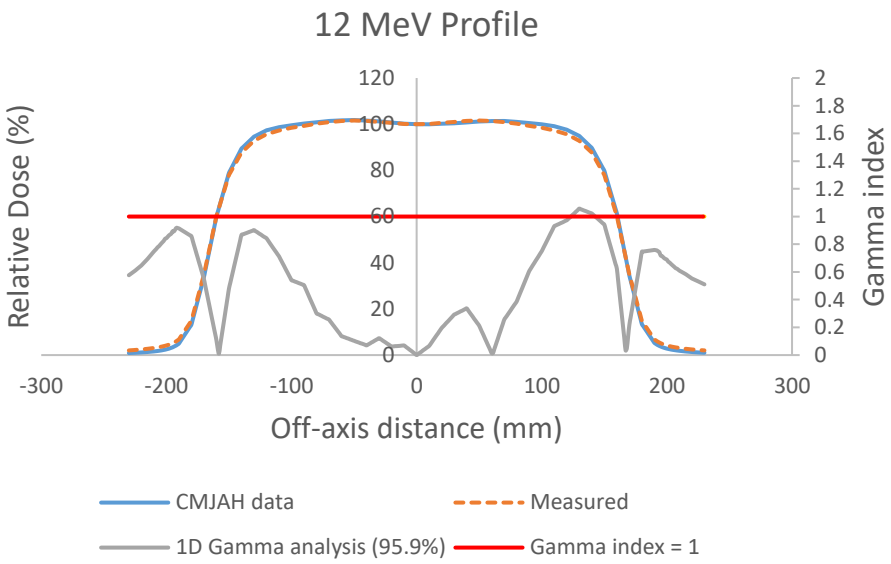

(c)

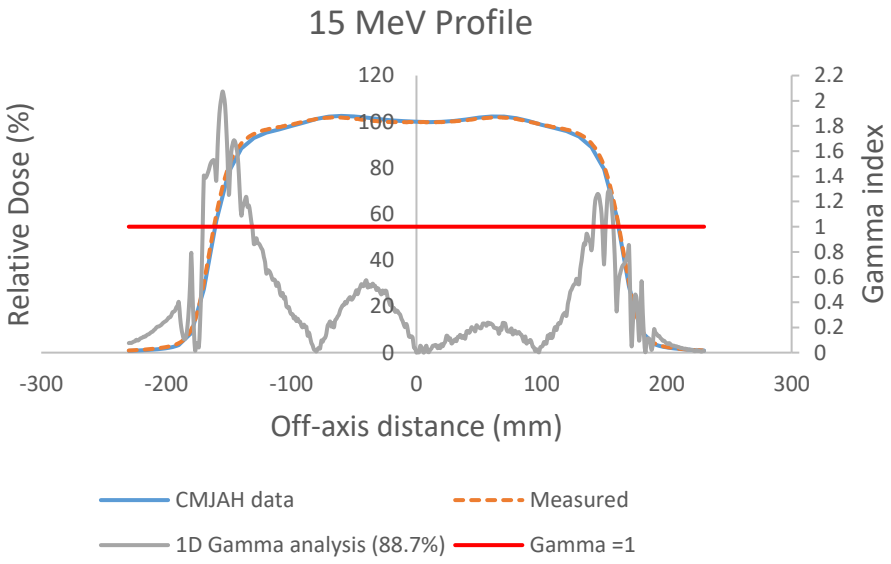

(d)

Figure 4.6: Cross-plane profiles in air with the field size set to 40 cm × 40 cm, Indicating the percentage difference obtained from 1D gamma analysis comparing measured and CMJAH profiles. The data are normalized to the central axis dose. (a) 6 MeV profile. (b) 9 MeV profile. (c) 12 MeV profile. (d) 15 MeV profile.

4.2. Validation Tests

4.2.1. Model verification

PDDs

The 1D gamma analysis technique with 3%/3 mm criterion was utilized to compare eMC-simulated profiles and PDDs with those measured using the PTW Semiflex 31021. Figures 4.7(a) to (d) and 4.8(a) to (d) compare measured and computed PDDs in water for beam energies of 6 MeV, 9 MeV, 12 MeV and 15 MeV, employing an applicator sized 6 cm x 6 cm and trapezoid-shaped cutout to confine the field, respectively. The SSD was set to 100 cm. Similarly, Figures 4.9(a) to (d) and 4.10(a) to (d) present the PDD comparisons at 110 cm SSD for the same beam energies, applicator and cutout. Tables 4.1 and 4.2 present the percentage difference obtained from 1D gamma analysis for all square applicators and a trapezoidal cutout at 100 cm and 110 cm SSD. In this study, the acceptance criteria required that at least 90% of the relative dose points that were compared meet the 3%/3 mm criterion. Electron beams with energies 6 MeV, 9 MeV and 12 MeV for all applicators met the 3%/3 mm criterion. Measurements at 15 MeV with the trapezoidal cutout had an overall pass rate of 85.9%.

For this case, 107 relative dose points were compared, with 92 points within 3%/3 mm. Between depths of 62 mm and 76 mm (see Figure 4.7(d)), the eMC algorithm overestimated the dose by an average of 4.2%. This discrepancy was due to the loss of scattering equilibrium, reducing the number of interactions and particles sampled, which contributed to inaccuracies in the calculated dose (Snyder, et al., 2019).

At 110 cm SSD, the PDD comparison for the trapezoidal cutout and the 6 cm × 6 cm applicator did not meet the 3%/3 mm criterion at 15 MeV, as shown in Table 4.2. The eMC algorithm overestimated by an average of 4.3% from depths of 33 mm to 49 mm and 58 mm to 75 mm. For the trapezoid cutout, 72% of the compared relative dose points were within 3%/3 mm, with an average deviation of 3.9% between depths of 31 mm to 51 mm and 3.3% between 67 mm to 73 mm.

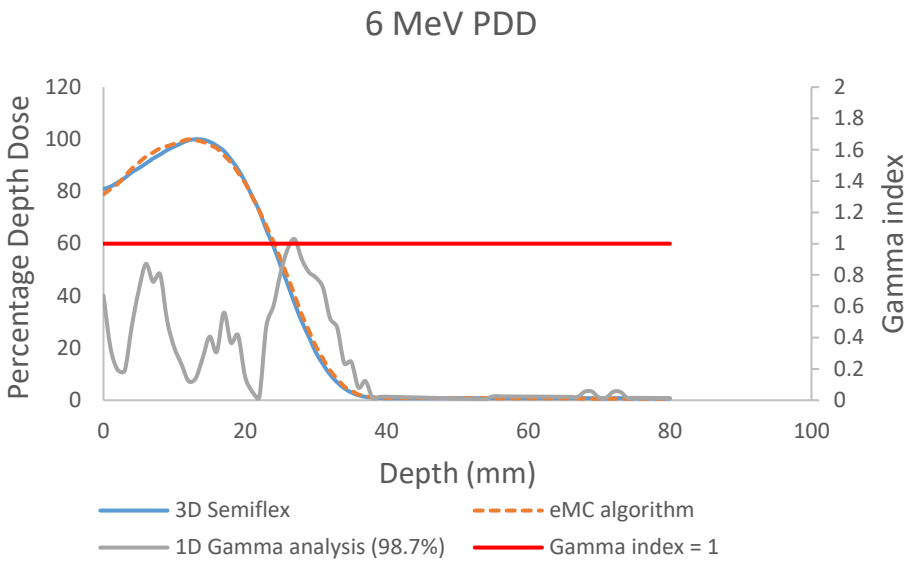
6 MeV PDD
Percentage Depth Dose
Gamma index
Depth (mm)
3D Semiflex
eMC algorithm
1D Gamma analysis (98.7%)
Gamma index = 1

(a)

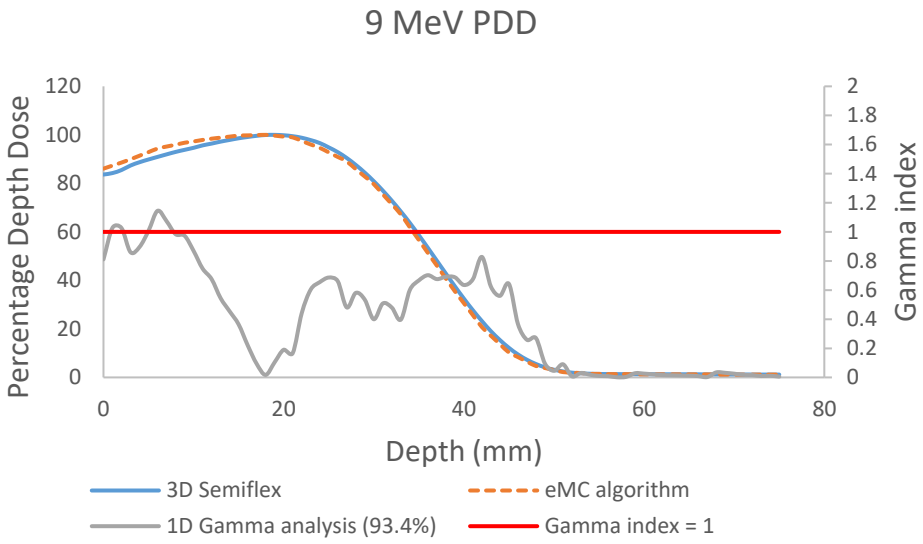
9 MeV PDD
Percentage Depth Dose
Gamma index
Depth (mm)
3D Semiflex
eMC algorithm
1D Gamma analysis (93.4%)
Gamma index = 1

(b)

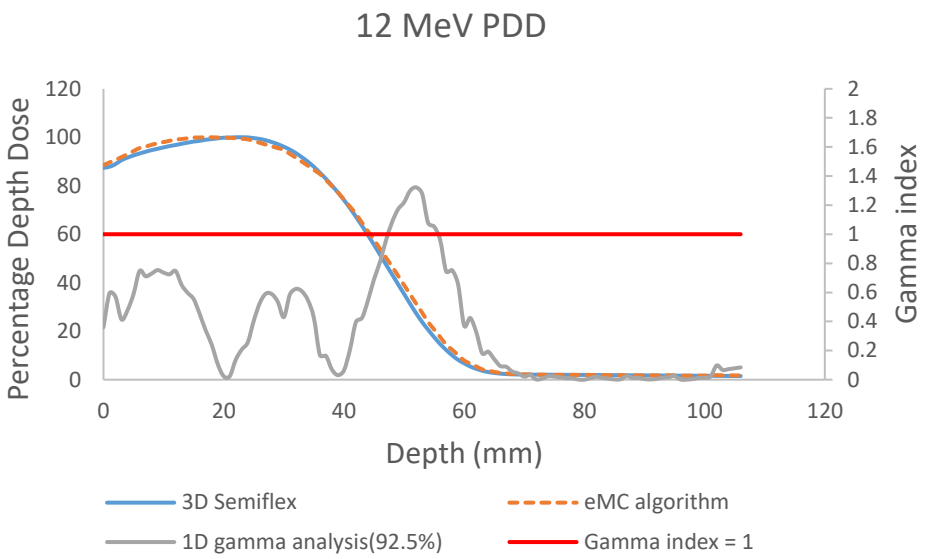

(c)

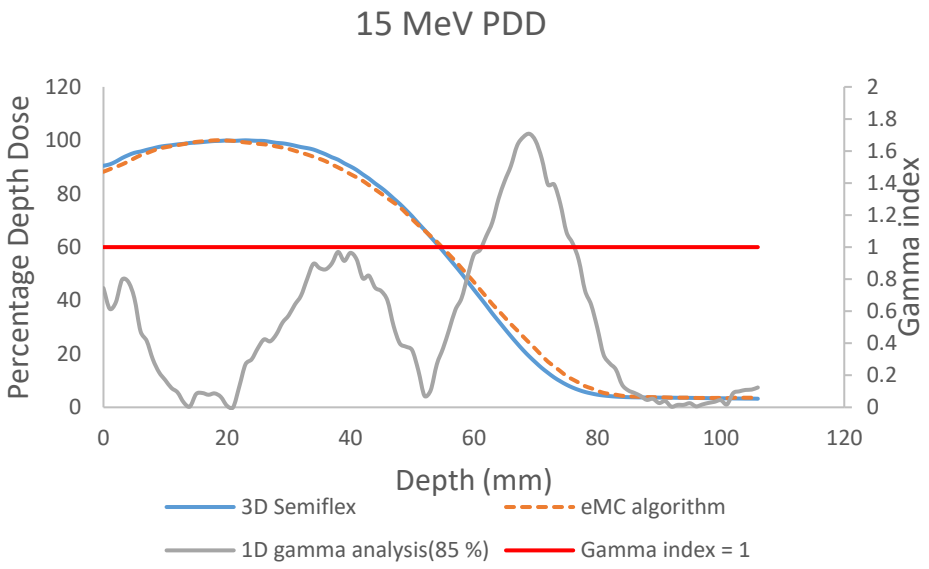

(d)

Figure 4.7: Comparison of computed and measured PDDs in water at 100 cm SSD, employing the trapezoid cutout to confine the field, indicating the percentage difference obtained from 1D gamma analysis. (a) 6 MeV. (b) 9 MeV. (c) 12 MeV. (d) 15 MeV.

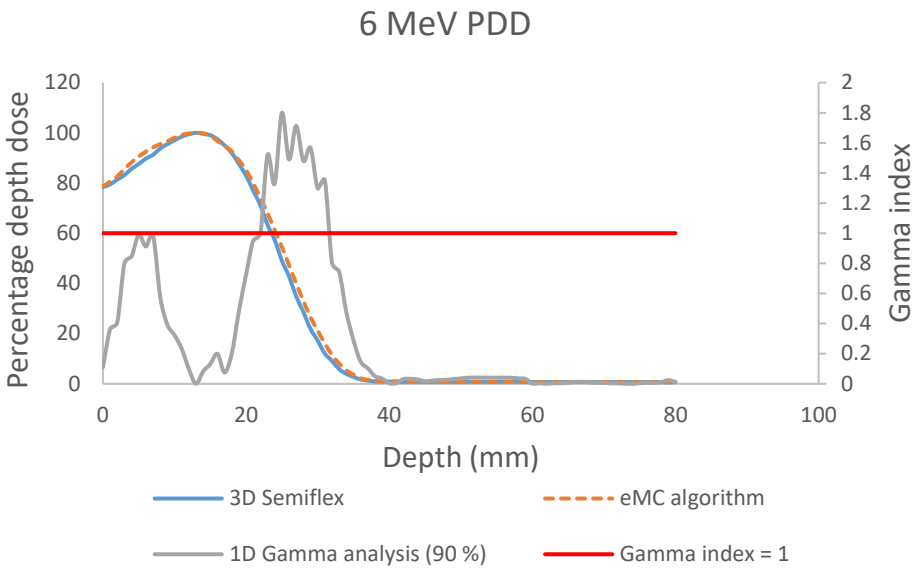
6 MeV PDD
Percentage depth dose
Gamma index
Depth (mm)
3D Semiflex
eMC algorithm
1D Gamma analysis (90 %)
Gamma index = 1

(a)

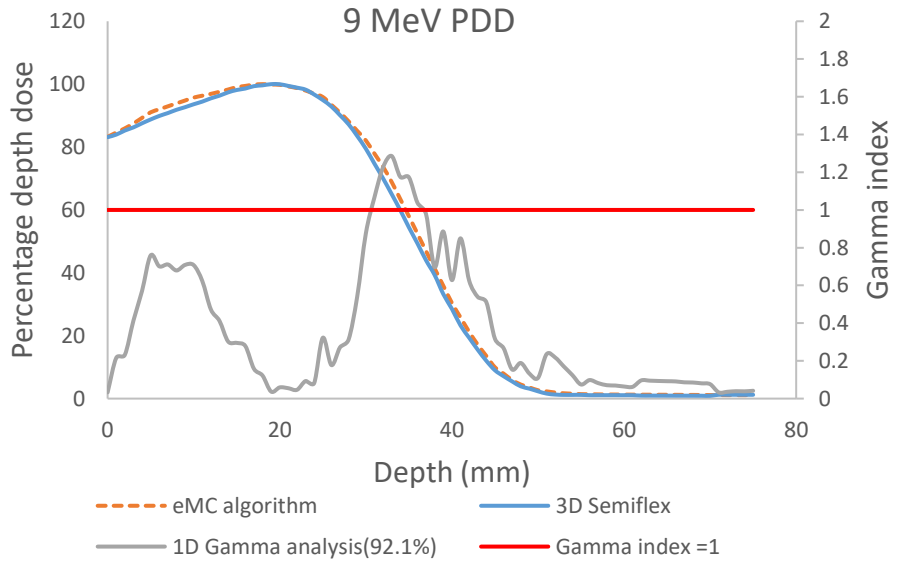
9 MeV PDD
Percentage depth dose
Gamma index
Depth (mm)
eMC algorithm
3D Semiflex
1D Gamma analysis(92.1%)
Gamma index =1

(b)

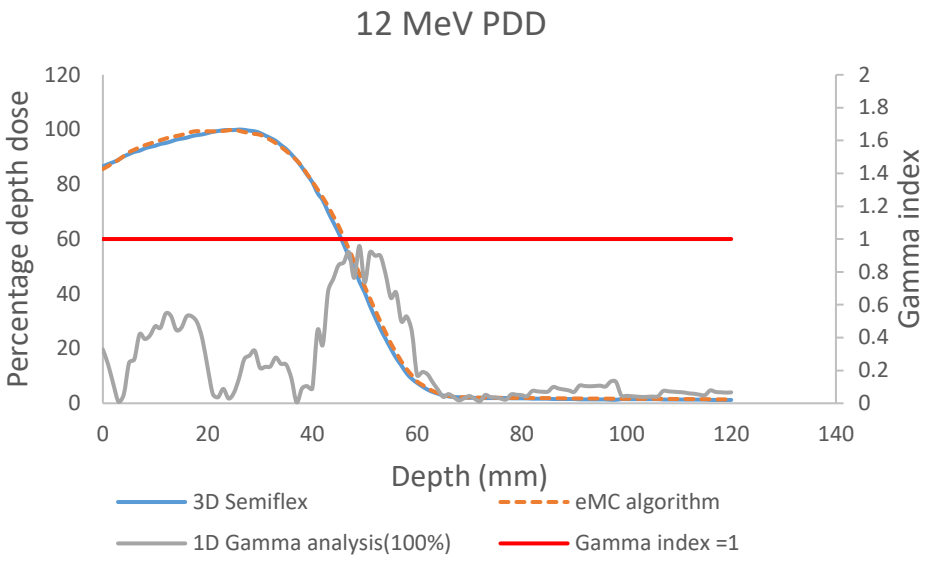

(c)

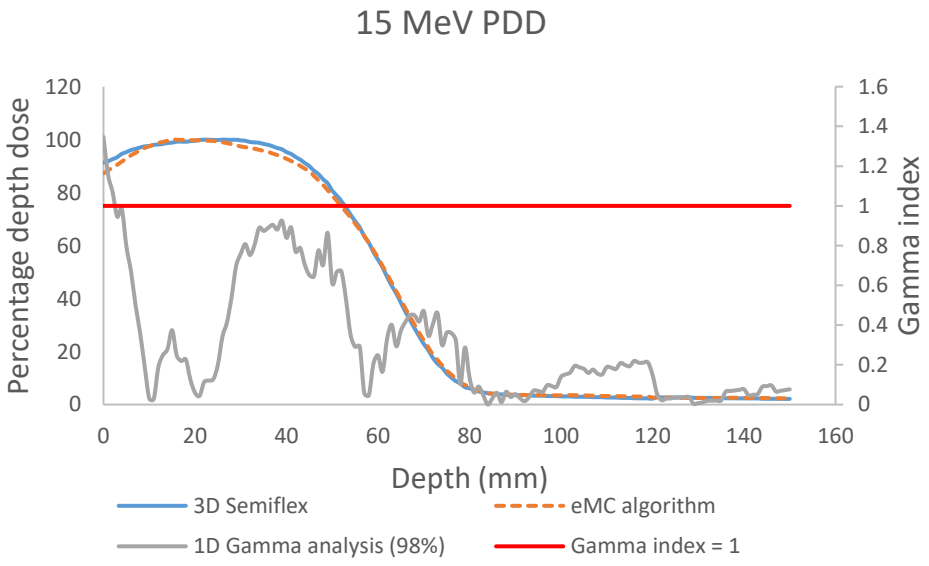

(d)

Figure 4.8: Comparison of measured and calculated PDDs in water, for an applicator sized 6 cm x 6 cm, indicating the percentage difference obtained from 1D gamma analysis at 100 cm SSD. (a) 6 MeV. (b) 9 MeV. (c) 12 MeV. (d) 15 MeV.

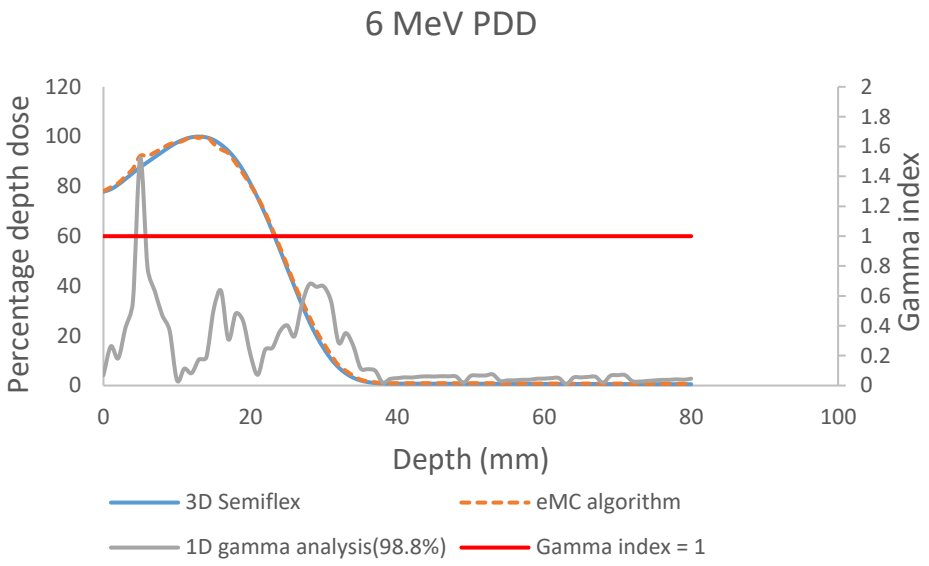
6 MeV PDD
Percentage depth dose
Gamma index
Depth (mm)
3D Semiflex
eMC algorithm
1D gamma analysis(98.8%)
Gamma index = 1

(a)

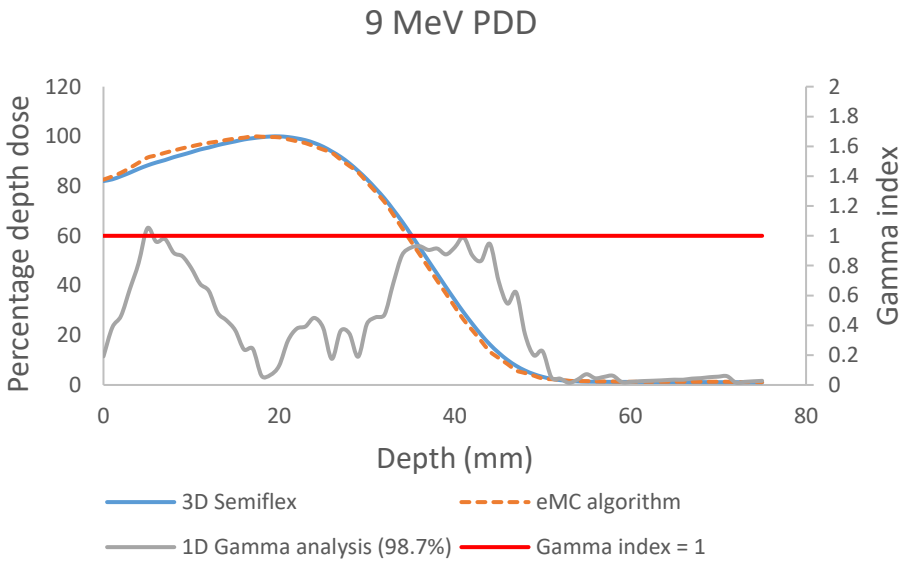
9 MeV PDD
Percentage depth dose
Gamma index
Depth (mm)
3D Semiflex
eMC algorithm
1D Gamma analysis (98.7%)
Gamma index = 1

(b)

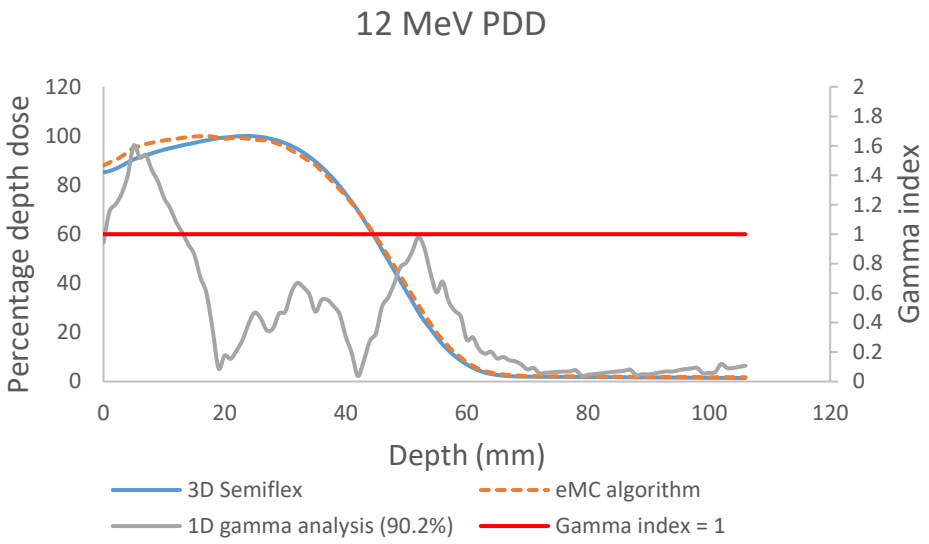

(c)

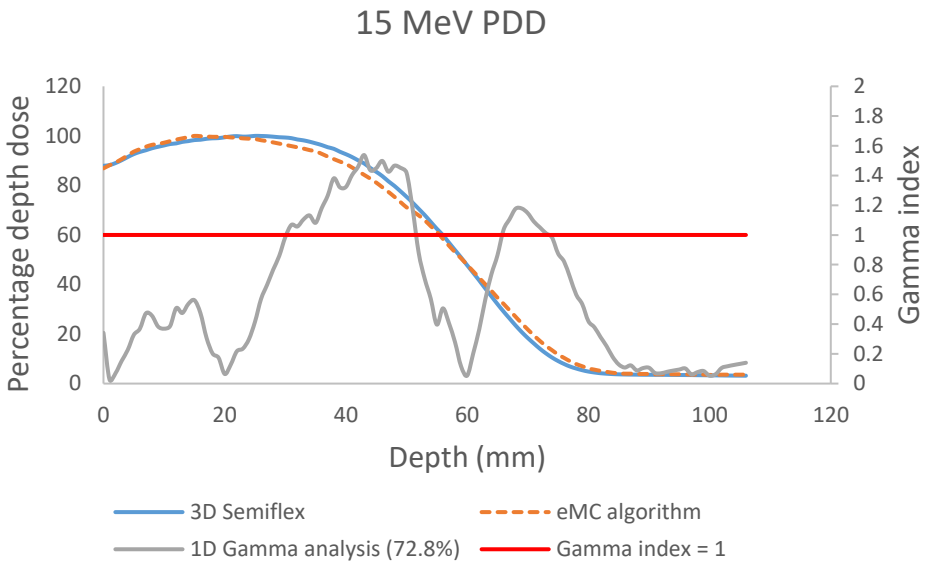

(d)

Figure 4.9: Comparison of measured and calculated PDDs in water at 110 cm SSD with a trapezoid cutout, indicating the percentage difference obtained from 1D gamma analysis. (a) 6 MeV. (b) 9 MeV. (c) 12 MeV. (d) 15 MeV.

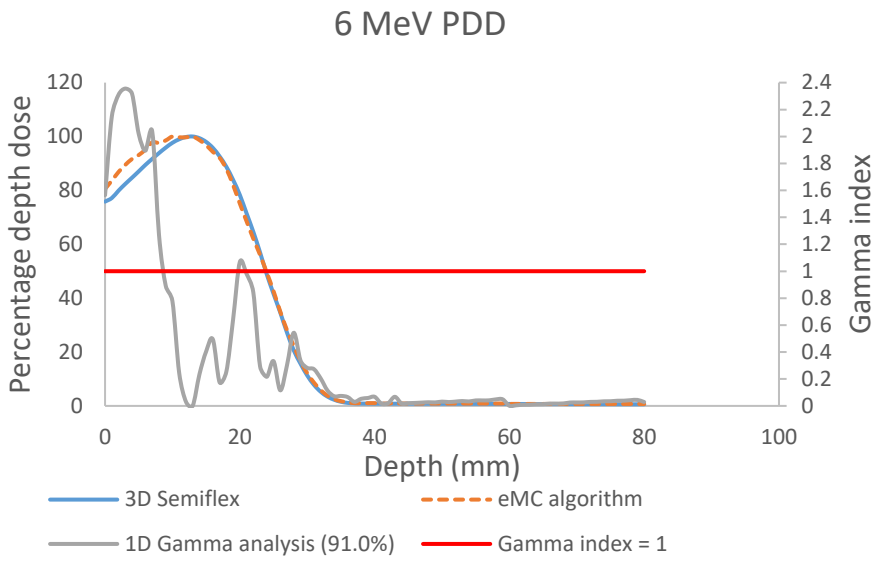
6 MeV PDD
Percentage depth dose
Gamma index
Depth (mm)
3D Semiflex
eMC algorithm
1D Gamma analysis (91.0%)
Gamma index = 1

(a)

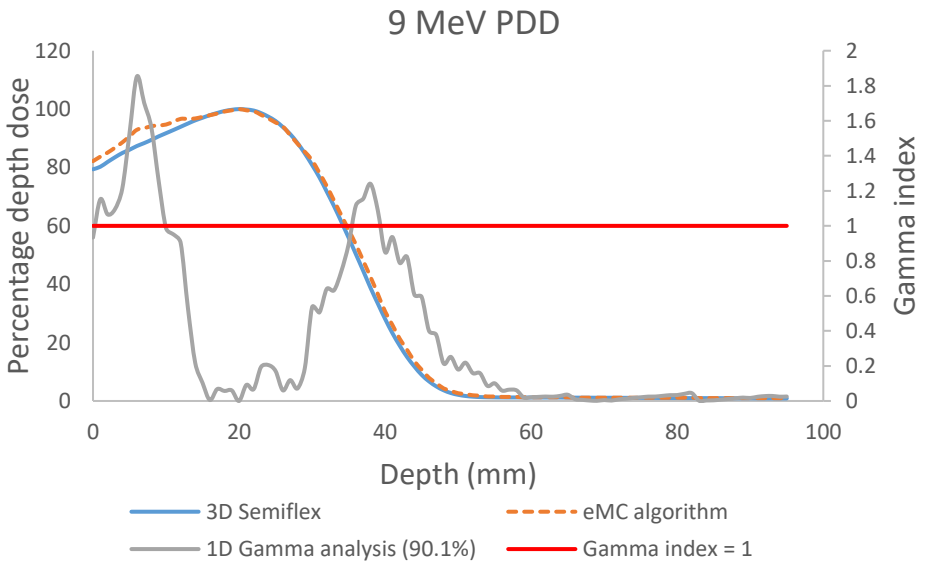
9 MeV PDD
Percentage depth dose
Gamma index
Depth (mm)
3D Semiflex
eMC algorithm
1D Gamma analysis (90.1%)
Gamma index = 1

(b)

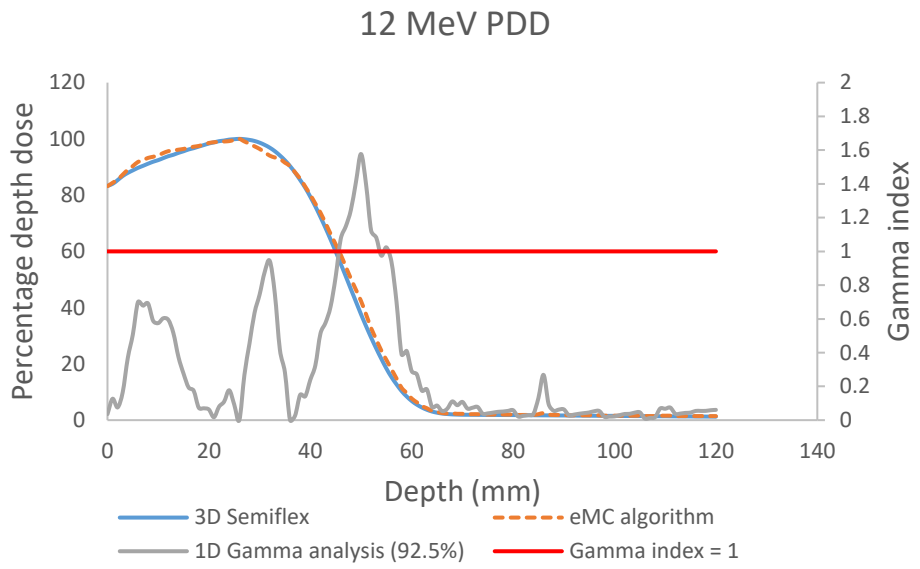

(c)

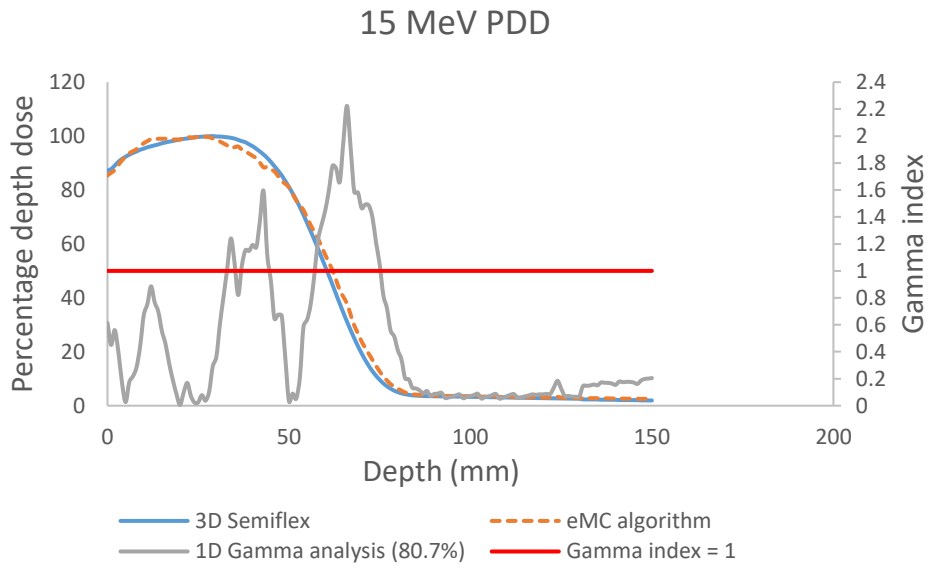

(d)

Figure 4.10: Comparison of calculated and measured PDDs in water, employing an applicator sized 6 cm x 6 cm to confine the field at 110 cm SSD, showing the percentage difference obtained from 1D gamma analysis. (a) 6 MeV. (b) 9 MeV. (c) 12 MeV. (d) 15 MeV.

Table 4.1: Summary of the 1D gamma analysis comparing calculated and measured PDDs in water, with the SSD of 100 cm, for different beam energies and applicators.

Applicator (cm^2)	Gamma analysis (%)			
	6 MeV	9 MeV	12 MeV	15 MeV
6 x 6	90.0	92.1	100	98.0
10 x 10	98.7	100	97.9	98.8
14 x 14	90.0	100	90.0	100
20 x 20	91.4	100	100	91.3
25 x 25	97.5	90.0	100	90.1
Trapezoid	98.7	93.4	92.5	85.9

Table 4.2: Summary of the 1D gamma analysis comparing computed and measured PDDs in water, with the SSD of 110 cm, for different electron beam energies and applicators.

Applicator (cm^2)	Gamma analysis (%)			
	6 MeV	9 MeV	12 MeV	15 MeV
6 x 6	90.0	90.1	92.5	80.8
10 x 10	91.4	96.1	90.1	99.3
14 x 14	93.8	92.7	100	90.0
20 x 20	93.8	92.3	90.9	91.2
25 x 25	98.7	92.3	97.9	100
Trapezoid	98.8	98.7	90.3	72.8

Profiles

Figure 4.11(a) to (d) and figure 4.12(a) to (d) present cross-plane profile comparisons between eMC-calculated and measured profiles utilizing the PTW Semiflex 31021 for beam energies of 6 MeV, 9 MeV, 12 MeV and 15 MeV with the 14 cm x 14 cm applicator, measured at depths of R_{90} and R_{50} at 110 cm SSD. The data were normalized to the central axis dose. The eMC algorithm computed profiles were consistent with the measured profiles, except for the 12 MeV profile measured at R_{90} and R_{50}. In these cases, the eMC algorithm underestimated the dose by an average of 4.1% from an off-axis distance of -79 mm to -56 mm at R_{90} and by 4.3% at R_{50}.

The comparison also included profiles acquired using an applicator sized 6 cm x 6 cm and a trapezoid cutout to confine the field at 110 cm and 100 cm SSD. For these fields, the computed profiles were within 3%/3 mm of the measured profiles, except for the 12 MeV trapezoid cutout profile measured at R_{90} with the SSD set to110 cm, which achieved a confidence level of 89.6 percent. Tables 4.3, 4.4,4.5 and 4.6 present the percentage difference obtained from the 1D gamma analysis for the electron beam energies and applicators referenced above.

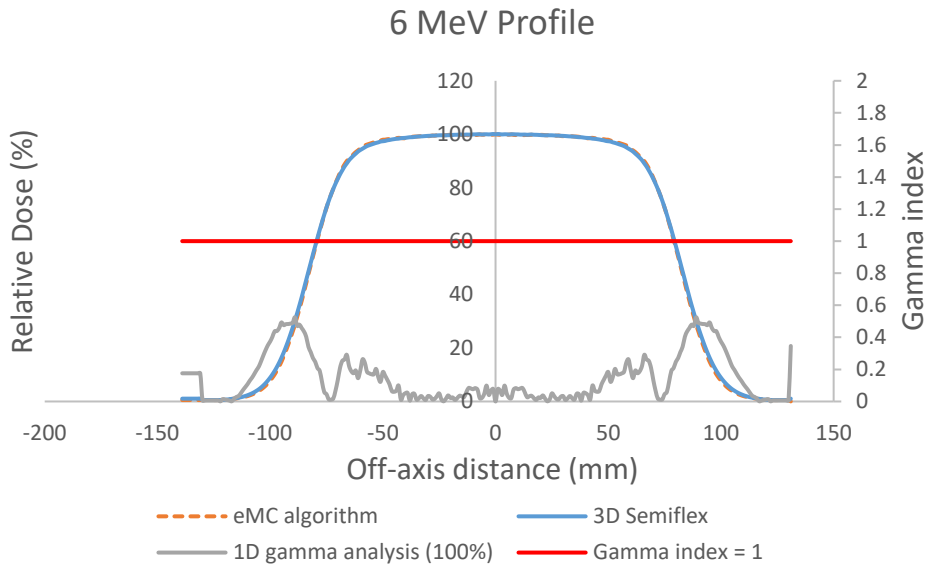

(a)

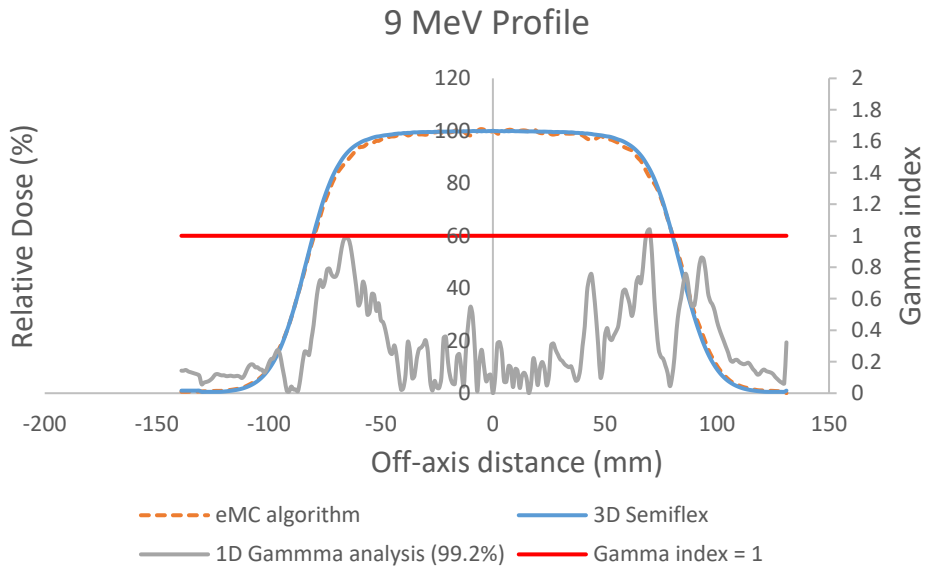

(b)

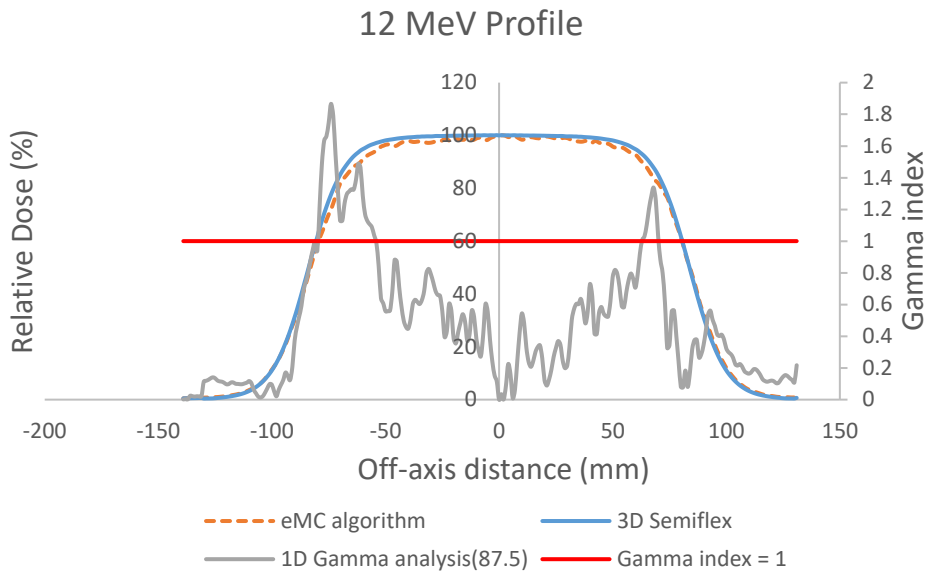

(c)

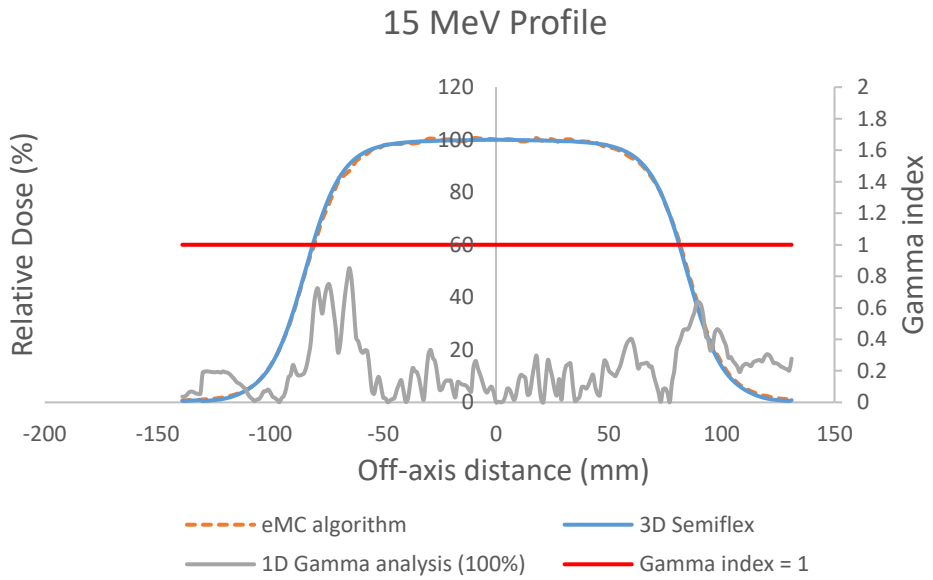

(d)

Figure 4.11: Cross-plane profiles in water at 110 cm SSD, employing an applicator sized 14 cm x 14 cm to confine the field, indicating the percentage difference obtained from 1D gamma analysis comparing measured and calculated profiles at R_{90}. (a) 6 MeV. (b) 9 MeV. (c) 12 MeV. (d) 15 MeV.

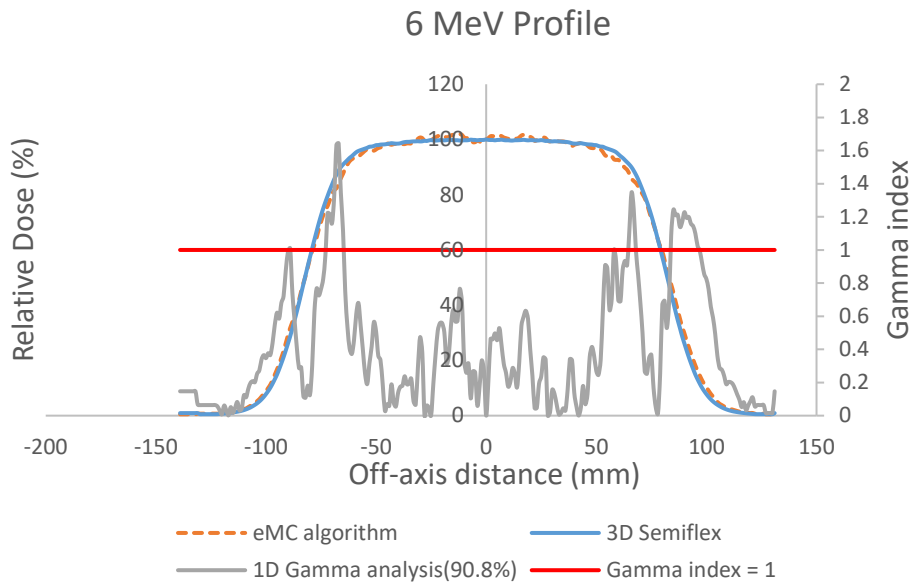
6 MeV Profile
Relative Dose (%)
Gamma index
Off-axis distance (mm)
120
100
80
60
40
20
0
2
1.8
1.6
1.4
1.2
1
0.8
0.6
0.4
0.2
0
-200
-150
-100
-50
0
50
100
150
eMC algorithm
3D Semiflex
1D Gamma analysis(90.8%)
Gamma index = 1

(a)

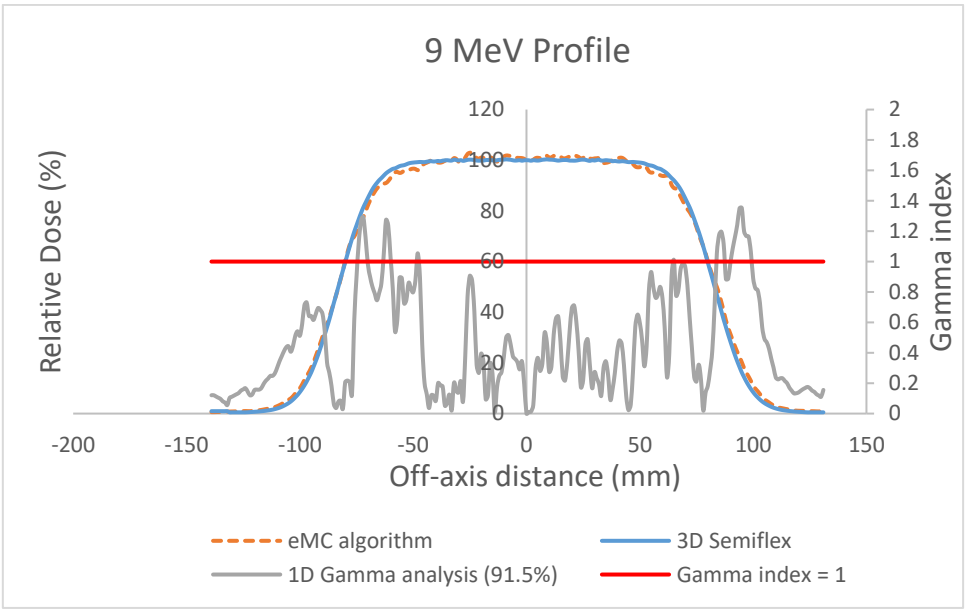
9 MeV Profile
Relative Dose (%)
Gamma index
Off-axis distance (mm)
120
100
80
60
40
20
0
2
1.8
1.6
1.4
1.2
1
0.8
0.6
0.4
0.2
0
-200
-150
-100
-50
0
50
100
150
eMC algorithm
3D Semiflex
1D Gamma analysis (91.5%)
Gamma index = 1

(b)

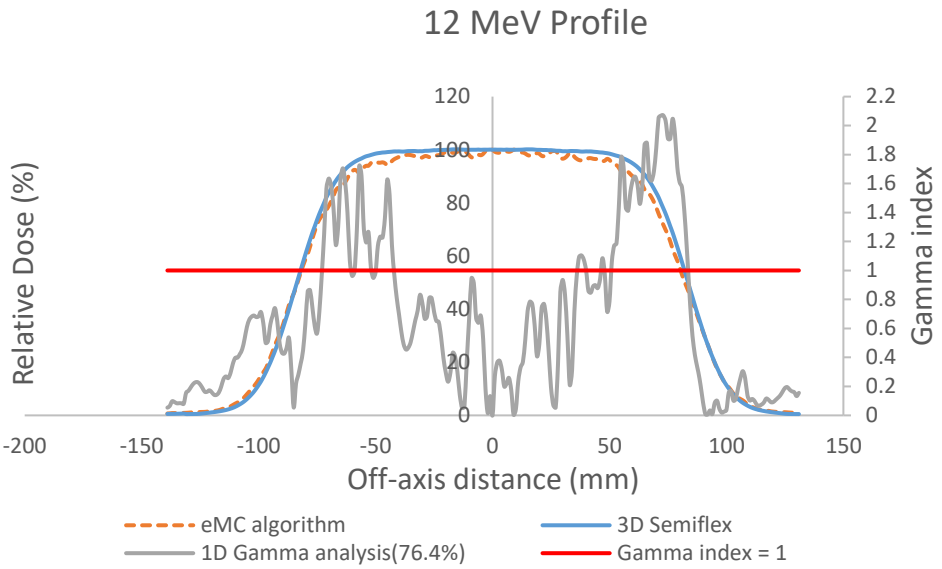

(c)

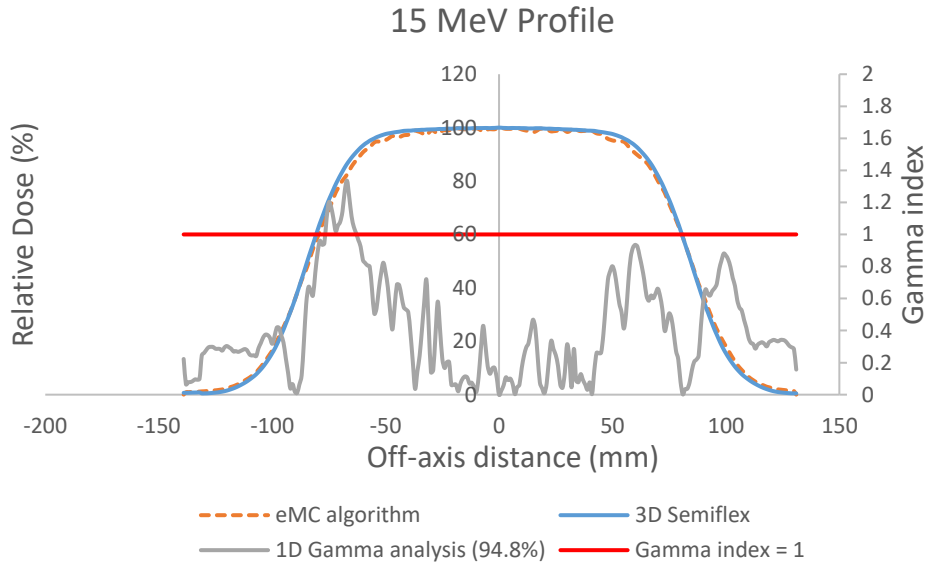

(d)

Figure 4.12: Cross-plane profiles at 110 cm SSD in water, for an applicator sized 14 cm × 14 cm, indicating the percentage difference obtained from 1D gamma analysis comparing measured and calculated profiles at R_{50}. (a) 6 MeV. (b) 9 MeV. (c) 12 MeV. (d) 15 MeV.

Table 4.3: Summary of the 1D gamma analysis comparing computed and measured cross-plane profiles, scanned at R_{90} in water at 100 cm SSD for the different applicators and the trapezoid cutout, for all energies.

Applicator (cm^2)	Gamma analysis (%)			
	6 MeV	9 MeV	12 MeV	15 MeV
6 x 6	91.8	95.6	100	99.6
14 x 14	99.6	99.2	100	92.9
Trapezoid	90.4	94.5	96.3	97.1

Table 4.4: Summary of the 1D gamma analysis comparing measured and computed cross-plane profiles, scanned at R_{50} in water with the SSD set to 100 cm, for the different applicators and the trapezoid cutout, for all energies.

Applicator (cm^2)	Gamma analysis (%)			
	6 MeV	9 MeV	12 MeV	15 MeV
6 x 6	98.9	99.3	100	100
14 x 14	93.7	99.3	97.1	98.5
Trapezoid	92.6	94.5	97.8	100

Table 4.5: Summary of the 1D gamma analysis comparing computed and measured profiles, scanned at R_{90} in water at 110 cm SSD, for the different applicators and the trapezoid cutout, for all energies.

Applicator (cm^2)	Gamma analysis (%)			
	6 MeV	9 MeV	12 MeV	15 MeV
6 x 6	99.6	100	100	100
14 x 14	100	99.2	87.5	100
Trapezoid	97.0	89.6	95.6	97.5

Table 4.6: Summary of the 1D gamma analysis comparing measured and computed cross-plane profiles, scanned at R_{50} in water with the SSD set to 110 cm, for the different applicators and the trapezoid cutout, for all energies.

Applicator (cm^2)	Gamma analysis (%)			
	6 MeV	9 MeV	12 MeV	15 MeV
6 x 6	96.7	100	100	95.2
14 x 14	90. 8	91.5	76.4	94.8
Trapezoid	96.7	93.2	96.3	100

Output factors

Table 4.7 presents a comparison between computed and measured output factors at the depth of maximum dose on the central axis for 100 cm SSD in a homogeneous water-equivalent phantom. The output factors computed by the eMC algorithm agreed with the measured values to within 2%, except for the 9 MeV beam utilizing an applicator sized 6 cm x 6 cm, and the 9 MeV and 6 MeV beams utilizing the trapezoid cutout to confine the field. The deviation between the eMC algorithm computed output factors and the measured values was 3.75% for the 6 MeV beam with a trapezoid cutout, while for the 9 MeV beam utilizing an applicator sized 6 cm x 6 cm, the deviation was -3.89%.

Table 4.8 presents a comparison of output factors between the eMC-calculated and the PTW Semiflex 31021 measurements at 110 cm SSD. All comparisons were within 2%, except for the 6 MeV and 15 MeV trapezoid fields, which showed deviations of 6.53% and 3.68%, respectively.

Table 4.7: The percentage differences obtained from comparing measured and computed output factors in water with the SSD set to 100 cm for the different applicators and the trapezoid cutout, for all energies.

Applicator (cm^2)	6 MeV			9 MeV			12 MeV		
	Measured ±0.02	eMC calc ±0.002	%difference	Measured ±0.02	eMC calc ±0.002	%difference	Measured ±0.02	eMC calc ±0.002	%difference
6 x 6	0.89	0.886	-0.45	0.95	0.913	-3.89	0.98	0.973	-0.71
10 x 10	1.00	1.000	0.00	1.00	1.000	0.00	1.00	1.000	0.00
14 x 14	1.03	1.024	-0.58	0.99	0.977	-1.31	0.99	0.973	-1.72
20 x 20	1.02	1.040	1.96	0.98	0.972	-0.82	0.99	0.978	-1.21
25 x 25	1.03	1.036	0.58	0.97	0.985	1.55	0.98	0.968	1.22
Trapezoid	0.96	0.996	3.75	0.96	0.981	2.19	0.97	0.986	1.64

Applicator (cm^2)	15 MeV		
	Measured ±0.02	eMC calc ±0.002	%difference
6 x 6	0.99	0.974	-1.62
10 x 10	1.00	1.000	0.00
14 x 14	0.98	0.970	-1.02
20 x 20	0.99	0.976	-1.41
25 x 25	0.99	0.980	-1.01
Trapezoid	0.97	0.980	1.03

Table 4.8: Percentage differences obtained from comparing measured and computed output factors in water with the SSD set to 110 cm for the different applicators and the trapezoid cutout, for all energies.

Applicator (cm^2)	6 MeV			9 MeV			12 MeV		
	Measured ±0.02	eMC calc ±0.002	%difference	Measured ±0.02	eMC calc ±0.002	%difference	Measured ±0.02	eMC calc ±0.002	%difference
6 x 6	0.67	0.665	-0.75	0.73	0.719	-1.51	0.77	0.755	-1.95
10 x 10	0.79	0.783	-0.89	0.81	0.810	0	0.81	0.812	0.25
14 x 14	0.83	0.829	-0.12	0.80	0.798	-0.25	0.81	0.823	1.61
20 x 20	0.83	0.846	1.93	0.81	0.809	-0.12	0.82	0.822	0.24
25 x 25	0.83	0.836	0.72	0.80	0.805	0.63	0.83	0.810	-2.41
Trapezoid	0.72	0.767	6.53	0.75	0.774	3.20	0.76	0.788	3.68

Applicator (cm^2)	15 MeV		
	Measured ±0.02	eMC calc ±0.002	%difference
6 x 6	0.78	0.786	0.77
10 x 10	0.81	0.802	-0.99
14 x 14	0.80	0.805	0.63
20 x 20	0.82	0.810	-1.22
25 x 25	0.81	0.801	-1.11
Trapezoid	0.78	0.796	2.05

4.2.2. Heterogeneity test

Lung equivalent material

The AAPM MPPG 5a recommends a 7% tolerance for comparing doses computed by a dose calculation algorithm with those measured by detectors in the presence of inhomogeneities. This study used a 1D Gamma analysis technique with criteria of 7%/3 mm, 4%/3 mm and 3%/3 mm to compare eMC algorithm calculated cross-plane profiles with measurements from the PTW Octavius detector 1500. Figure 4.13(a) to (d) presents a comparison of measured and computed cross-plane profiles for different electron beam energies at 100 cm SSD, where an interface was created along the in-plane axis by offsetting the lung-equivalent material and Perspex to half of the field. Table 4.9 summarizes these results.

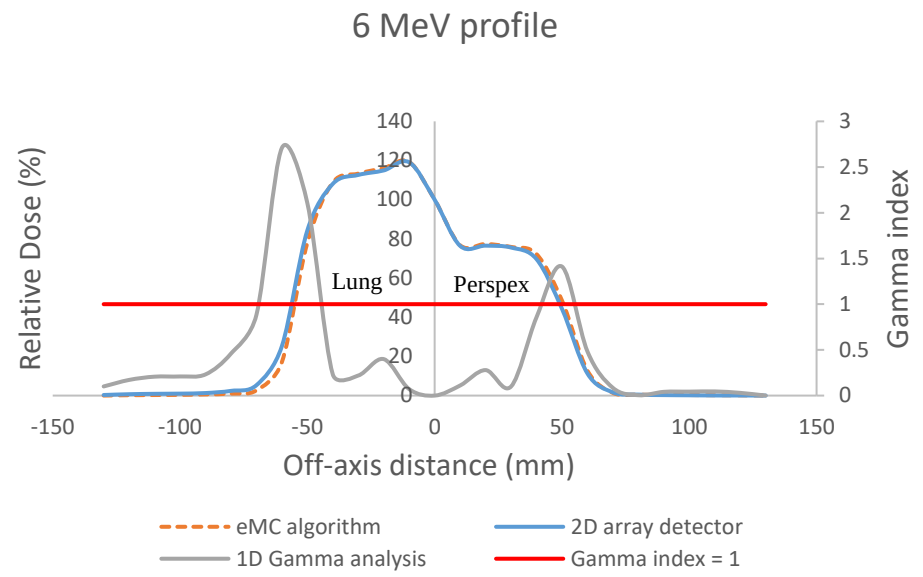
6 MeV profile
Relative Dose (%)
Gamma index
Lung
Perspex
Off-axis distance (mm)
eMC algorithm
2D array detector
1D Gamma analysis
Gamma index = 1

(a)

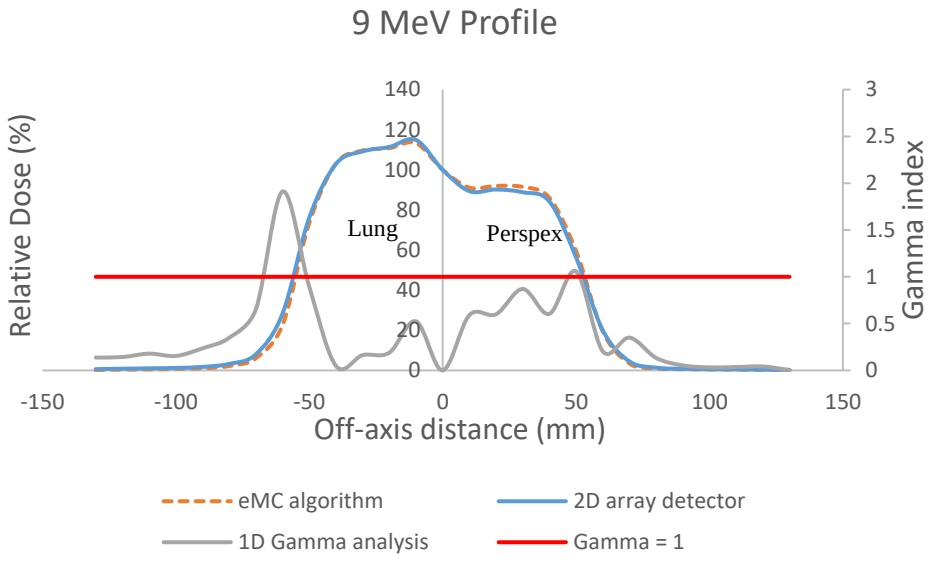
9 MeV Profile
Relative Dose (%)
Gamma index
Lung
Perspex
Off-axis distance (mm)
eMC algorithm
2D array detector
1D Gamma analysis
Gamma = 1

(b)

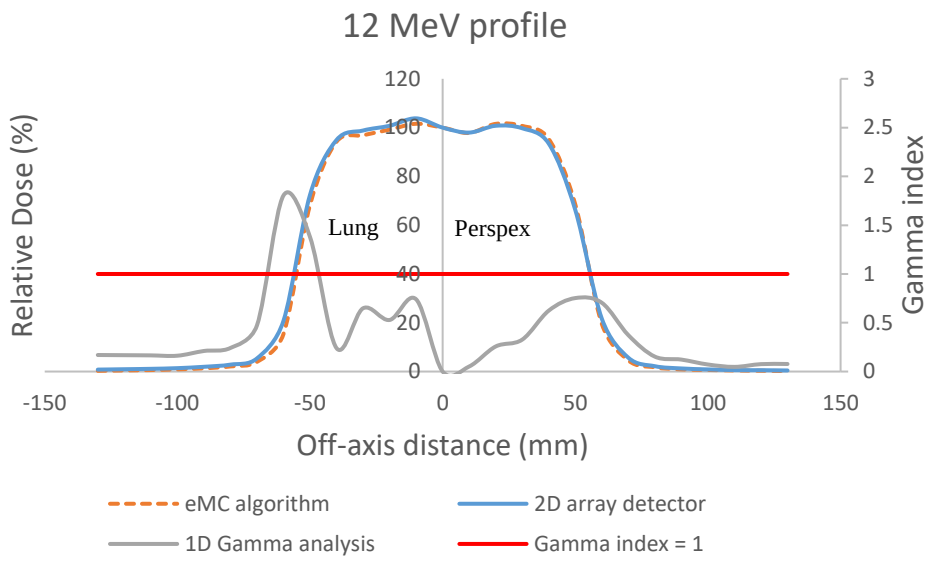

(c)

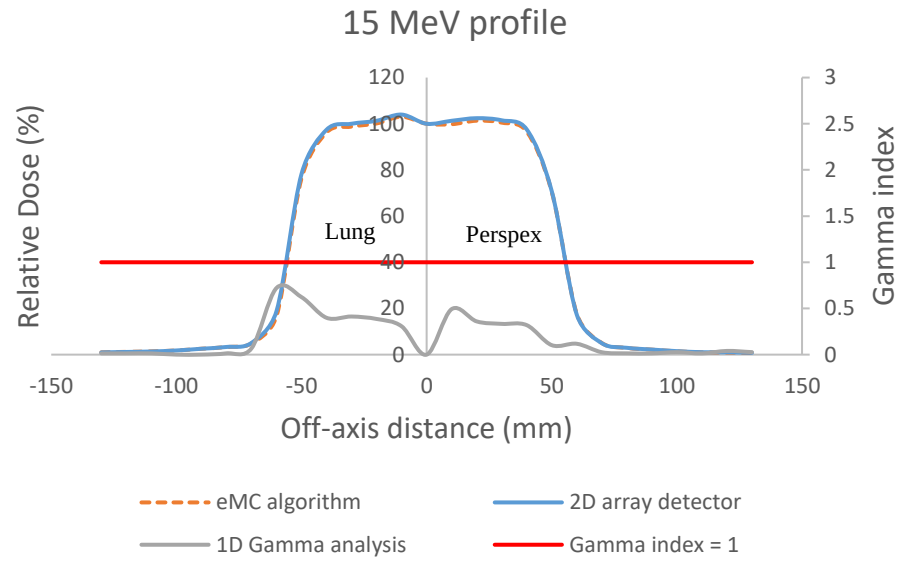

(d)

Figure 4.13: Cross-plane profiles at 100 cm SSD with the lung and Perspex offset to half of the field, indicating the 1D gamma analysis comparing computed and measured profiles. The data are normalized to the central axis dose. (a) 6 MeV profile measured at 1.9 cm depth. (b) 9 MeV profile measured at 2.7 cm. (c) 12 MeV profile measured at 2.7 cm. (d) 15 MeV profile measured at 2.7 cm depth.

Table 4.9: Summary of the 1D gamma analysis comparing computed and measured cross-plane profiles for different electron beam energies and 1D gamma analysis criteria, with the lung and Perspex offset to half of the field.

Energy (MeV)	1D Gamma analysis criteria		
	3 %| 3 mm	4 %| 3 mm	7 %| 3 mm
6	88.9 %	88.9 %	96.2 %
9	92.5 %	96.3 %	100 %
12	92.6 %	92.6 %	100 %
15	100 %	100 %	100 %

A total of 27 relative dose points were compared across the different electron beam energies, and all met the 7%/3 mm, 3%/3 mm and 4%/3 mm criteria, except for the 6 MeV beam when evaluated with the 3%/3 mm and 4%/3 mm criteria. In this case, 89% of the points met the specified criteria. The eMC algorithm demonstrated an underestimation of dose by an average of 7.2% at an off-axis distance of –60 mm and –50 mm, while overestimating by 4.2% at an off-axis distance of 50 mm. This trend was consistent across cross-plane profiles for the 6 MeV, 9 MeV and 12 MeV beams, particularly at an off-axis distance of -60 mm, where the eMC algorithm showed an average underestimation of 6.2%.

Figure 4.14(a) to (d) presents a comparison between cross-plane profiles simulated using the eMC algorithm and profiles measured with the PTW Octavius detector 1500 when lung-equivalent material was positioned within the 10 cm × 10 cm field. All profile comparisons met the 7%/3 mm, 3%/3 mm and 4%/3 mm criteria, with a maximum average deviation of 4.1% at an off-axis distance of –60 mm. Table 4.10 present the 1D gamma analysis results for all beam energies when lung-equivalent material was positioned within the field.

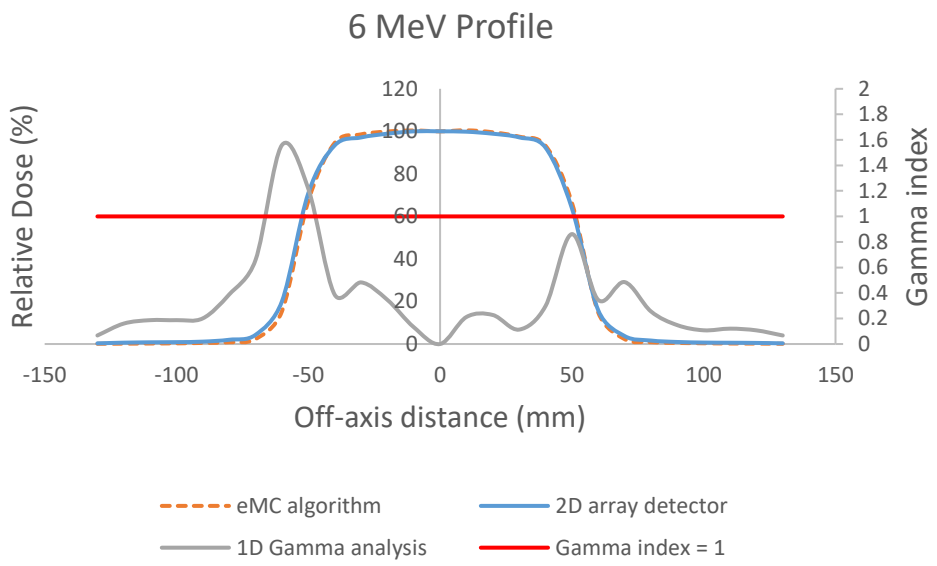
6 MeV Profile
Relative Dose (%)
Gamma index
Off-axis distance (mm)
120
100
80
60
40
20
0
2
1.8
1.6
1.4
1.2
1
0.8
0.6
0.4
0.2
0
-150
-100
-50
0
50
100
150
eMC algorithm
2D array detector
1D Gamma analysis
Gamma index = 1

(a)

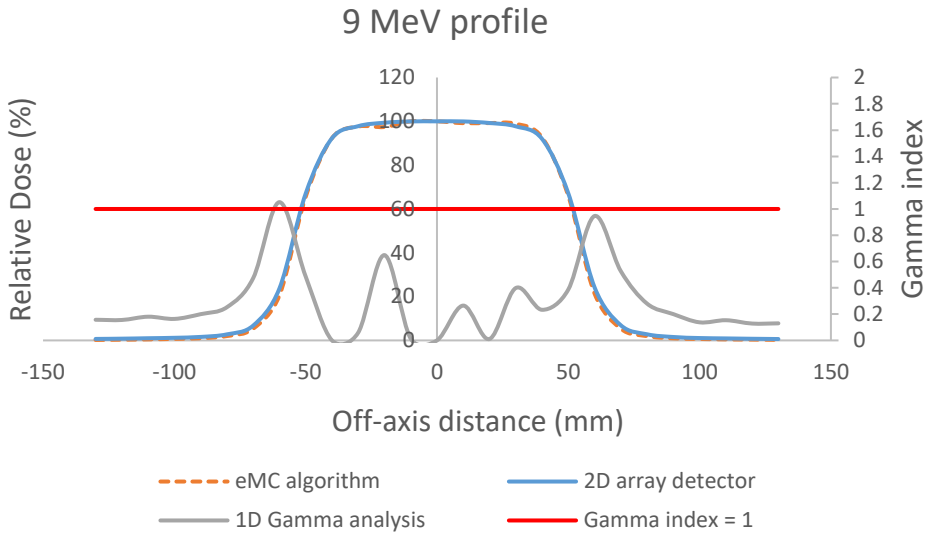
9 MeV profile
Relative Dose (%)
Gamma index
Off-axis distance (mm)
120
100
80
60
40
20
0
2
1.8
1.6
1.4
1.2
1
0.8
0.6
0.4
0.2
0
-150
-100
-50
0
50
100
150
eMC algorithm
2D array detector
1D Gamma analysis
Gamma index = 1

(b)

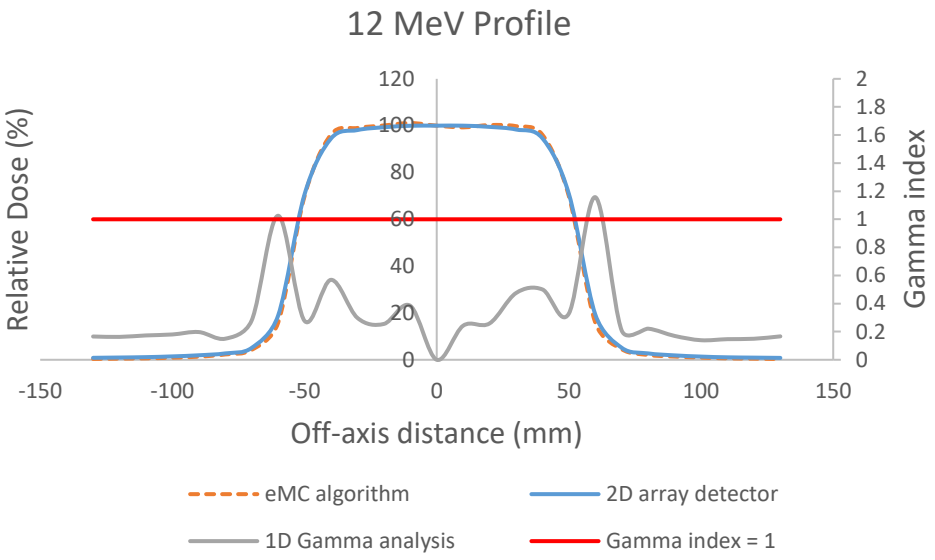

(c)

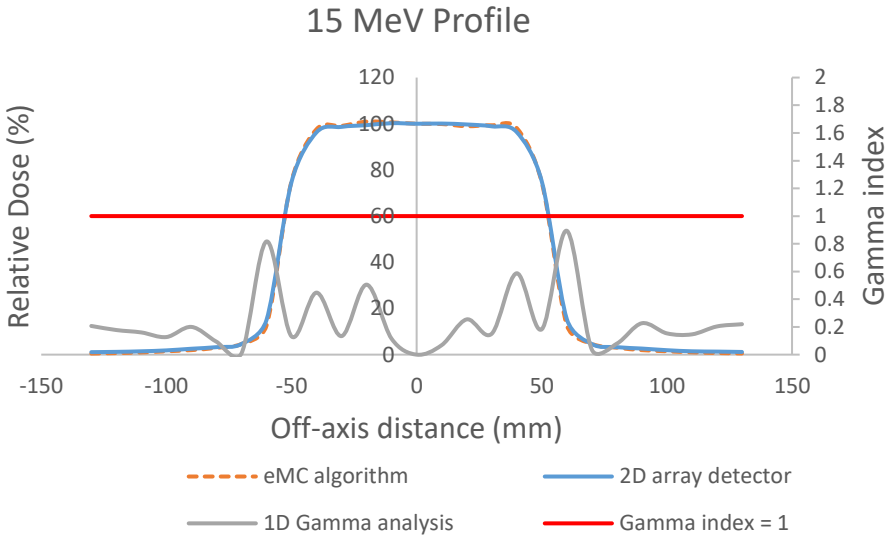

(d)

Figure 4.14: Cross-plane profiles at 100 cm SSD with lung-equivalent material positioned within the 10 cm × 10 cm field, indicating the 1D gamma analysis comparing calculated and measured profiles. (a) 6 MeV profile measured at 1.9 cm depth. (b) 9 MeV profile measured at 2.7 cm depth. (c) 12 MeV profile measured at 2.7 cm. (d) 15 MeV profile measured at 2.7 cm.

Table 4.10: Summary of the 1D gamma analysis comparing calculated and measured cross-plane profiles for different electron beam energies and 1D gamma analysis criteria at 100 cm SSD, with the lung-equivalent material positioned within field.

Energy (MeV)	1D Gamma analysis criteria		
	3 %| 3 mm	4 %| 3 mm	7 %| 3 mm
6	92.6 %	92.6 %	100 %
9	96.3 %	100 %	100 %
12	92.6 %	92.6 %	100 %
15	100 %	100 %	100 %

Bone equivalent material (POP)

Figure 4.15(a) to (d) presents a comparison between cross-plane profiles simulated by the eMC algorithm and those measured using an Octavius detector 1500 in a phantom, where POP and Perspex materials were offset to half of the field, creating an interface along the in-plane axis. The profiles simulated by the eMC algorithm matched the measured profiles when the 7%/3 mm criterion was applied. However, when the 3%/3 mm and 4%/3 mm criteria were applied, less than 90% of the compared relative dose points met the criteria for the 6 MeV beam. The maximum deviation for this profile was 8.6% at an off-axis distance of -60 mm. Similarly, for the 9 MeV beam, 81.5% of the compared relative dose points met the 3%/3 mm criterion, with the maximum deviation at an off-axis distance of -60 mm. Table 4.11 provides the gamma analysis percentages for all beam energies.

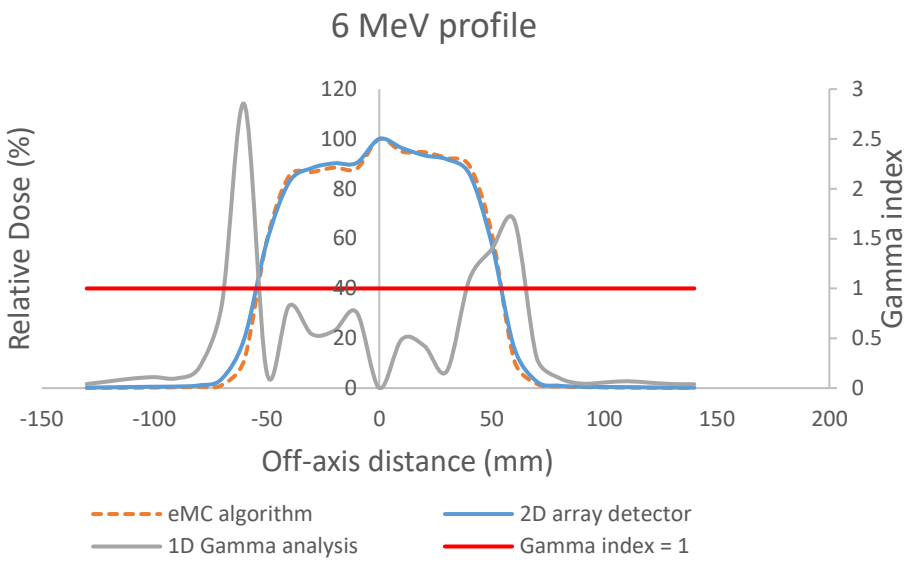
6 MeV profile
Relative Dose (%)
Gamma index
Off-axis distance (mm)
120
100
80
60
40
20
0
3
2.5
2
1.5
1
0.5
0
-150
-100
-50
0
50
100
150
200
eMC algorithm
2D array detector
1D Gamma analysis
Gamma index = 1

(a)

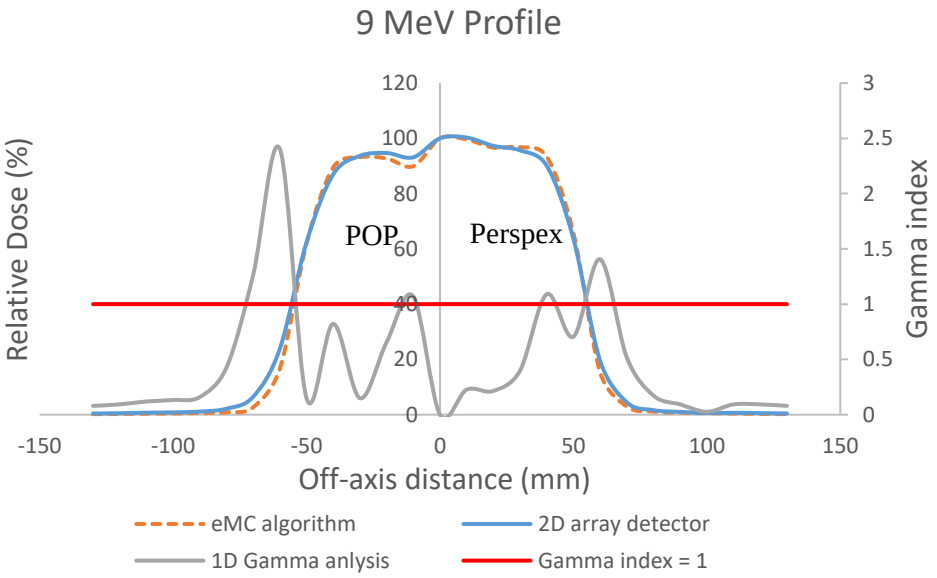
9 MeV Profile
Relative Dose (%)
Gamma index
Off-axis distance (mm)
POP
Perspex
120
100
80
60
40
20
0
3
2.5
2
1.5
1
0.5
0
-150
-100
-50
0
50
100
150
eMC algorithm
2D array detector
1D Gamma anlysis
Gamma index = 1

(b)

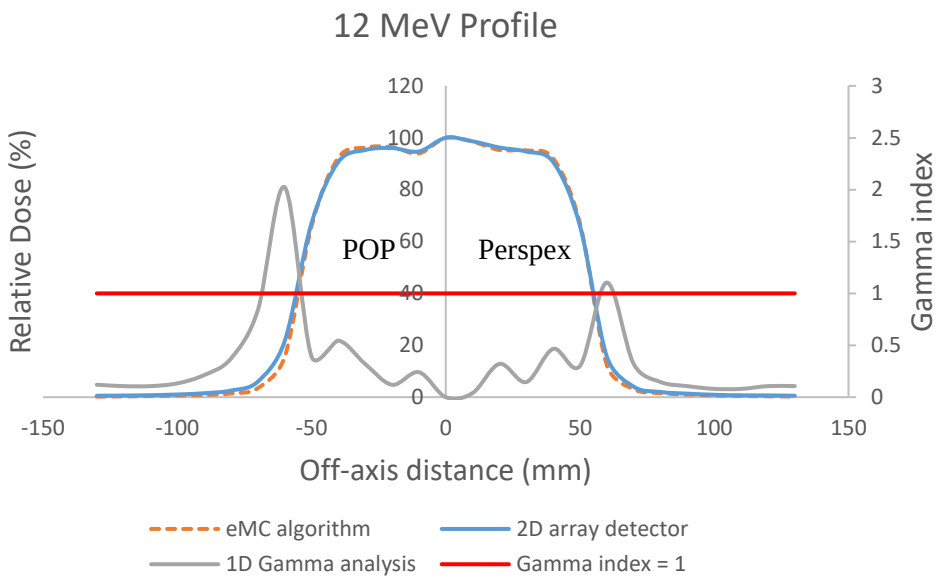

(c)

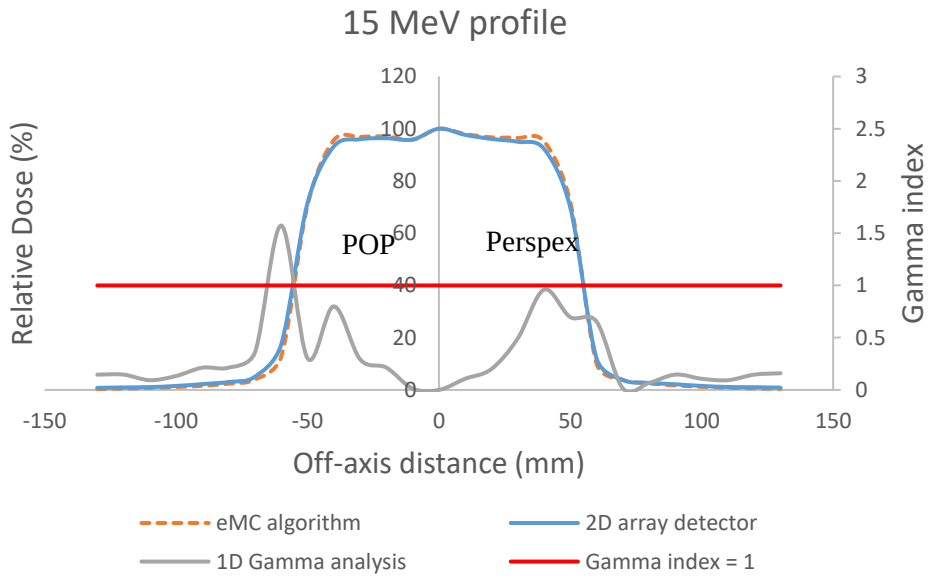

(d)

Figure 4.15: Cross-plane profiles at 100 cm SSD with the POP and Perspex offset to half the field, indicating the 1D gamma analysis comparing computed and measured profiles. The data are normalized to the central axis dose. (a) 6 MeV profile measured at 1.6 cm depth. (b) 9 MeV profile measured at 2.4 cm depth. (c) 12 MeV profile measured at 2.4 cm. (d) 15 MeV profile measured at 2.4 cm depth.

Table 4.11: Summary of the 1D gamma analysis comparing calculated and measured cross-plane profiles for different 1D gamma analysis criteria and beam energies, with POP and Perspex offset to half of the field.

Energy (MeV)	1D Gamma analysis criteria		
	3 %| 3 mm	4 %| 3 mm	7 %| 3 mm
6	85.7 %	88.8 %	96.4 %
9	81.5 %	92.3 %	96.3 %
12	92.6 %	96.3 %	100 %
15	96.3 %	96.3 %	100 %

Figure 4.16(a) to (d) presents a comparison between cross-plane profiles simulated by the eMC algorithm and those measured using an Octavius detector 1500 in a phantom where the POP material was positioned within the 10 cm × 10 cm applicator-defined field. The simulated profiles matched the measured profiles when the 7%/3 mm criterion was applied. However, when the 3%/3 mm and 4%/3 mm criteria were applied, the 9 MeV and 6 MeV profile comparisons did not achieve a confidence level above 90% (see Table 4.12). The maximum deviation in both instances occurred at an off-axis distance of -60 mm and 60 mm.

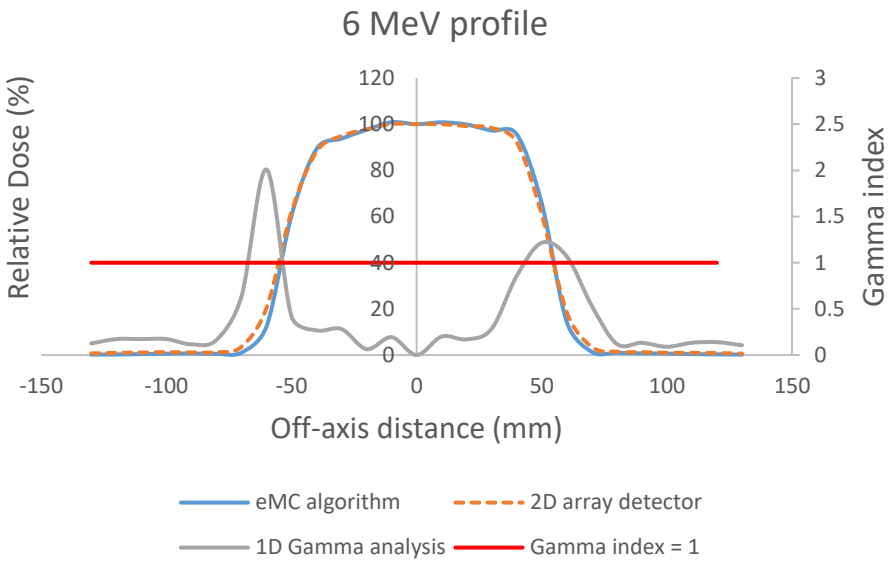
6 MeV profile
Relative Dose (%)
Gamma index
Off-axis distance (mm)
120
100
80
60
40
20
0
3
2.5
2
1.5
1
0.5
0
-150
-100
-50
0
50
100
150
eMC algorithm
2D array detector
1D Gamma analysis
Gamma index = 1

(a)

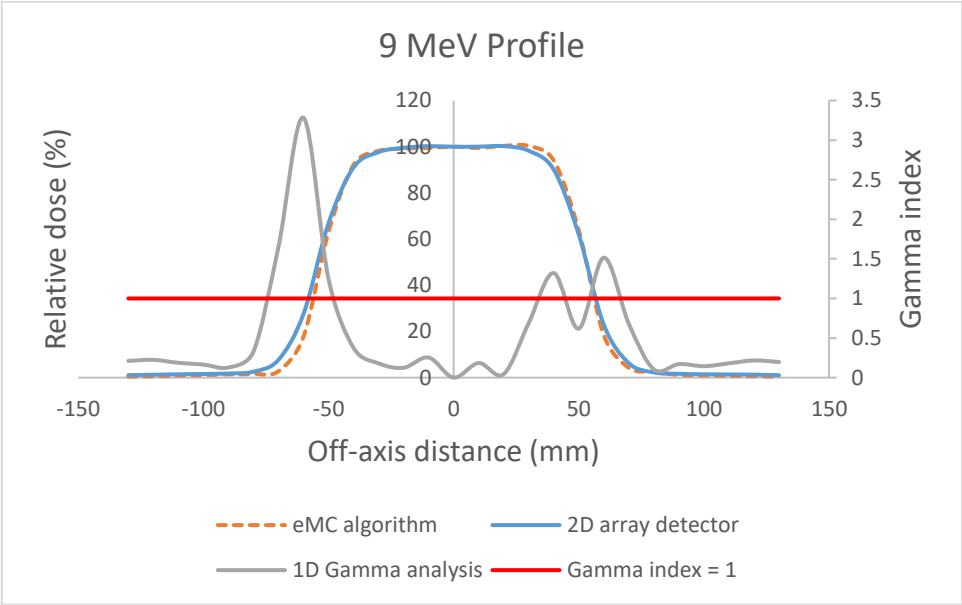
9 MeV Profile
Relative dose (%)
Gamma index
Off-axis distance (mm)
120
100
80
60
40
20
0
3.5
3
2.5
2
1.5
1
0.5
0
-150
-100
-50
0
50
100
150
eMC algorithm
2D array detector
1D Gamma analysis
Gamma index = 1

(b)

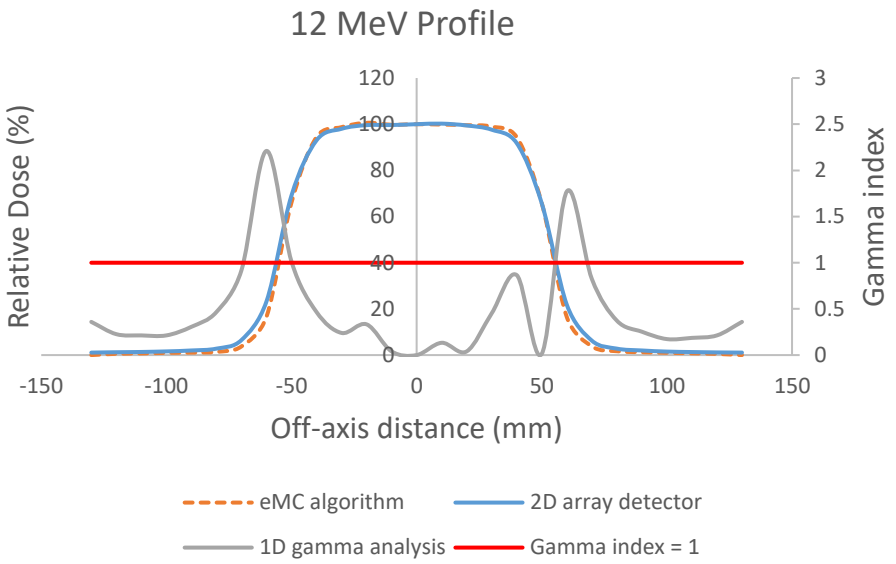

(c)

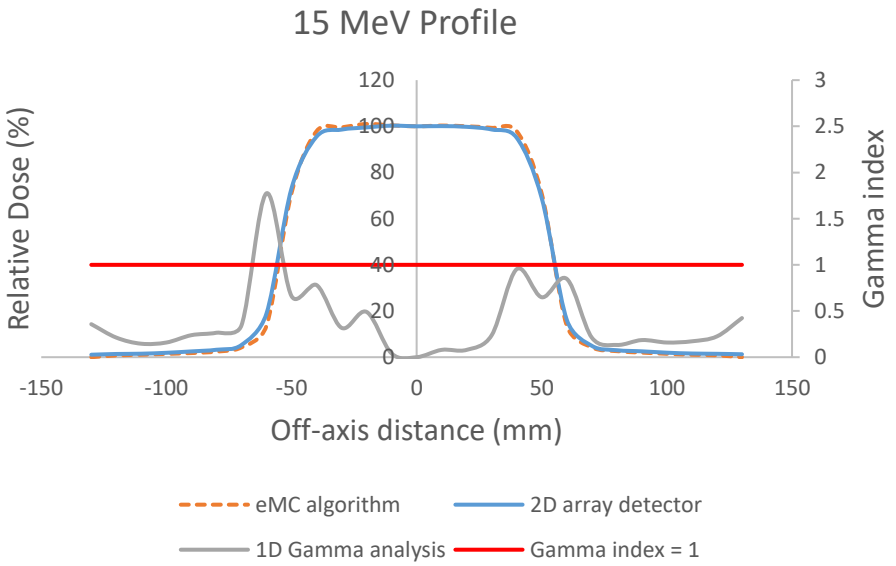

(d)

Figure 4.16: Cross-plane profiles at 100 cm SSD with the POP material positioned within the field, indicating the 1D gamma analysis comparing measured and calculated profiles. (a) 6 MeV profile measured at 1.6 cm depth. (b) 9 MeV profile measured at 2.4 cm depth. (c) 12 MeV profile measured at 2.4 cm. (d) 15 MeV profile measured at 2.4 cm depth.

Table 4.12: Summary of the 1D gamma analysis comparing calculated and measured cross-plane profiles for different beam energies and 1D gamma analysis criteria, with the POP material positioned within the field.

Energy (MeV)	1D Gamma analysis criteria		
	3 %| 3 mm	4 %| 3 mm	7 %| 3 mm
6	85.2 %	88.8 %	96.3%
9	74.0 %	81.5 %	92.6 %
12	92.6 %	92.6 %	100 %
15	96.3 %	96.3 %	100 %

4.2.3. Oblique incidence test

The PDDs calculated by the eMC algorithm at a 20° gantry angle in water, utilizing an applicator sized 10 cm x 10 cm to confine the field at 100 cm SSD, were compared for all beam energies with those measured using the PTW Semiflex 31021 under the same conditions. Figure 4.17(a) to (d) presents a comparison between computed and measured PDDs obtained during the oblique incidence test. The eMC-calculated PDDs agreed with the measurements when the 1D gamma analysis with the 5%/3 mm criterion of tolerance was applied (Huq, et al., 2015). However, when the 3%/3 mm criterion was used, the passing rate exceeded 90% for 9 MeV and 6 MeV beams, reaching 100% for 6 MeV and 96% for 9 MeV, while 12 MeV and 15 MeV achieved 83% and 87%, respectively. The eMC algorithm overestimated the dose by an average of 3.8% between depths of 40 mm and 53 mm for 12 MeV and by 4.1% between depths of 58 mm and 72 mm for 15 MeV. Despite these deviations, the beam quality parameters remained within 2 mm.

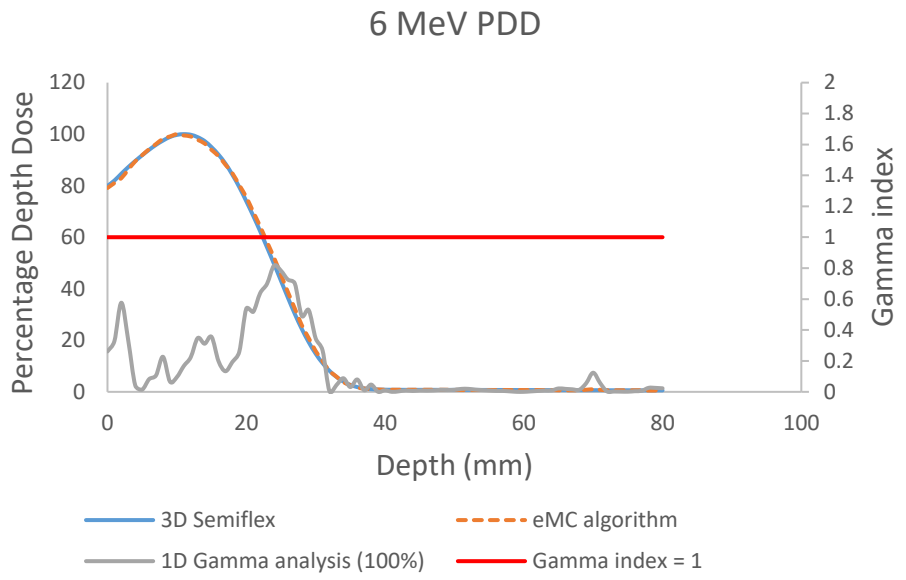
6 MeV PDD
Percentage Depth Dose
Gamma index
Depth (mm)
3D Semiflex
eMC algorithm
1D Gamma analysis (100%)
Gamma index = 1

(a)

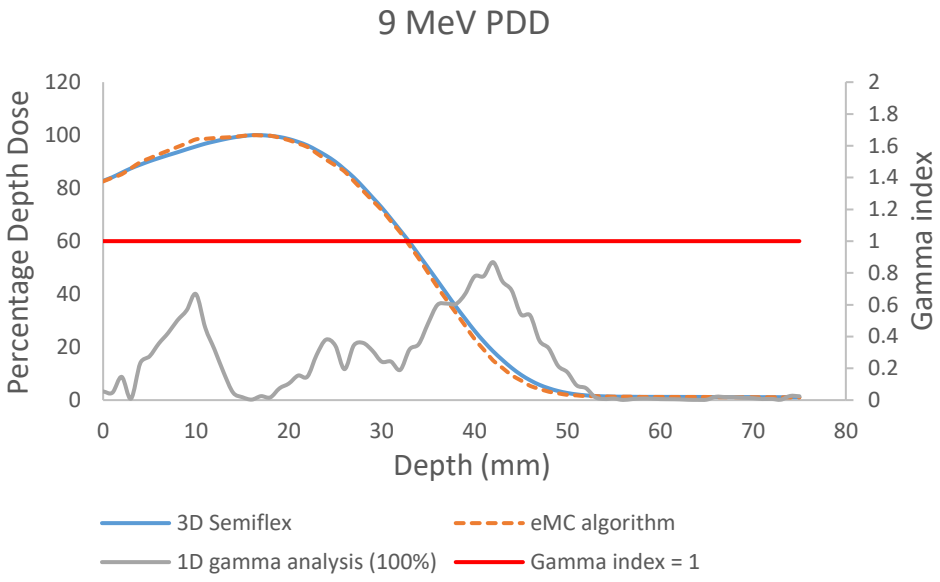
9 MeV PDD
Percentage Depth Dose
Gamma index
Depth (mm)
3D Semiflex
eMC algorithm
1D gamma analysis (100%)
Gamma index = 1

(b)

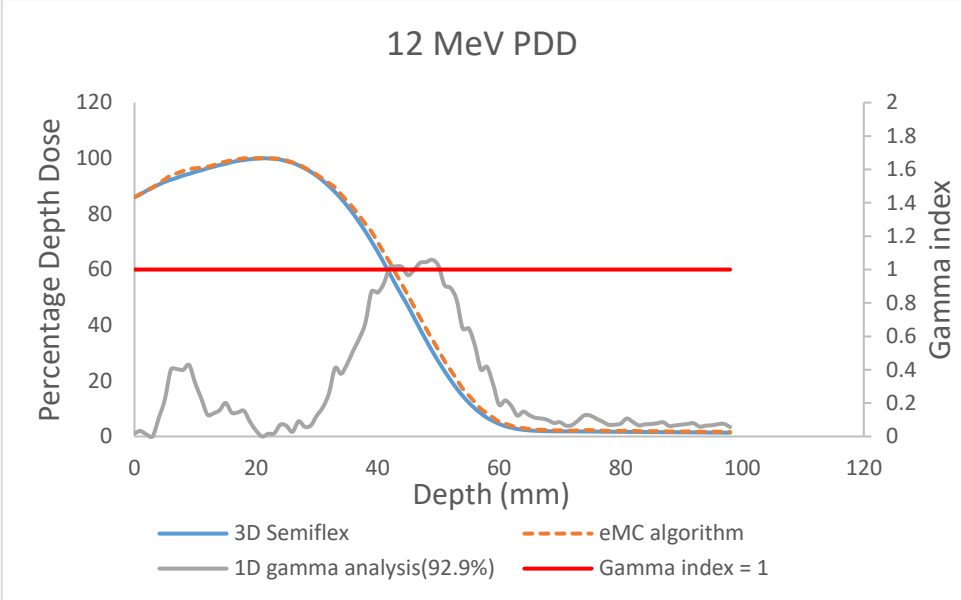

(c)

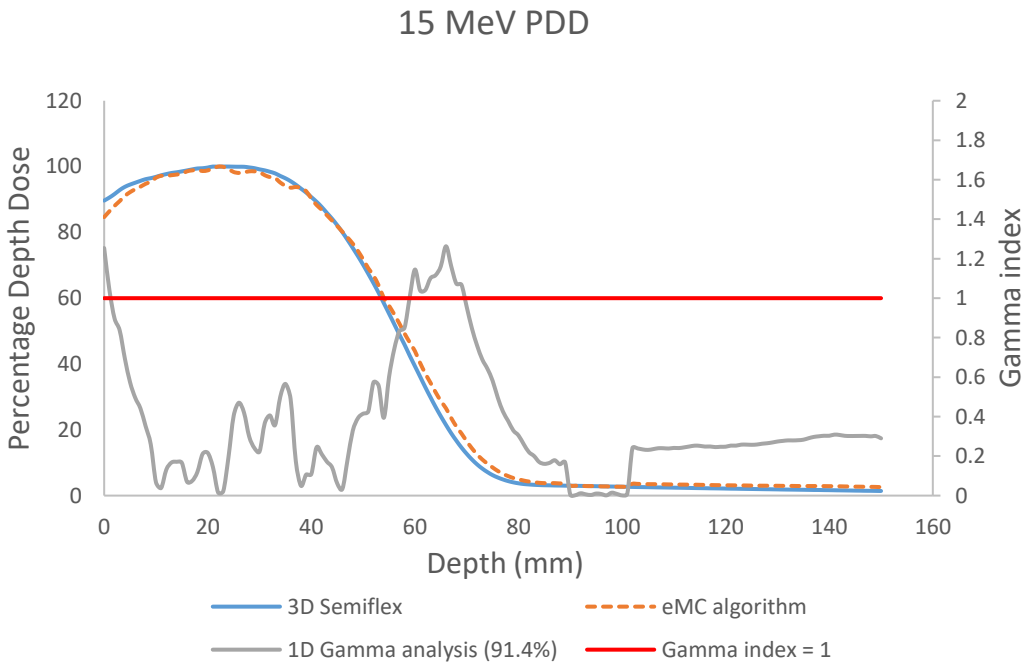

(d)

Figure 4.17: A comparison of computed and measured PDDs in water at a gantry angle of 20 degrees, indicating the percentage difference obtained from 1D gamma analysis. (a) 6 MeV. (b) 9 MeV. (c) 12 MeV. (d) 15 MeV.

Figure 4.18(a) to (d) presents a comparison between measured and computed cross-plane profiles in water at R_{90}, with the gantry angle set to 20°. All profiles met the 5% tolerance

suggested by the AAPM MPPG 5a. However, under the 3%/3 mm criterion, only the 12 MeV profile had 90% of the compared relative dose points within the tolerance range, while 6 MeV, 9 MeV and 15 MeV had 88%, 87% and 86%, respectively. At an off-axis distance of -82 mm to 48 mm, the eMC algorithm underestimated by an average of 8.1% at 9 MeV and 6 MeV, and 7.5% at 15 MeV, which corresponded to a systematic shift of 2mm at the field edge.

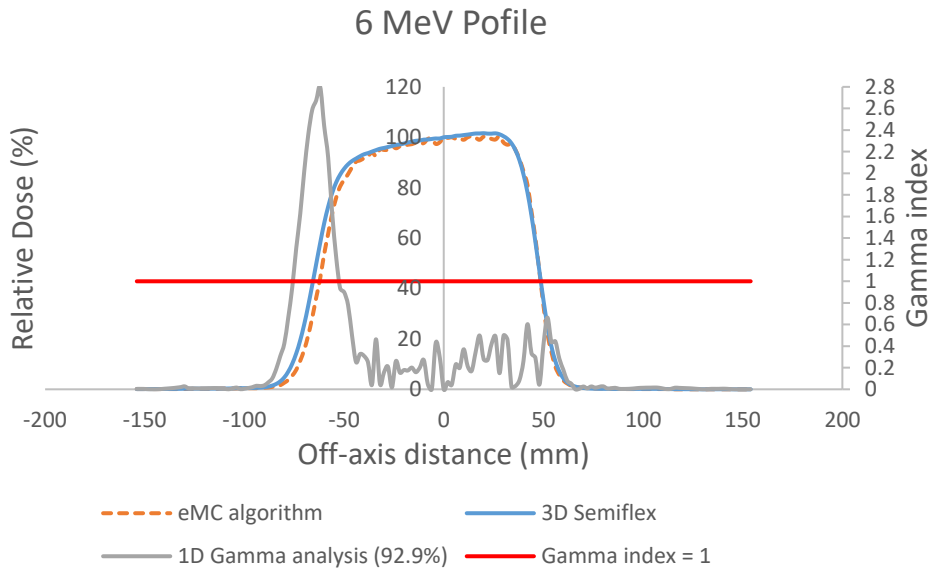

(a)

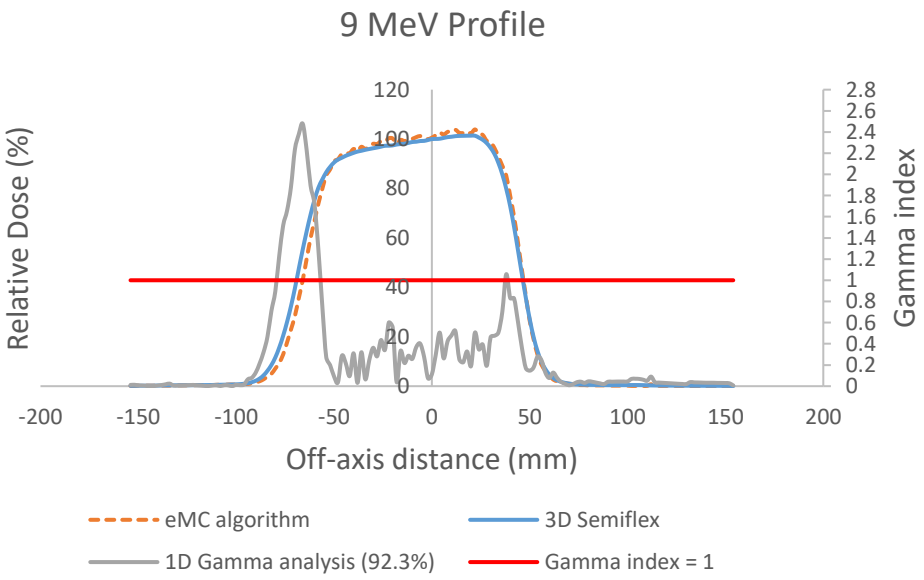

(b)

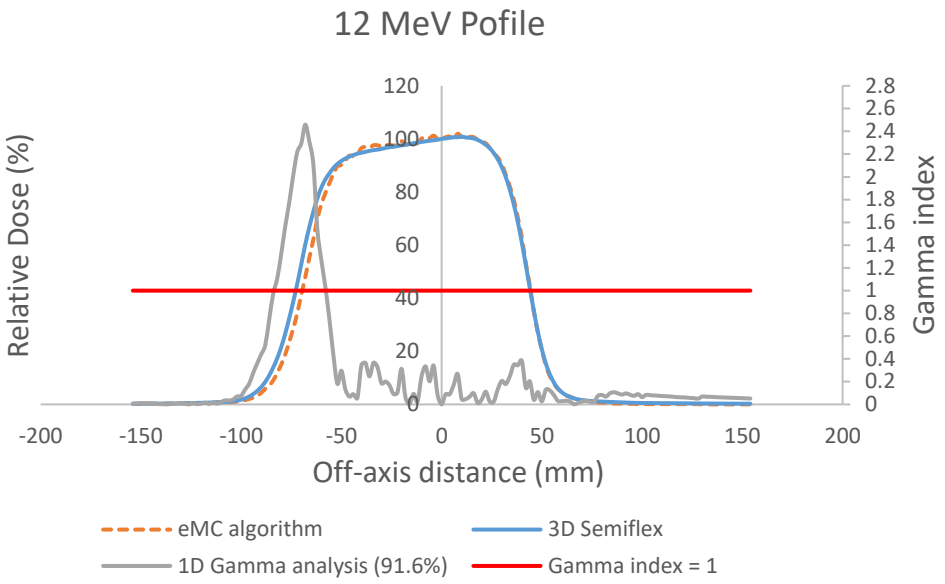

(c)

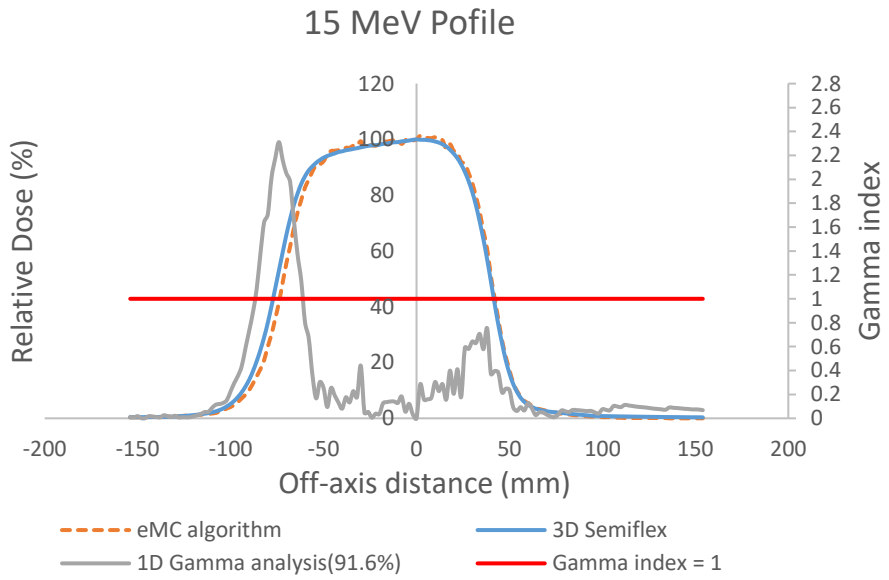

(d)

Figure 4.18: Cross-plane profiles in water at a depth of R_{90}, with the gantry angle set to 20 degrees, indicating the percentage difference obtained from 1D gamma analysis comparing calculated and measured profiles. (a) 6 MeV. (b) 9 MeV. (c) 12 MeV. (d) 15 MeV.

4.3. Input parameters

Grid spacing

The grid spacing for the eMC algorithm was varied from 0.1 cm to 0.8 cm to simulate PDDs in water, which were then compared to the measured PDDs. The number of histories was fixed at 500,000 for all electron beam energies. An applicator sized 10 cm × 10 cm was utilized to confine the field, and the SSD was set to one hundred centimetres. A 1D gamma analysis with 3%/3mm criterion was employed to compare the PDDs. Figure 4.19(a) to (d) presents this comparison for the 9 MeV beam, while Table 4.13 summarizes the 1D gamma analysis for all beam energies when the grid spacing was varied.

For the 9 MeV beam, simulated PDDs from the eMC algorithm agreed with measurements when the grid spacing was between 0.1 cm and 0.5 cm. Similar agreement was observed for the 15 MeV and 12 MeV beam. However, for the 6 MeV beam, agreement with measured PDDs occurred only at 0.15 cm and 0.2 cm grid spacings. When the grid spacing was set to 0.1 cm, the eMC algorithm produced discrepancies, calculating the surface dose in the homogeneous water-equivalent phantom to be 0.0 Gy. This pattern was consistent across all beam energies.

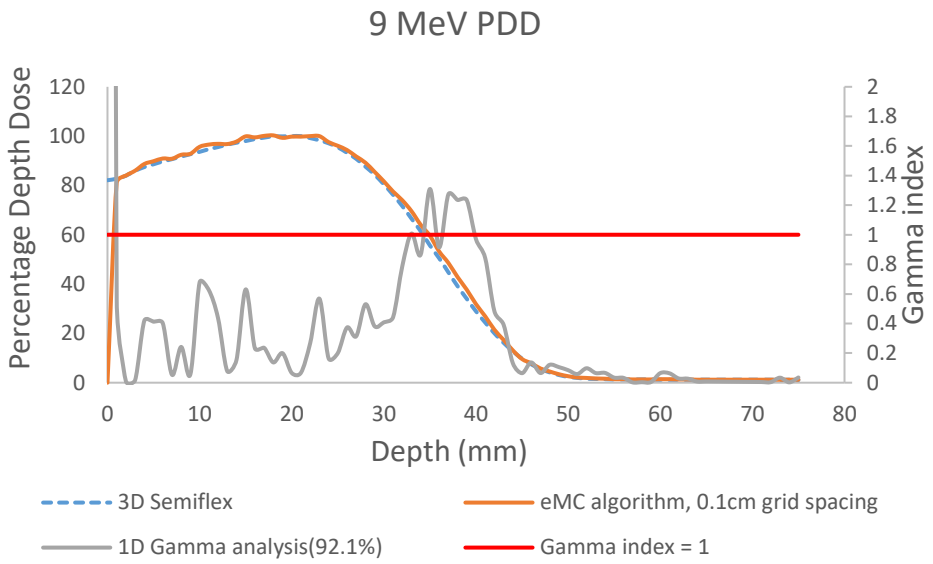
9 MeV PDD
Percentage Depth Dose
Gamma index
Depth (mm)
3D Semiflex
eMC algorithm, 0.1cm grid spacing
1D Gamma analysis(92.1%)
Gamma index = 1

(a)

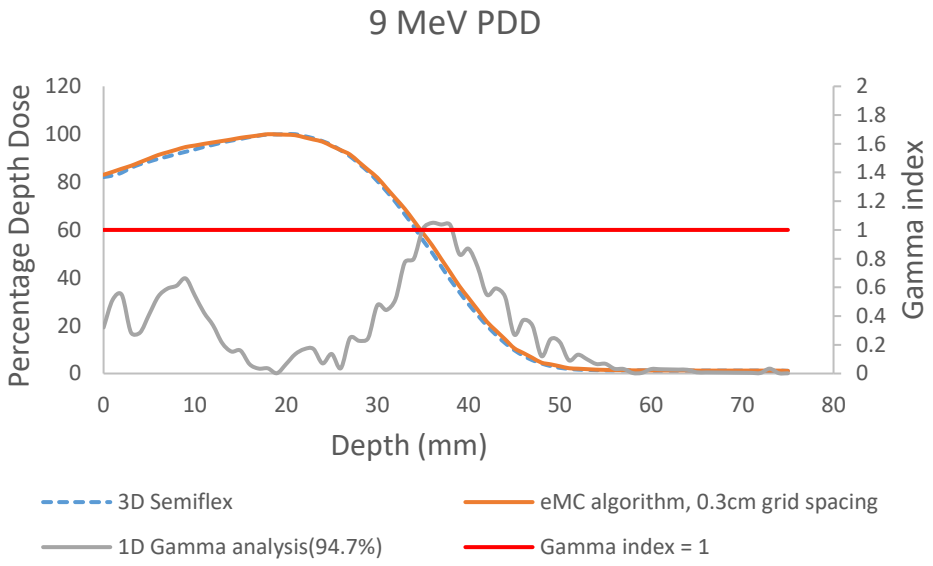
9 MeV PDD
Percentage Depth Dose
Gamma index
Depth (mm)
3D Semiflex
eMC algorithm, 0.3cm grid spacing
1D Gamma analysis(94.7%)
Gamma index = 1

(b)

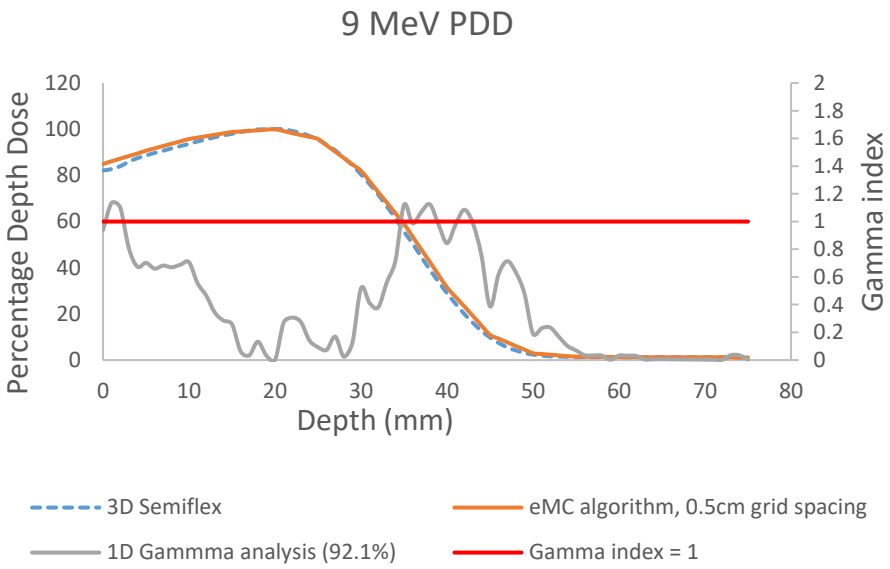

(c)

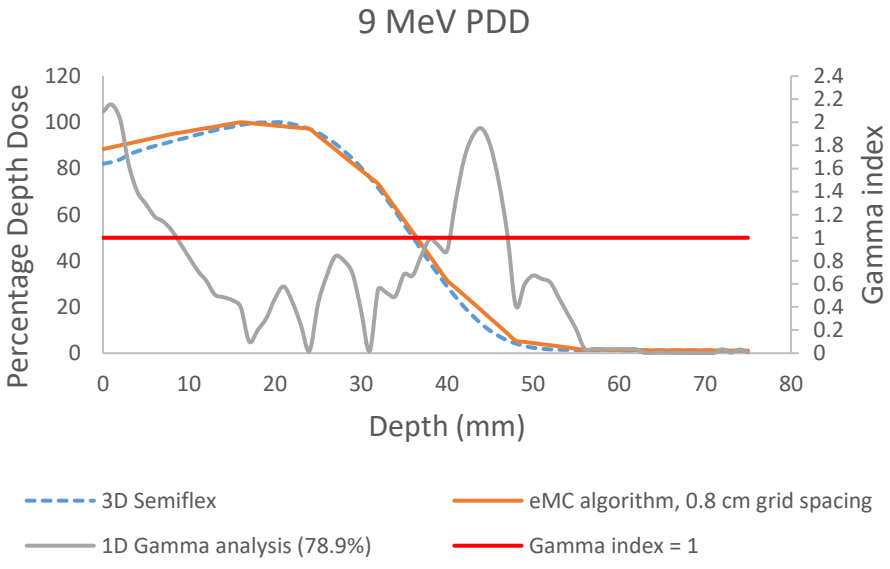

(d)

Figure 4.19: 9 MeV PDDs in water at 100 cm SSD, indicating the percentage difference obtained from 1D gamma analysis comparing computed and measured PDDs for different grid spacings. (a) 0.1 cm grid spacing (b) 0.3 cm grid spacing. (c) 0.5 cm grid spacing. (d) 0.8 cm grid spacing.

Table 4.1: Summary of the 1D gamma analysis comparing measured and computed PDDs for different grid spacings and beam energies.

Grid spacing (cm)	1D Gamma analysis (%)			
	6 MeV	9 MeV	12 MeV	15 MeV
0.10	81 .6	92.1	90.7	78.9
0.15	96.8	100	91.1	96.1
0.20	98.6	94.7	93.4	97.4
0.25	82.9	98.7	90.0	97.4
0.30	82.9	94.7	97.4	98.6
0.40	82.8	100	93.4	100
0.50	75.0	92.0	97.4	94.3
0.60	67.1	88.1	81.5	76.3
0.70	73.7	76.3	78.9	73.6
0.80	65.8	78.9	71.1	77.6

Number of histories

The number of histories varied from 50,000 to one million, with the grid spacing kept constant at 0.2 cm to simulate PDDs with the eMC algorithm. The PDDs were simulated in a water-equivalent phantom, utilizing an applicator sized 10 cm × 10 cm to confine the field, with the SSD set to one hundred centimetres. The simulated PDDs were compared with those measured using a PTW Semiflex 31021, employing a 1D gamma analysis technique with 3%/3 mm criterion. Figure 4.20(a) to (d) presents a comparison between measured and simulated PDDs for the 9 MeV beam. From 50,000 to 200,000 histories, the calculated PDDs did not match the measured PDDs, as the percentage differences were below the 90% confidence level. As the number of histories increased, the levels of noise decreased, and the accuracy improved. This pattern was observed across all beam energies used in this study. Table 4.14 presents the percentage difference obtained from 1D gamma analysis for all electron beam energies. From the table, the 6 MeV PDD comparison achieved a confidence level greater than 90% only when the grid spacing of 0.2 cm and 500,000 histories were used. In contrast, the 12 MeV and 15

MeV PDD comparisons exceeded the 90% confidence level for histories ranging between 200,000 and 1 million.

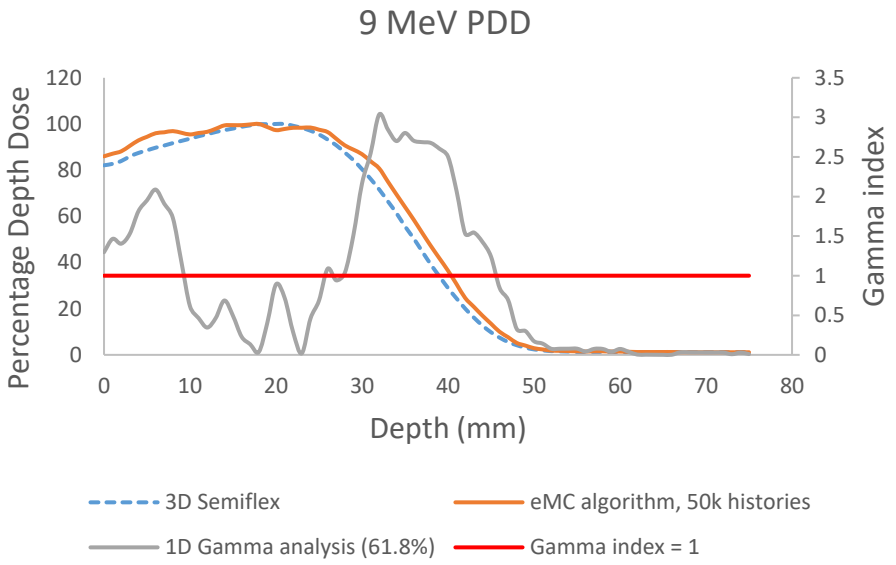

(a)

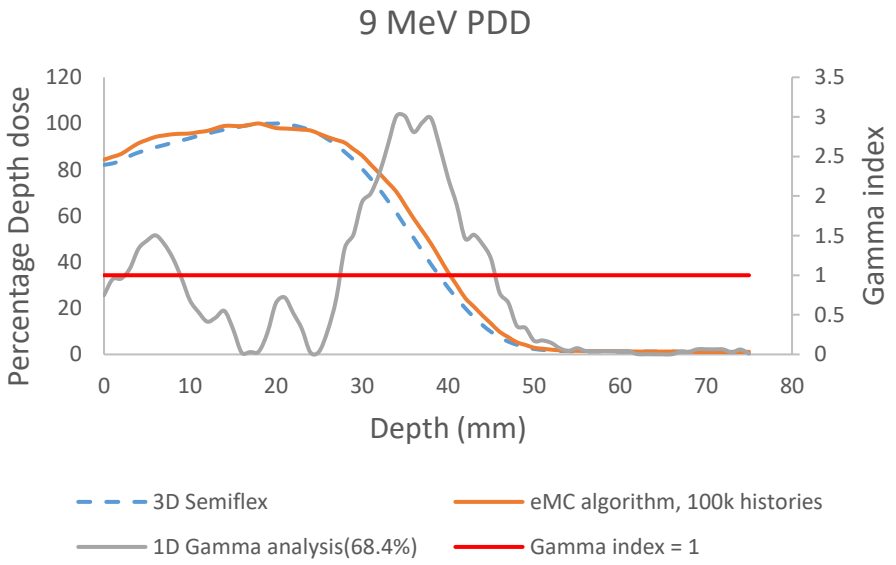

(b)

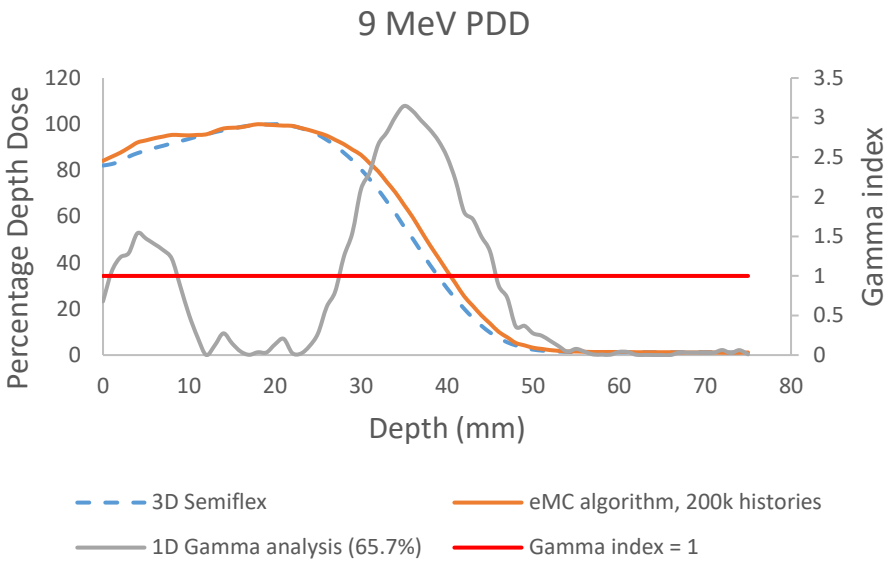

(c)

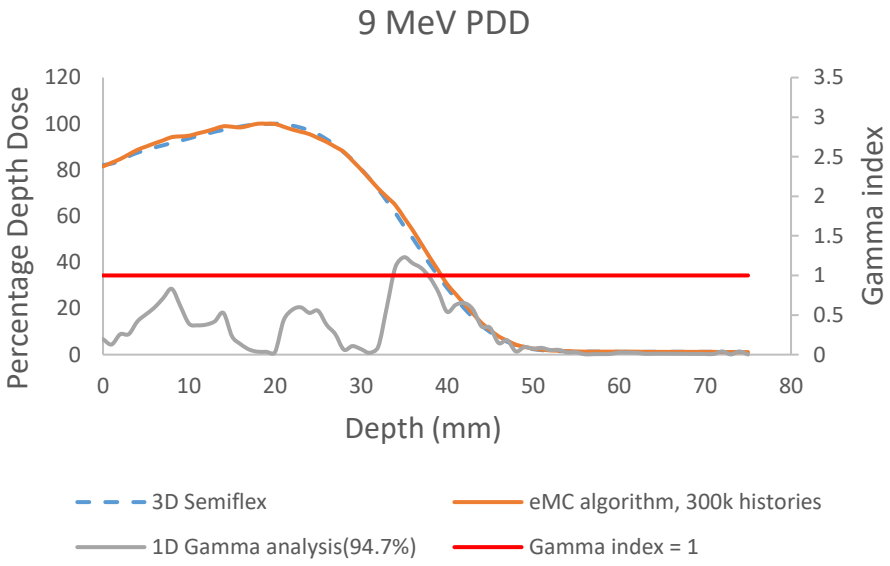

(d)

Figure 4.20: Comparison of measured and computed PDDs in water for the 9 MeV beam, indicating the percentage difference obtained from 1D gamma analysis for different number of histories. (a) 50 000 histories. (b) 100 000 histories. (c) 200 000 histories. (d) 300 000 histories

Table 4.2: Summary of the 1D gamma analysis comparing calculated and measured PDDs for different electron beam energies and number of histories.

Number of histories	1D Gamma analysis (%)			
	6 MeV	9 MeV	12 MeV	15 MeV
50000	80.3	61.8	88.2	63.2
100000	84.2	68.4	81.6	73.7
200000	85.5	65.8	93.4	92.1
300000	84.2	94.7	90.1	94.1
400000	84.8	94.7	92.1	94.1
500000	98.6	94.7	93.4	97.4
600000	84.2	93.4	93.4	93.1
700000	84.2	92.1	94.7	96.0
800000	84.2	92.1	92.1	97.0
900000	82.9	93.4	92.1	97.0
1000000	84.2	93.4	93.4	97.0

5. Discussion

Commissioning and validation of dose calculation algorithms are essential to ensure accurate dose calculation in clinical practice. The transition from manual dose calculations and pencil beam algorithms to MC algorithms offers enhanced accuracy in dose calculation, as MC algorithms are considered to be more accurate (Snyder, et al., 2019). However, all TPS algorithms should be validated before clinical use to determine their limitations. This study aimed to commission the eMC algorithm integrated into the Elekta Monaco (version 6.1.2) TPS by evaluating the functionality of the algorithm in homogeneous and inhomogeneous phantoms, in accordance with the AAPM MPPG 5a (Huq, et al., 2015). This was achieved by validating the beam data used for beam modelling and performing three additional validation tests: model verification, oblique incidence and heterogeneity tests. According to the AAPM Task Group Report 106, discrepancies between beam data measured by different physicists should be less or equal to one percent (AAPM, 2008). The CMJAH beam data were compared to the measured beam data utilising 1D gamma analysis with 2%/2 mm criterion. The results demonstrated that there was agreement to within 2% in the measured PDDs and profiles both in air and water (see figure 4.1 to 4.6). The overall comparability of the entire beam data set was 98.9%.

Chamberland et al. (2015) and Cygler et al. (2004) compared the performance of dose computation algorithms, specifically the eMC and pencil beam algorithms, in calculating dose distributions in homogeneous water-equivalent phantoms. Chamberland et al. used the Macro Monte Carlo (MMC) algorithm, whereas this study used VMC++. The calculated PDDs and profiles were compared to the measured data, and neither algorithm demonstrated superiority over the other, as both produced accurate dose calculations under the tested conditions. In both studies, the calculated PDDs and profiles matched the measured data to within 3%. These results align with the findings of this study, as the measured and computed profiles and PDDs in water matched within 3%. However, deviations were observed for the 15 MeV beam with the irregular trapezoid cutout at 110 cm and 100 cm SSD, with a maximum deviation of 4.2%. The reasons for these deviations are unknown, but this could be due to the loss of scattering equilibrium and the absence of beam data for field sizes below 6 cm x 6 cm during beam modelling. Additionally, Xu et al. (2009) evaluated the performance of the eMC algorithm (MMC) in calculating dose distributions for small fields in a homogeneous water-equivalent phantom. The eMC algorithm demonstrated greater accuracy (2.5%) in calculating doses for

small fields compared to earlier algorithms, including the pencil beam algorithm. This suggests that while both algorithms perform similarly in water for field sizes above 6 cm x 6 cm, the eMC algorithm provide greater accuracy for small-field dose calculations.

Snyder et al. (2019) compared output factors computed by the eMC algorithm (VMC++) with measured values in water for the same beam energies and applicators used in this study. The computed output factors matched the measured values within 2% for all electron beam energies and applicators. Similarly, Huang et al. (2019) reported that eMC-computed output factors matched the measured values within 2% for all applicators and beam energies. However, discrepancies were observed for small fields, particularly for the 6 MeV beam, with a maximum error of 9.8%. These errors were attributed to a loss of side scatter equilibrium and limitations within the TPS (Huang, et al., 2019). Huang et al. used a RayStation TPS, which like the Monaco TPS used here, does not permit users to input measured output factors, as is possible with the Pinnacle TPS. The findings of both studies were consistent with the results of this study, as the computed matched the measured values to within 2% for all applicators and beam energies at 110 cm and 100 cm SSD. However, for the trapezoid cutout, the output factor comparison exceeded the 2% tolerance at 100 cm SSD for 9 MeV and 6 MeV, and for 6 MeV, 12 MeV and 15 MeV at 110 cm SSD, with a maximum deviation of 6.53%; this can also be attributed to the loss of scattering equilibrium.

Ding et al. (2005) compared measured output factors to those computed utilizing the eMC algorithm (MMC) and the pencil beam algorithm in water at both standard and extended SSDs for all electron beam energies. The eMC algorithm outperformed the pencil beam algorithm in calculating output factors. Specifically, the pencil beam algorithm accurately calculated output factors for high energies (18 MeV), but for beam energies of 12 MeV and 6 MeV, errors greater than 10% occurred. These errors were due to the algorithm overestimating the effect of scatter, particularly for elongated fields. Additionally, the pencil beam algorithm was more accurate in calculating dose distributions than the eMC algorithm for gantry angles of 30° at extended SSDs. The inaccuracies in the eMC algorithm resulted from the use of large grid spacing (0.49 cm), which introduced systematic uncertainties and affected the accuracy of the results (Ding, et al., 2005). This research found that the calculated profiles and PDDs at the gantry angle of 20° in water matched the measured data to within 5%, which did not align with the findings of Ding et al. but corresponded with the findings of Huang et al. (2019). An offset of 2mm in the penumbra regions nearest to the gantry was observed at all energies, which could be attributed

to a systematic geometric setup error during the measurement or deficiencies in the modelling of the applicator endface.

Additionally, Ding et al. (2005) compared the performance of the pencil beam algorithm and the eMC algorithm in the presence of inhomogeneities. The eMC algorithm computed accurate dose distributions for adjacent inhomogeneities, while the pencil beam algorithm struggled to predict large dose perturbations near the edges of inhomogeneities. Similarly, Chamberland et al. (2015) compared calculated dose distributions by these two algorithms with those measured using film. The eMC algorithm calculated dose distributions that match the film measurements for lung tissue, with a discrepancy of only 4%. In contrast, the pencil beam algorithm could not accurately predict dose perturbations caused by small inhomogeneities, especially in low-density materials, where the algorithm failed to model electron scattering effectively. This study used low-density polystyrene (lung equivalent) and solid POP (bone equivalent) for the heterogeneity test. Two setups were tested: one with the inhomogeneity positioned entirely within the field, with water equivalent buildup and backscatter (Perspex) and another where the inhomogeneity and Perspex were offset to half of the field, to create an interface along the in-plane axis. A 1D gamma analysis with a 7%/3 mm criterion was employed to compare measured and computed cross-plane profiles, and the percentage difference was above 90% for all electron beam energies. This was consistent with the studies referenced above. However, when the 3%/3 mm criterion was applied, the percentage difference remained above 90% for lung-equivalent material but dropped below 90% for bone-equivalent material at 6 MeV and 9 MeV beams (see table 4.9 to 4.12). The reasons for these discrepancies are unknown but the eMC algorithm struggled to compute accurate doses in low-dose regions, particularly at off-axis distances of ±60 mm, which may be due to calculation uncertainties related to grid spacing size.

Popple et al. (2006) recommended that the grid spacing for an eMC algorithm should be set to "0.1 cm for 6 MeV, 0.15 cm for 9 MeV, 0.2 cm for 12 MeV and 0.25 cm for 15 MeV" to ensure accurate dose calculation. The results of this study were consistent with recommendations for the 15 MeV, 12 MeV and 9 MeV beams (see Table 4.13), as the percentage difference obtained from the 1D gamma analysis using 3%/3mm criterion to compare calculated and measured PDDs in water, was above 90%. However, this was not the case for 6 MeV, as the percentage difference fell below the 90% pass rate. Setting the grid spacing to 0.1 cm for 6 MeV resulted in inaccurate dose estimation on the phantom surface, as the algorithm estimated surface dose to be 0.00 Gy. This issue was observed for all electron beam energies. Unlike Popple et al.,

Huang et al. (2019) recommended setting the grid spacing to 0.2 cm and the number of histories to 500,000 to ensure accurate dose calculations when using the eMC algorithm (VMC++) for all electron beam energies. The findings of this research were consistent with this recommendation, as the percentage difference from the 1D gamma analysis exceeded 90% for all beam energies when comparing the calculated and measured PDDs in water utilizing the 3%/3 mm criterion. When the number of histories varied from 50,000 to one million, the eMC-calculated PDDs agreed to within 3% of the measured PDDs when the number of histories was set to 300,000 and above. This agreement was observed for 9 MeV, 12 MeV and 15 MeV beams. However, for 6 MeV beam, the 1D gamma analysis percentage exceeded 90% only when a minimum of 500,000 histories was used.

The uncertainties associated with MC calculations arise from several sources: particle sampling statistics, beam source modeling, CT to density conversion, voxelization, transport model approximations and cross section libraries (Reynaert, et al., 2006). The overall standard uncertainty of MC algorithm is estimated at 2 % to 3 % (Reynaert, et al., 2006). The uncertainties associated with the PTW Semiflex 31021 3D chamber arise from the calibration coefficient, temperature and pressure, ion recombination, polarity effects, positioning accuracy, electrometer precision and volume averaging in dose gradients. To determine the combined uncertainty between VMC++ and the Semiflex detector, the independent standard uncertainties, namely the VMC++ statistical uncertainty, the Semiflex measurement error, the depth positioning error and the normalization or setup variation were summed in quadrature. This resulted in a combined uncertainty of approximately 2.3 %. Under this combined uncertainty, 91 % of the compared PDDs and profiles in water met the one dimensional gamma analysis criterion of 3 % /3 mm. Similarly, when combining the uncertainties of the PTW Octavius detector 1500 with those of VMC++, the resulting total uncertainty was 2.5 %. Under this uncertainty, 100 % of the beam profiles calculated by VMC++ and those measured met the 7 %/3 mm criterion recommended by the AAPM MPPG 5a (Huq, et al., 2015), while 69 % met the stricter 3 %/3 mm criterion. The uncertainty related to CT to density conversion may explain the dose deviations computed by the algorithm in heterogeneous media such as bone and lung, where the maximum deviation occurred in the umbra region.

The limitations of this study, particularly when performing the model verification test, was the process of generating PDDs, profiles and output factors. These were generated manually by inserting points of interest within the calculated dose distribution. During this process, it was challenging to accurately identify the location at which the dose distribution begins on the

surface and to pinpoint the exact location of the peak dose along the central axis of the beam. A dedicated software application developed by Elekta, which automates the generation of output factors, profiles and PDDs, is now available and should be integrated into the Monaco TPS for improved efficiency and accuracy during commissioning. Additionally, the Octavius detector 1500 used to measure profiles during the inhomogeneity tests provided planar dose distributions only at a specified depth rather than a comprehensive transverse dose distribution within the entire phantom. This limitation made identifying the exact position of the actual cold and hot spots impossible, as these could occur at different depths for each energy. The Octavius detector 1500 has a thick housing, which makes placement in certain depths in the phantom difficult. Unlike the Octavius detector 1500, high-resolution film can be positioned easily (and at several depths) in a slab phantom, allowing for a more comprehensive dose distribution measurement.

Future evaluations of the eMC algorithm at CMJAH could focus on fields smaller than 6 cm x 6 cm for all shapes, which were not addressed in this study. Further investigations could also explore the algorithm's performance in more complex phantoms. Additionally, simultaneous variation of grid spacing and histories could be examined to identify optimal combinations.

6. Conclusion

This study validated and commissioned the eMC algorithm integrated into the Elekta Monaco TPS (version 6.1.2) in accordance with the AAPM MPPG 5a (Huq, et al., 2015). The CMJAH beam data agreed to within 2% with the measured beam data, and model verification tests conducted in a homogeneous water-equivalent phantom confirmed accurate calculations of PDDs, profiles and output factors for all applicators and beam energies at standard and extended SSDs. The oblique incidence and heterogeneity tests further demonstrated the use of the algorithm under these conditions. The use of the algorithm for applicator inserts smaller than 6 cm x 6 cm is not advised, and a more extensive study is needed for small field sizes. The optimal input parameter settings were determined to be 0.2 cm grid spacing and 500,000 histories to optimize the accuracy of dose distributions at all beam energies.

References

AAPM, 1994. *Physical Aspects of Quality Assurance in Radiation Therapy (Report No. 13).* [Online]
Available at: https://www.aapm.org/pubs/reports/rpt_13.pdf
[Accessed 20 January 2024].

AAPM, 2004. *Tissue Inhomogeneity Correction for Megavoltage Photon Beams (Report No. 85),* College Park, MD: American Association of Physicists in Medicine.

AAPM, 2008. Accelerator beam data commissioning equipment and procedures: Report of TG-106 of the Therapy Physics Committee of the AAPM. *Medical Physics,* 35(9), pp. 4186–4215.

AAPM, 2009. *Recommendations for clinical electron beam dosimetry: The report of TG-70. Supplement to the recommendations of Task Group 25 (Report No. 70),* College Park, MD: American Association of Physicists in Medicine.

Ali, I., Alsbou, N. & Ahmad, S., 2022. Quantitative evaluation of dosimetric uncertainties in electron therapy by measurement and calculation using the electron Monte Carlo dose algorithm in the Eclipse treatment planning system. *Applied Clinical Medical Physics,* 23(1), p. e13478.

Amestoy, W., 2015. *Review of medical dosimetry: A study guide.* 1st ed. New York: Springer.

Amjad, H. & Muhammad, W., 2017. Treatment planning in radiation therapy. In: *An introduction to medical physics.* Cham, Switzerland: Springer International Publishing, pp. 63–115.

Andreo, P., 1991. Monte Carlo techniques in medical radiation physics. *Physics in Medicine and Biology,* 36(7), pp. 861–920.

Andreo, P., 2018. Monte Carlo simulation in radiotherapy dosimetry. *Radiation Oncology,* 13(1), p. 121.

Aubry, J. F., Bouchard, H., Bessières, I. & Lacroix, F., 2011. Validation of an electron Monte Carlo dose calculation algorithm in the presence of heterogeneities using EGSnrc and radiochromic film measurements. *Journal of Applied Clinical Medical Physics,* 12(4), pp. 2-14.

Bedford, J. L., Nilawar, R., Nill, S. & Oelfke, U., 2022. A phase space model of a Versa HD linear accelerator for application to Monte Carlo dose calculation in real-time adaptive workflow. *Applied Clinical Medical Physics,* 23(9), p. e13732.

Beilajew, A., 2013. History of Monte Carlo. In: J. Seco & F. Verhaegen, eds. *Monte Carlo techniques in radiation therapy.* Boca Raton, FL: CRC Press, pp. 14-28.

Carolan, M. G., 2010. *Pencil beam algorithm.* [Online]
Available at: https://radonc.wdfiles.com/local--files/pencil-beam-algorithm/PencilBeamDoseCalculationAlgorithm.pdf
[Accessed 25 October 2024].

Chamberland, E., Beaulieu, L. & Lachance, B., 2015. Evaluation of an electron Monte Carlo dose calculation algorithm for treatment planning. *Journal of Applied Clinical Medical Physics,* 16(3), pp. 60–79.

Chetty, I. J., Curran, B. & Cygler, J., 2007. Report of the AAPM Task Group No. 105: Issues associated with clinical implementation of Monte Carlo-based photon and electron external beam treatment planning. *Medical Physics,* 34(12), pp. 4818–4853.

Chowdhary, M., Chhabra, A., Kharod, S. & Marwaha, G., 2016. Total skin electron beam therapy in the treatment of mycosis fungoides: A review of conventional and low-dose regimens. *Clinical Lymphoma, Myeloma & Leukemia,* 16(10), pp. 580–586.

Clement, M., 2018. Monaco treatment planning system tools and optimization processes. *Medical Dosimetry,* 43(2), p. 106–117.

Cygler, J. E., Daskalov, G. M., Chan, G. H. & Ding, G., 2004. Evaluation of the first commercial Monte Carlo dose calculation engine for electron beam treatment planning. *Medical Physics,* 31(1), pp. 142–153.

Cygler, J. E. et al., 2005. Clinical use of a commercial Monte Carlo treatment planning system for electron beams. *Physics in Medicine and Biology,* 50(20), pp. 1031–1046.

Ding, G. X. et al., 2005. A comparison of electron beam dose calculation accuracy between treatment planning systems using either a pencil beam or a Monte Carlo algorithm. *International Journal of Radiation Oncology, Biology, Physics,* 63(2), pp. 622–633.

Duong, T. T. et al., 2023. An open-source software for calculating 1D gamma index in radiation therapy. *Saudi Journal of Biological Sciences,* 35(10), pp. 29–37.

Ebert, M. A. & Goodall, S. K., 2020. Recommended dose voxel size and statistical uncertainty parameters for precision of Monte Carlo dose calculation in stereotactic radiotherapy. *Applied Clinical Medical Physics,* 21(12), pp. 120-130.

Ekstrand, K. E. & Dixon, R. L., 1982. The problem of obliquely incident beams in electron-beam treatment planning. *Medical Physics,* 9(2), pp. 276-278.

Ferretti, A., Martignano, A., Simonato, F. & Paiusco, M., 2014. Validation of a commercial TPS based on the VMC(++) Monte Carlo code for electron beams: Commissioning and dosimetric comparison with EGSnrc in homogeneous and heterogeneous phantoms. *Physics in Medicine and Biology,* 30(1), pp. 25–35.

Fraass, B. A. & James, S., 2003. Summary and recommendations of a National Cancer Institute workshop on issues limiting the clinical use of Monte Carlo dose calculation algorithms for megavoltage external beam radiation therapy. *Medical Physics,* 30(12), pp. 3206–3216.

Gardner, J. K., 2005. *Integration of VMC++ into a Commercial Treatment Planning System.* [Online]
Available at: http://scholarscompass.vcu.edu/etd
[Accessed 10 April 2023].

Herwiningsih, S., 2017. *Dosimetric verification of stereotactic body therapy treatment plans for early stage non-small cell lung cancer using Monte Carlo simulation.* [Online]

Available at: https://eprints.qut.edu.au/109755/1/Sri_Herwiningsih_Thesis.pdf
[Accessed 22 February 2025].

Huang, J. Y., Dunkerley, D. & Smilowitz, J., 2019. Evaluation of a commercial Monte Carlo dose calculation. *Journal of Applied Clinical Medical Physics,* 20(6), pp. 184-193.

Huq, M. S. et al., 2015. AAPM Medical Physics Practice Guideline 5.a: Commissioning and QA of treatment planning dose calculations—Megavoltage photon and electron beams. *Applied Clinical Medical Physics,* 16(5), pp. 14-34.

IAEA, 2004. *Commissioning and quality assurance of computerized planning systems for radiation treatment of cancer,* Vienna: IAEA.

IAEA, 2006. Commissioning and quality assurance of computerized planning systems for radiation treatment of cancer (Technical Reports Series No. 430). *Medical Physics,* 33(2), pp. 561-661.

IAEA, 2024. *Absorbed dose determination in external beam radiotherapy: Technical Reports Series No. 398,* Vienna: International Atomic Energy Agency.

Imad, A. & Alsbou, N. S., 2021. Quantitative evaluation of dosimetric uncertainties in electron therapy by measurement and calculation using the electron Monte Carlo dose algorithm in the Eclipse treatment planning system. *Journal of Applied Clinical Medical Physics,* 23(1), p. e13295.

Jabbari, K., 2012. Review of fast Monte Carlo codes for dose calculation in radiation therapy treatment planning. *Journal of Medical Signals and Sensors,* 2(2), pp. 61–72.

Kawrakow, I., 2001. VMC++: Electron and photon Monte Carlo calculations optimized for radiation treatment planning. In: A. Kling, et al. eds. *Advanced Monte Carlo for Radiation Physics, Particle Transport Simulation and Applications.* Berlin: Springer, pp. 229-236.

Kawrakow, I. & Fippel, M., 2000. *VMC++: A Monte Carlo algorithm optimized for electron and photon beam dose calculations for radiation treatment planning. In: Proceedings of the 22nd Annual International Conference of the IEEE Engineering in Medicine and Biology Society (EMBS).* Chicago, Engineering in Medicine and Biology Society.

Kawrakow, I., Fippel, M. & Friedrich, K., 1996. 3D electron dose calculation using a voxel-based Monte Carlo algorithm (VMC). *Medical Physics,* 23(3), pp. 445-457.

Khan, F. M., 2014. *The Physics of Radiation Therapy.* 5th ed. Philadelphia: Lippincott Williams & Wilkins.

Khan, F. M., Doppke, K. P., Hogstrom, K. R. & Kutcher, G. J., 1991. Clinical electron-beam dosimetry: Report of AAPM Radiation Therapy Committee Task Group No. 25. *Medical Physics,* 18(1), pp. 73-109.

Li, H. et al., 2021. AAPM Task Group 198 report: An implementation guide for TG-142 quality assurance of medical accelerators. *Medical Physics,* 48(10), pp. 830–885.

Low, D. A., Harms, W. B., Mutic, S. & Purdy, J. A., 1998. A technique for the quantitative evaluation of dose distributions. *Medical Physics,* 25(5), pp. 587–595.

Metcalfe, P. et al., 2007. Medical linear accelerators. In: *The Physics of Radiotherapy X-Rays and Electrons.* Madison, WI: Medical Physics Publishing, pp. 2-40.

Okumura, Y., 1972. Correction of Dose Distribution for Air Space. *Radiology,* 103(1), pp. 183–185.

Oncology Medical Physics, 2020. *Electron Therapy Physics.* [Online]
Available at: https://oncologymedicalphysics.com/electron-therapy-physics/
[Accessed 20 February 2024].

Pascal, H. M. et al., 2022. Monte Carlo modeling of the Elekta Versa HD and patient dose calculation with EGSnrc/BEAMnrc. *Journal of Applied Clinical Medical Physics,* 23(9), p. e13715.

Podgorsak, E. B., 2005. *Radiation Oncology Physics: A Handbook for Teachers and Students.* Vienna: IAEA.

Popple, R. et al., 2006. Comprehensive evaluation of a commercial macro Monte Carlo electron dose calculation implementation using a standard verification data set. *Medical Physics,* 33(6), pp. 1540-1551.

Quizlet, 2023. *Penumbra beam direction.* [Online]
Available at: https://quizlet.com/750848066/penumbra-beam-direction-flash-cards/
[Accessed 23 February 2024].

Reynaert, N., van der Marck, S., Tomse, M. & Jansen, J., 2006. Monte Carlo treatment planning for photon and electron beams. *Radiation Physics and Chemistry*, 76(4), pp. 643–686.

Rinks, M., 2012. *Computerised treatment planning systems:*. [Online]
Available at: https://onlinelibrary.wiley.com
[Accessed 7 February 2024].

Rogers, D., 1991. The role of Monte Carlo simulation of electron transport in radiation dosimetry. *International Journal of Radiation Applications and Instrumentation,* 42(10), pp. 965–974.

Snyder, J. E. et al., 2019. The commissioning and validation of the Monaco treatment planning system on an Elekta VersaHD linear accelerator. *Medical Physics,* 20(1), pp. 184–193.

Xing, A., 2007. *Dosimetric investigation of electron arc therapy delivered using Siemens trapezoidal aperture.* [Online]
Available at: https://ir.canterbury.ac.nz/server/api/core/bitstreams/f6fa6c5b-33bc-42e1-b918-c67d085c1999/content
[Accessed 22 February 2025].

Xu, Z. E., Walsh, T., Telivala, A. & Yang, M. G., 2009. Evaluation of the Eclipse electron Monte Carlo dose calculation for small fields. *Journal of Applied Clinical Medical Physics,* 10(3), pp. 75-85.

APPENDIX

Appendix I: Elekta electron beam data document



ELEKTA

Monaco

Electron Beam Data Collection List

ELECTRON BEAM DATA MEASUREMENTS RECOMMENDATIONS

1. Water Phantom

A water phantom is needed that is large enough to measure profiles at 20 cm depth across the maximum possible field size, with the isocenter positioned at a depth of 10 cm. It must also allow measuring depth dose curves along the central axis down to a depth of at least 35 cm. The control software of the water phantom must allow movements parallel to the main axes, as well as scans on a constant depth along lines through the isocenter at arbitrary angles.

For the smallest field sizes it is recommended to check the centering of the detector for two different depths before data collection.

2. Recommendations for Scanning Measurements

Scans must be performed from the bottom of the tank up to the surface to reduce scan hysteresis and surface artifacts.

Accurate adjustment of the detector z-position is essential for these measurements. When gathering water tank scans, set the origin of coordinates to coincide accurately with the water surface and then check the water level regularly as the measurements proceed.

Be careful to reset the background level of the field and reference detectors after every change of the detector gain/range parameters.

The choice of detector is particularly important in electron beam measurements. In charged particle fields, large gradients may occur and detectors with adequate resolution are preferred. The recommended detector is an electron diode or a scanning chamber with a collection volume of 0.13 cm or smaller. The semiconductor detector is also suited for the in-air fluence measurements. It should therefore be the primary choice of detector. If ionization chambers are used for measurements in water, the reading must be converted to dose. A number of countries have implemented specific dosimetry protocols that deal with this issue.

3. Recommendations for Point Dose Measurements

When measuring Output Factors, be careful to measure the relative outputs using a diode or an ionization chamber no larger than a standard CC-13 scanning chamber. Do not use a parallel plate chamber, because large chambers distort the central-axis dose measurement for small fields. If the measurement set includes field sizes less than 5 cm across, it is best to use a detector even smaller than a CC-13 chamber. Please record the type of chamber used.

When measuring output factors, be careful to let the temperature equilibrate before starting a series of relative measurements.

IMPAC Medical Systems, Inc., 13723 Riverport Drive, Suite 100 Maryland Heights, MO 63043
USA
Tel +1 .800.488.4672 Fax +1.408.830.8003

ELEKTA

ELECTRON BEAM DATA REQUIREMENTS

Oncentra users do not need any additional measurements. However, Monaco® users need to make additional measurements, which include additional measurements for 3D conventional modes.

XiO® Electron Monte Carlo and XiO® Electron Pencil Beam users need to make additional measurements. Please refer to XiO eMC Data requirements (LSSXIO0013) and XiO Pencil Beam data requirements (LSSXIO0012) documents for further information.

IN-AIR MEASUREMENTS

All measurements are at 70 cm and 90 cm SDD (Source to Detector Distance). If 70 cm SDD is not possible for technical reasons, then another SDD may be chosen, as long as the distance of 20 cm between the two SDD planes is maintained.

The in-air measurements are to be carried out free in air without any applicator or build-up cap and the detector should be located in an empty water tank.

In-air measurements should be normalized to 1.0 for an 8 x 20 cm^2 field size at 70 cm SSD.

1. Inplane and Crossplane profiles, Output Factors.

Field Sizes (cm) Upper BLD X Lower BLD	8 x 8	8 x 20	8 x Max	Max x Max

NOTE: These field sizes are conformed to the proper upper and lower Beam Limiting Device (BLD), depending on the head geometry of the LINAC. If possible, profiles should include at least 6 cm on each side outside the geometrical field.

IN-WATER MEASUREMENTS

All measurements are at 100 cm SSD.

For each applicator size, Inplane and Crossplane Jaw positions are needed.

1. Without Applicator

a. Depth Dose Scans for the maximum field size.

NOTE: PDD should be measured from a depth 5-10 cm beyond the practical range to at least 0.5 cm above the water surface. For a beam of nominal energy N MeV, N ≤ 10, a suitable initial scan depth is (N/2 + 5) cm (e.g., 8 cm for a 6-MeV beam); for N ≥ 10, a suitable initial scan depth is N cm (e.g., 20 cm for a 20-MeV beam). Set a depth increment of 1 mm for Energies < 12 MeV and use 1 – 2 mm for Energies > 12 MeV.

2. With Applicator

a. Depth Dose Scans for each applicator.

NOTE:

PDD should be measured from a depth 5-10 cm beyond the practical range to at least 0.5 cm above the water surface. For a beam of nominal energy N MeV, N ≤ 10, a suitable initial scan depth is (N/2 + 5) cm (e.g., 8 cm for a 6-MeV beam); for N ≥ 10, a suitable initial scan depth is N cm (e.g., 20 cm for a 20-MeV beam). Set a depth increment of 1 mm for Energies < 12 MeV and use 1 – 2 mm for Energies > 12 MeV.

b. Profiles along Inplane and Crossplane direction at the recommended depth for the specific energy, d = d_{norm}

Nominal Electron Energy, E_{nom} [MeV]	d_{norm} [cm]
4 MeV ≤ E_{nom} ≤ 6 MeV	1.0
6 MeV < E_{nom} ≤ 15 MeV	2.0
15 MeV < E_{nom} ≤ 50 MeV	3.0

NOTE: If possible, scan 6 cm outside the field edge. Set a scan increment of no more than 2 mm.

c. Bremsstrahlung profiles along X- and Y-direction at the recommended depth for the specific energy, d = d_{brem}

Nominal Electron Energy, E_{nom} [MeV]	d_{brem} [cm]
4 MeV ≤ E_{nom} ≤ 6 MeV	5.0
6 MeV < E_{nom} ≤ 15 MeV	10.0
15 MeV < E_{nom} ≤ 25 MeV	15.0
25 MeV < E_{nom} ≤ 35 MeV	20.0
35 MeV < E_{nom} ≤ 50 MeV	30.0

NOTE: If possible, scan 6 cm outside the field edge. Set a scan increment of no more than 2 mm.

3. Absolute dose for a fixed number of MU for each applicator for the same SSD (100 cm) at the recommended depth according to the nationally recommended dosimetry protocol, d_{cal}.

ADDITIONAL DATA

Customer needs to provide machine specific parameters such as

- Treatment unit head geometry
- Wedge and Collimator materials
- Multileaf Collimator – Specific parameters
- Geometry and Units for Relative Dose distributions

- Applicator Design Data for Electrons

Please refer to *LWBMON0001Beam Data Collection Worksheet for further information.*

CE 0086

Elekta Business Area Software Systems

IMPAC Medical Systems, Inc., 13723 Riverport Drive, Suite 100 Maryland Heights, MO 63043

USA

Tel +1 .800.488.4672 Fax +1.408.830.8003

ELEKTA

IMPAC Medical System Inc.

13723 Riverport Drive

Suite 100

Maryland Heights, MO 63043

USA

Phone +1 800 878 4267

Fax: +1 314 812 4491

IMPAC Medical Systems, Inc., the Elekta logo, and our product names are trademarks of Elekta. All other brand names or trademarks are the property of their respective holders. 0 2014 IMPAC Medical Systems, Inc.

IMPAC Medical Systems, Inc., 13723 Riverport Drive, Suite 100 Maryland Heights, MO 63043
USA

Tel +1 .800.488.4672 Fax +1.408.830.8003
LSSMON0007 / 1.0 / 25-Mar-14 ELEKTA